Development of a Permittivity Measurement Technique based on the Resonant Properties of Split Ring Resonator Metamaterial Structure

A THESIS
submitted to the

UNIVERSITY OF CALICUT

for the award of the degree
of

DOCTOR OF PHILOSOPHY

in

PHYSICS

by

SREEDEVI P. CHAKYAR

POST GRADUATE AND RESEARCH
DEPARTMENT OF PHYSICS
CHRIST COLLEGE (AUTONOMOUS), IRINJALAKUDA
MAY 2019

Dedicated to
My Family

THESIS CERTIFICATE

This is to certify that the thesis titled **Development of a Permittivity Measurement Technique based on the Resonant Properties of Split Ring Resonator metamaterial structure**, submitted by **Sreedevi P. Chakyar**, to the University of Calicut for the award of the degree of **Doctor of Philosophy**, is a bona fide record of the research work done by her under my supervision. The contents of this thesis, in full or in parts, have not been submitted to any other Institute or University for the award of any other degree.

Dr. V. P. Joseph
Research Guide
Associate Professor
Department of Physics
Christ College (Autonomous)
Irinjalakuda
680 125.

Place: Irinjalakuda
Date: 15 May 2019

DECLARATION

I hereby declare that the thesis entitled **Development of a Permittivity Measurement Technique based on the Resonant Properties of Split Ring Resonator metamaterial structure**, is an independent work carried out by me and it has not been submitted to any other institute or university for the award of any other degree.

Sreedevi P. Chakyar

Place: Irinjalakuda
Date: 15 May 2019

ACKNOWLEDGEMENTS

I wish to express my deep sense of gratitude to my research guide Dr. V. P. Joseph for his guidance, immense support and continuous encouragement. I am also thankful to the inspiration, love and care that he showered upon me during the years of my Ph.D. work.

It is my immense pleasure to express my sincere gratitude to Dr. Fr. Jolly Andrews, Assistant Professor, Dept. of Physics, Christ College (Autonomous), Irinjalakuda, for his constant support and interest shown throughout my research. I would also like to thank Dr. K. T. Mathew, Professor Emeritus, Department of Electronics, CUSAT for his technical assistance for doing simulation works.

I also express my gratitude to Dr. Mathew Paul Ukken, Principal, Christ college (Autonomous), Irinjalakuda. I take this opportunity to express my heartfelt gratitude to late Dr. Fr. T. M. Jose, former principal of Christ college (Autonomous), Irinjalakuda, for his constant encouragement and support for my research. I also thank Prof. V. P. Anto, HoD, Department of Physics for his motivation and support. I also thank all the faculty members of the department of Physics for their support. I am also thankful to Dr. Antony Joseph, Professor, Department of Physics, University of Calicut, Dr. Balu T. Kuzhivelil, Professor (Rtd.), Deartment of Zoology, Christ College (Autonomous), Irinjalakuda, and other RAC members for their valuable suggestions and comments which helped me throughout the research.

I gratefully acknowledge the University Grants Commission (UGC), Government of India, for providing financial support to complete my research in the form of UGC-JRF.

I take this opportunity to express my heartfelt gratitude to all my colleagues - Nees Paul, Joe Kizhakooden, Jovia Jose, Sikha Simon K., Bindu C., Umadevi K. S. and Anju Sebastian - for their helps and suggestions given when it needed most .

My gratitude also extends to Mrs. Prathibha P., late Mrs. Priya Rajan, Research Scholars of Christ College (Autonomous), Irinjalakuda, for their helps in various ways.

I am very much thankful to the former and present lab assistants of department of physics, all office and library staffs at Christ college for their support and assistance at different times of my Ph. D. work.

I am extremely thankful to my parents and sister for their encouragement and support. Their prayers and blessing were the reason for all my achievements. I am very much indebted to my husband Sreenath and daughter Durga for their patience and support given to me during stressful days of my research.

I bow my head before the God Almighty who lead me through darkest and toughest ways of life.

SREEDEVI P. CHAKYAR

PREFACE

Metamaterials have been a topic of extensive research during last two decades. Due to their negative permeability, negative permittivity and negative refractive index properties they show exotic characteristics leading to a variety of applications. The negative permeability Split Ring Resonator (SRR) structure has been an important object of study and its properties have been analyzed widely and are investigated for various applications. Dielectric measurements have also been an interesting research topic since several decades and continues to be so. Several techniques were developed to find the complex permittivity in various conditions especially in the microwave regime. The advancements in the technologies and the demands in various applications paved way to formulate different methods and design different experiments for such measurements. This thesis investigates novel dielectric measurement techniques using Split Ring Resonator metamaterial structure.

The concept of metamaterial, its history, recent trends and applications are introduced in **chapter 1**. It also presents an analysis of material property - dielectric constant or permittivity. A comprehensive review on different measurement methods for dielectric constant at microwave frequencies are also discussed.

The structure, origin of negative permeability and resonant nature of SRR are discussed in detail in **chapter 2**. The structure of SRR consists of two concentric flat metallic rings of equal width but of different radii. Each of the ring possesses a small split at diametrically opposite ends. The resonant nature of SRR arises from the intrinsic capacitance and inductance of the structure. The structural and substrate parameters define the capacitance and inductance and hence the resonant frequency. An alternating electromagnetic field with its magnetic component perpendicular to SRR surface will excite the structure which leads to the power absorption at the resonant frequency. The negative permeability arises from the interaction of SRR with the magnetic part of the interacting electromagnetic field. Different other structures designed to modify the properties of SRR are briefly discussed. A review of literature on structural and substrate tunability of the resonant frequency is also presented. Slight variation in the structural and substrate parameters can be used to tune the resonant frequency of SRR and this finds numerous applications in the field of sensors. They include applications such as displacement sensors, rotation sensors, strain sensors and movement sensors. Several other applications of SRR regarding dielectric measurements are also reviewed. The relevance of the work done in this thesis in relation to the existing literature is also briefly discussed.

In **chapter 3** a new equation for resonant frequency of SRR in terms of structural and substrate parameters is derived by analyzing the distribution of electric field on the surface of SRR. The methodology adopted in this work for the fabrication technique of the SRR along with the experimental setup for measuring the resonant properties are elaborated here. SRRs are fabricated in different dimensions on printed circuit boards using photochemical etching methods. Resonant frequency measurements are done by exciting the SRR by placing it in between transmitting and receiving probes connected to Vector Network Analyser (VNA). The electric field distribution on the surface of SRR is analyzed theoretically and verified experimentally. It is found that both the surfaces of SRR have equal distribution of charges and fields. This concept is a new approach and based on this, a new formulation for the effective capacitance of SRR is derived. Expression for resonant frequency in terms of the derived capacitance and intrinsic inductance is also presented. Experiments and simulations are used to verify the derived expressions.

A novel, compact, direct and efficient method for complex permittivity measurement is presented in **chapter 4**. The presence of a dielectric sample on the surface of SRR alters the resonant frequency due to the change in the effective capacitance. Equations for obtaining the real and imaginary part of permittivity are derived from the resonant parameters of SRR. By measuring the resonant frequencies of SRR with and without the presence of the sample, the permittivity of the unknown sample can be found out using the proposed equation. An equation for measurement of unknown permittivity of the substrate is also derived in terms of the resonant frequency. The loss tangent of sample also can be calculated using Q - factors of SRR resonance curves measured with and without the sample in contact. The derived equations for real part of permittivity and loss tangent are used to find out the complex permittivity of different solid samples using four different SRR test probes. The measured values are verified using standard cavity perturbation technique. Another method using a calibration curve for measuring the real part of the permittivity is also presented. In order to do this a calibration curve is drawn from the known values of permittivity of some standard samples and the corresponding resonant frequencies of the SRR. The unknown permittivity values are then found from the calibration curve using the obtained resonant frequency values. Measurement of permittivity values for some powdered food samples like pulses and cereals using extrapolation method is also presented.

Temperature dependent permittivity measurement of different type of solid samples are addressed in **chapter 5**. The temperature variations of various dielectrics are important for scientific and commercial applications. Both methods described in the fourth chapter are used to calculate the dielectric constant at a wide range of temperature. The temperature dependent dielectric studies on various flame retardant circuit boards may be a novel approach for the analysis of non-linear effects of the performance of microwave and electronic circuits. Another sample selected for the study is wax which may find applications in cosmetics, paints and dye industry. Other samples like plastic and perspex are also analyzed using these proposed methods.

A brief summary of all works presented is included in **chapter 6**. The studies presented in this thesis can be extremely helpful in the measurement of dielectric constant of solid materials and this can be extended to liquid samples also. The analytical formulation of the resonance of SRR can be extended to other resonating structures. The methods proposed for permittivity measurements can be helpful in microwave circuit designing, antenna designing, food quality checking and preservation. The future scope on the topics presented in thesis and the possible extensions are also discussed.

Contents

List of Tables

List of Figures

Chapter 1

Introduction

This chapter gives a brief introduction to the thesis. A discussion on metamaterials, dielectric constant and different permittivity measurement techniques is included in this chapter. Properties of metamaterials and their physical realization are briefly discussed. Several applications of metamaterials are also presented. Theory of dielectrics and importance of dielectric constant are briefly explained. Several permittivity measurement techniques used at microwave frequencies are reviewed.

The light and its interplay with materials have fascinated human minds since the dawn of civilization. Ever since scientific pursuit have commenced, humans have pondered over the cause of behavioral differences of each material in the presence of light. Upon keenly observing the properties of materials in the presence of light, it was understood that these differences can be partly explained by a property called refractive index. A deeper understanding of refractive index occurred only after James Clerk Maxwell astonishingly, painstakingly and intuitively showed that light is an electromagnetic wave.

Optical properties of any material can be explained by carefully studying the propagation of light through that material medium. The behavior of a material when an electromagnetic wave passes through it can be quantified using two intrinsic parameters, electric permittivity (ε) and magnetic permeability (μ). Electric permittivity is related to polarization happening in the medium in the presence of an interacting electric field. Similarly, permeability can be explained in terms of magnetization occurring in the medium due to interaction with the external magnetic field. In terms of electric permittivity and magnetic permeability, refractive index of a material is given by $n = \sqrt{\varepsilon\mu}$. Most commonly found materials in nature possess positive values of electric permittivity and magnetic permeability. Positive values for ε and μ ensure that the wave vector $\vec{k}$ associated with the propagation, points in the same direction as that of the flow of light energy as indicated by the Poynting vector $\vec{S}$. This naturally leads to an interesting question - whether one can find materials with negative values of μ and ε so as to obtain materials with unique optical properties.

1.1 History of metamaterials

Several attempts were made in order to modify the electromagnetic properties of materials and to manipulate the propagation of electromagnetic waves in order to suit different applications. Some examples of such attempts include chiral media, stratified media and photonic band-gap structures. As early as 1898, J. C. Bose used twisted jute fibers to rotate the plane of polarization of light [1]. Since 1948, artificial dielectrics have been in use as microwave lenses which were lighter and smaller than conventional ones. Winston E. Kock in 1946 proposed an application for light weight lenses as an artificial dielectric by using metallic antennas [2]. Rotman proposed a model of artificial plasma media using rod structures and parallel plate structures [3]. Photonic band gap structures which are three dimensional periodic dielectric structures in which forbidden bands for electromag-

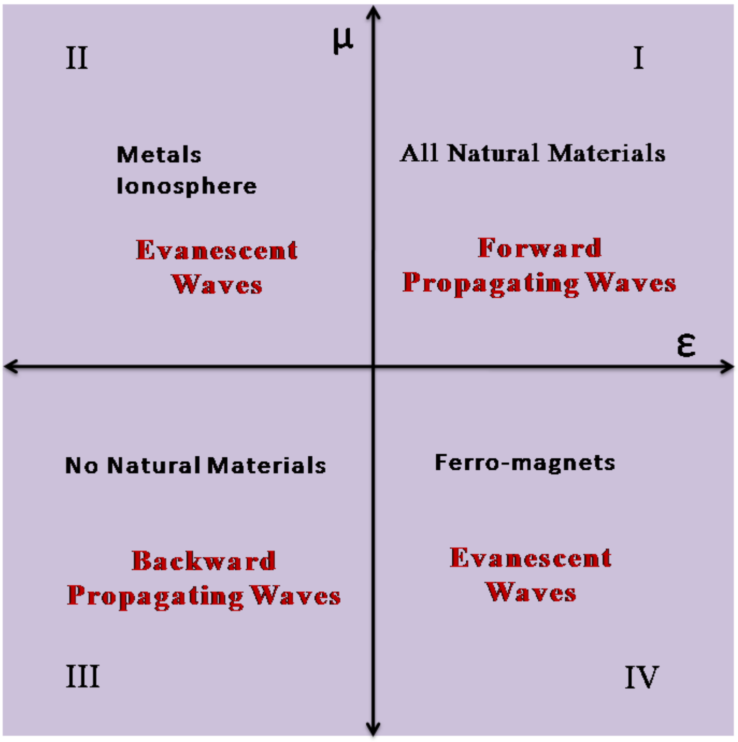

Figure 1.1: Classification of materials based on permittivity and permeability.

netic waves are present have also been proposed [4].

Metamaterials are another class of materials proposed for manipulating electromagnetic waves. The origin of the term metamaterial is from the Greek word ’meta’ which means ’beyond’, that is, they are materials having exotic properties not found in nature. The term ’Metamaterial’ was coined by Roger. M. Walser. He defined them as “Macroscopic composites having a man-made, three-dimensional, periodic cellular architecture designed to produce an optimized combination, not available in nature, of two or more responses to specific excitation ”[5]. They are thus artificially engineered structures having properties of negative permittivity and negative permeability arranged periodically to form a homogeneous bulk material in relation to the interacting electromagnetic wave. Properties of metamaterials are derived from their physical nature or structure of their composites and not from their chemical nature.

1.1.1 Classification of materials based on permittivity and permeability

As the permittivity and permeability are the deciding factors of optical properties of materials when electromagnetic wave interact with them, we can classify materials based on these parameters.

The materials can be represented in a space divided into four quadrants defined by axes representing permittivity (ε) and permeability (μ) as in Fig. 1.1. First quadrant includes all common natural materials possessing positive values of permittivity and permeability. Electromagnetic waves undergo forward propagation through these materials. Second quadrant includes materials with negative values of permittivity and positive values of permeability. Metals with good conductivity display negative permittivity towards electromagnetic wave with frequencies lower than visible light. All types of ionized medium including ionosphere may be added to this category. Ferro-magnetic materials can be included in the fourth quadrant as their permeability values are negative while permittivity is positive. Electromagnetic wave propagation through materials of second and fourth quadrant will be in the evanescent mode. The third quadrant, where both permittivity and permeability are negative and hence having negative refractive index is literally unoccupied as no natural materials have been found with such properties. The possibility of negative refractive index medium was thought to be non - existent as it is not generally observed in nature. But, if such materials are artificially engineered, they will show backward propagation where the direction of wave vector $\vec{k}$ will be opposite to the direction of the energy flow ($\vec{S}$).

It was Russian scientist Victor G. Veselago who first investigated the possibility of negative index of refraction theoretically and presented its various interesting consequences [6]. In usual media the electric field vector $\vec{E}$, magnetic field vector $\vec{H}$and the direction of propagation $\vec{k}$ form a right handed triplet as represented in Fig. 1.2(a).The corresponding equations related to the propagation of light of frequency ω are given by

$$\vec{k} \times \vec{E} = \omega\mu\vec{H} \tag{1.1}$$

$$\vec{k} \times \vec{H} = -\omega\varepsilon\vec{E} \tag{1.2}$$

In metamaterial media having negative refractive index all these three field vectors form a left handed triplet as represented by the following Eqns. 1.3 and 1.4 and hence are also known as 'Left Handed Materials' (LHM) (Fig. 1.2(b)).

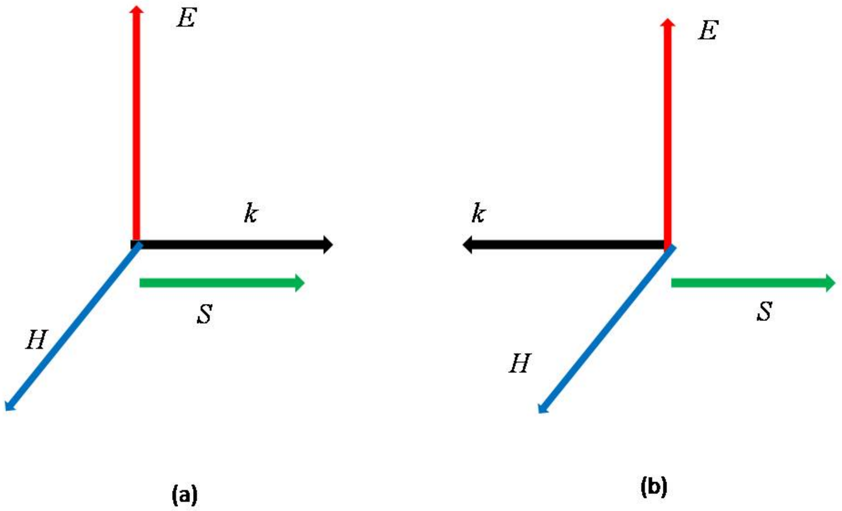

Figure 1.2: Direction of electric field ($\vec{E}$), magnetic field ($\vec{H}$), wave vector ($\vec{k}$) and poynting vector ($\vec{S}$) in (a) right handed medium and (b) left handed medium.

$$\vec{k} \times \vec{E} = -\omega\mu\vec{H} \tag{1.3}$$

$$\vec{k} \times \vec{H} = \omega\varepsilon\vec{E} \tag{1.4}$$

Here the poynting vector $\vec{S} = \vec{E} \times \vec{H}$ will not change its direction since permeability and permittivity are both negative.

He also explained the possibility of negative refraction (reversal of Snell's law) and focusing of light by planar lenses and also discussed other effects of negative refractive index such as reversal of Doppler effect and Cerenkov effect.

1.1.2 Origin of negative refractive index

Permittivity and permeability are complex quantities and hence their negative values can be represented as

$$\varepsilon = -\varepsilon_0\varepsilon_r = \varepsilon_0\varepsilon_r e^{i\pi} \tag{1.5}$$

$$\mu = -\mu_0\mu_r = \mu_0\mu_r e^{i\pi} \tag{1.6}$$

where ε_0 and μ_0 are permittivity and permeability for free space. The refractive index n is given by

$$n = \sqrt{\varepsilon\mu} \tag{1.7}$$

Substituting the expressions for ε and μ, one obtains

$$\begin{aligned} n &= \sqrt{\varepsilon_0\mu_0\varepsilon_r\mu_r}e^{i\pi} \\ &= -\sqrt{\varepsilon_0\mu_0\varepsilon_r\mu_r} \end{aligned}$$

Thus the refractive index becomes negative if the permittivity and permeability are negative. Hence, negative index medium is also called as 'Double Negative medium' (DNG medium).

1.1.3 Consequences of negative refractive index

The negative refractive index of a medium affects the propagation of electromagnetic wave in several ways. Some of the effects include reversal of Snell's law, inverse Doppler effect and inverse Cerenkov effect.

1.1.3.1 Reversal of Snell's law

When light travels from one medium to another it is refracted at an angle and it is described by Snell's law as,

$$\frac{sin\theta_1}{sin\theta_2} = \frac{n_2}{n_1} \tag{1.8}$$

where, θ_1 and θ_2 are angle of incidence and angle of refraction respectively and n_1 and n_2 are refractive indices of the first and second medium respectively (Fig. 1.3(a)).

For ordinary medium, n_1 and n_2 are positive quantities and hence the angles are also positive. That is the incident ray and refracted ray are in opposite sides of the normal as shown in Fig. 1.3(a).

When the refractive index of the second medium is negative, the Eqn. 1.8 becomes

$$\frac{sin\theta_1}{sin\theta_2} = -\frac{n_2}{n_1} \tag{1.9}$$

If the incident angle is positive then the refracted angle should be negative. That is, the refracted ray is in the same side of the normal as that of the incident ray as in Fig. 1.3(b). This phenomena is known as the reversal of Snell's law.

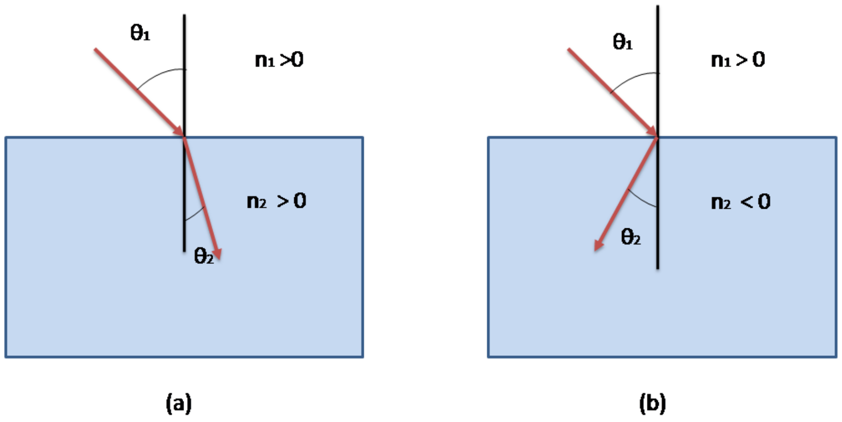

Figure 1.3: Schematic representation of Snell's law when light ray passes through (a) positive index medium and (b) negative index medium.

1.1.3.2 Inverse Doppler effect

Doppler effect refers to the shift in frequency observed by the receiver due to the relative velocity of the receiver with respect to the source. The shift in frequency is expressed as

$$\Delta\omega = \omega_0 \frac{nv}{c} \tag{1.10}$$

where v is the velocity of the source with respect to the observer and ω_0 is the original frequency. If the receiver is moving away, the frequency observed by the receiver decreases where as measured frequency increases if the receiver is moving towards the source. In the left handed medium, when the refractive index becomes negative, the expression becomes

$$\Delta\omega = -\omega_0 \frac{nv}{c} \tag{1.11}$$

Because of the negative sign the Doppler effect will be reversed, i.e., the receiver moving away will observe a higher frequency and that moving towards the source will measure a lower frequency.

1.1.3.3 Inverse Cerenkov effect

Charged particle moving through a medium with velocity v greater than the velocity of light c in that medium gives rise to a shock wave which travel forward at an angle θ. The expression for the angle at which the shock wave propagates is given by

$$cos\theta = \frac{c}{nv} \tag{1.12}$$

When the refractive index become negative, the equation changes as

$$cos\theta = -\frac{c}{nv} \tag{1.13}$$

Here the angle becomes obtuse and hence the shock wave travels backwards. This reversal of the direction of propagation of shock wave in a medium of negative refractive index is known as inverse Cerenkov effect.

1.1.4 Realization of negative refractive index

Even though the possibility of negative refractive index was proposed in late 1960s, its experimental realization did not occur till early twenty first century. As there are no natural materials which posses negative refractive index, artificial engineering of materials with simultaneous values of negative permittivity and permeability is required to realize metamaterials.

1.1.4.1 Negative permittivity

Metals below their plasma frequency can show a negative permittivity. The equation for permittivity of a plasma is given by,

$$\varepsilon = \varepsilon_0[1 - \frac{\omega_p^2}{\omega^2}] \tag{1.14}$$

where, ω is the interacting electromagnetic frequency and ω_p is the plasma frequency. The plasma frequency of a medium, the frequency below which the electromagnetic wave does not propagate through that medium, is given by,

$$\omega_p^2 = \frac{N_e e^2}{m^* \varepsilon_0} \tag{1.15}$$

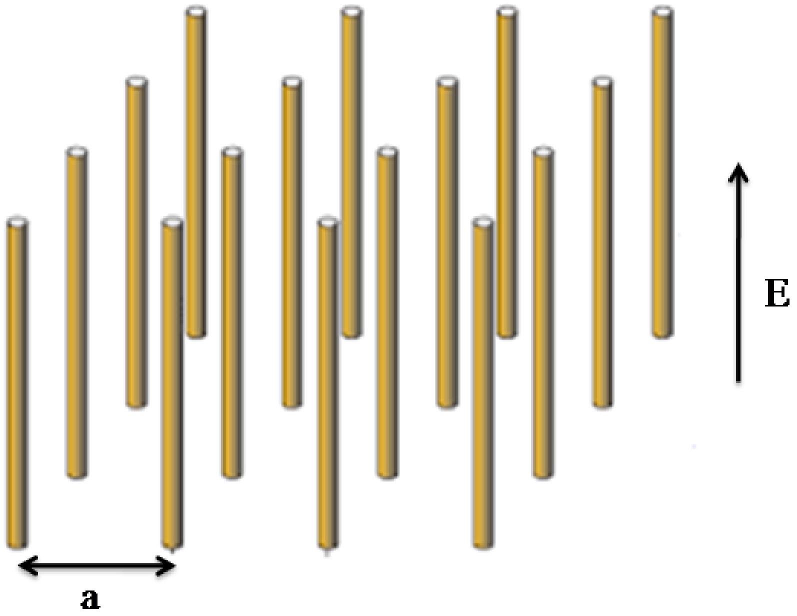

Figure 1.4: Schematic representaton of a wire mesh structure.

where, N_e is the electron density, e is the electronic charge and m^* is the effective mass of the electron. As one can see from Eqn. 1.14, for frequencies below the plasma frequency, the permittivity becomes negative. Usually metals have plasma frequency in the ultraviolet region. The plasma frequency will vary in accordance with the effective mass and number density of electron. A periodic array of thin metallic wires has been shown to have negative permittivity in the microwave frequencies (Fig. 1.4) [7]. The arrangement of thin wires reduces the electronic number density considerably and effective mass of electron is increased due to the self inductance produced in the wires. A detailed explanation and experimental confirmation of the proposed structure is presented by Pendry *et al.* [8]. The transmission characteristics for such a wire medium with typical plasma frequency of around 3 GHz is shown in Fig. 1.5.

1.1.4.2 Negative permeability

The discussion on possibility of negative permeability materials at microwave region was initiated by J. B. Pendry *et al.* [9] after realizing that artificial magnetic materials can be designed using magnetic moments generated from circulating current elements. He proposed a Split Ring Resonator (SRR) structure which became the stepping stone to the development of negative permeability. A detailed analysis of the structure, properties

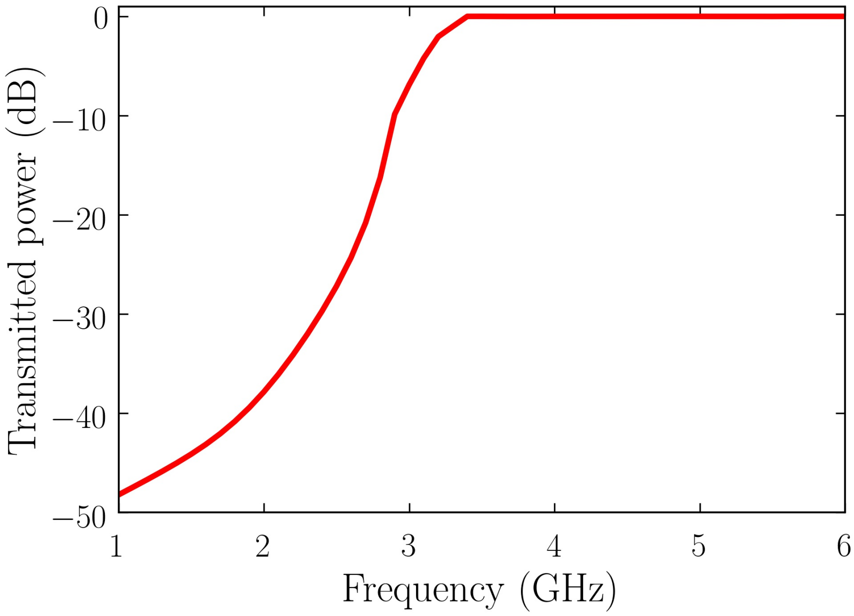

Figure 1.5: Transmission characteristics of a wire mesh structure with lattice spaing *l*.

and application of SRR is presented in the next chapter.

1.1.4.3 Negative refractive index

Negative refractive index media or double negative media can be conceived as a combination of two single negative medium of permittivity and permeability. The practical realization of double negative media is done by fabricating a composite medium using an array of SRRs and thin conducting wires. Such an array showing negative refractive index at microwave frequencies was fabricated by Smith *et al.* [10] (Fig. 1.6). The effective[10] permittivity and permeability of this medium was determined from reflection and transmission coefficients and was shown to be negative [11, 12]. For composite medium made of SRRs and thin wires, the transmission curve with respect to frequency shows a specific transmission region where both the constituent structures show absolutely no transmission of power. This transmission corresponds to the negative refractive index of DNG medium (Fig. 1.7). Reversal of Snell's law has been experimentally verified using SRR - wire composites by Shelby *et al.* [13]. Two dimensional left handed material in microwave frequencies has been fabricated and verified through simulations by Shelby *et al.* [14].

At the early stages of development of metamaterials, the design and fabrication involved photochemical etching. The dimensions of the structures constructed were in the order of millimeters and centimeters and the operating frequencies were in microwave

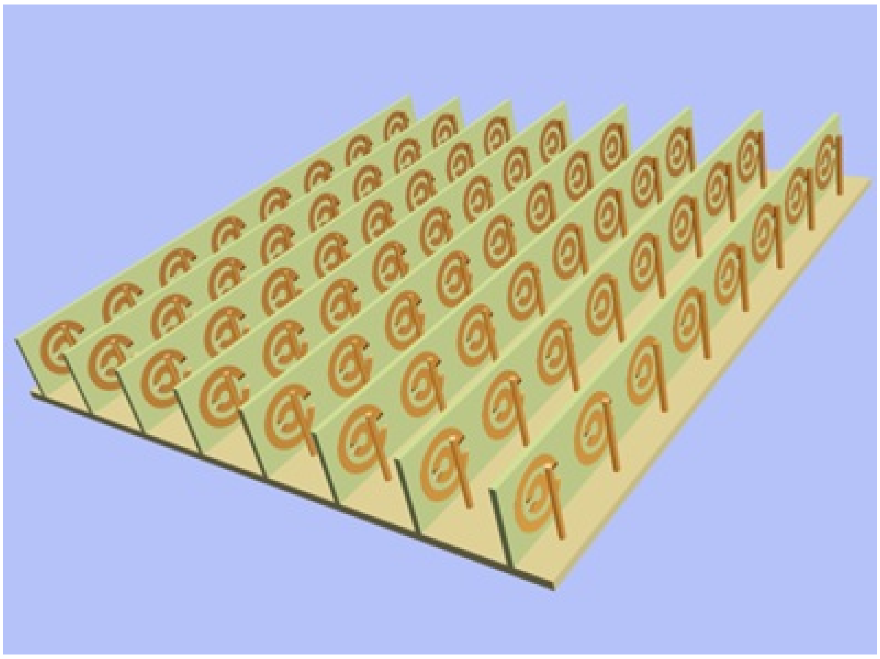

Figure 1.6: Composite medium of wire and split ring resonator structures which show negative refractive index.

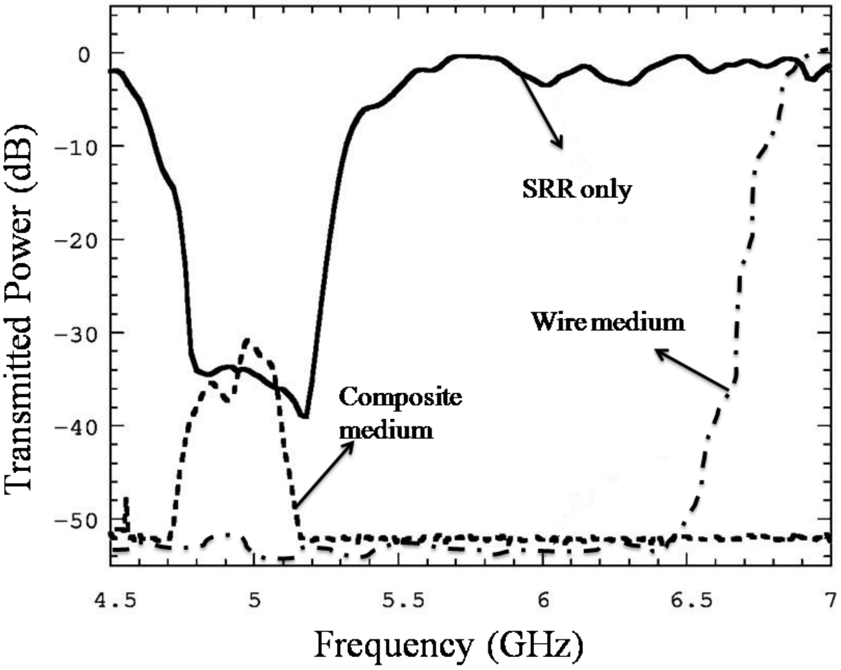

Figure 1.7: Plot showing transmission characteristics of a SRR-medium, wire mesh and SRR-wire composite structure.

frequencies (GHz). The advent of new technology enabled the miniaturization of structures into nanoscales and the increasing of operating frequencies to terahertz regions [15, 16, 17]. Intense research is going on to raise the operating frequency of metamaterials to even the visible region [18, 19].

1.2 Applications of metamaterials

Owing to the interesting properties of metamaterials, a number of applications were proposed in different frequency domains. Some of the important applications are discussed below.

1.2.1 Sensors

Several sensing applications have been developed using metamaterial resonating structures. It has been shown that variations in resonant frequency can be used in applications such as dielectric sensors, pressure sensors, vibration sensors, biomedical sensors etc. [20, 21, 22]. Wireless strain sensors have also been developed for application in engineering, medicine and avionics [23, 24].

Several dielectric measurement techniques have been developed using the resonant frequency variations of different metamaterial resonating structures [25, 26, 27, 28]. They provide comparatively easy and precise measurements using simple experimental setups.

1.2.2 Antennas

Simulations of dipole antennas embedded in metamaterial substrates by Wu *et al.* [29], showed that they have an improved directivity. Enoch *et al.* [30] have analyzed the microwave radiation from a source embedded in metamaterial slab and showed that it will be directed in a narrow cone. A featherlight horn antenna constructed using artificial plasma sheets using thin metallic wires have been proposed for astronomical applications [31]. Such a structure with negative permittivity can be used to replace the conventional horn antenna. Several application have been reported in literature where the functionality of the antennas are effectively tuned using suitable meta-structure inclusions [32, 33].

1.2.3 Perfect absorbers

The advent of metamaterials have opened up a useful and efficient area in the state-of-the-art absorber technology. A review of broadband metamaterial perfect absorbers, their fabrication methods and various applications is presented by Yu *et al.* [34]. To be specific, some noticeable proposals are mentioned below. An absorber at terahertz frequencies using metamaterial structures which has maximum absorption by using the tuning of the electrical permittivity and magnetic permeability has been presented [35]. Similarly, a dual band metamaterial perfect absorber using gold-nano rings have been studied for applications in optical filters, photo detectors etc. [36].

1.2.4 Metamaterial cloaking

An interesting application of metamaterials is cloaking. The negative refraction property allows the electromagnetic field to bend around an object making it invisible. Numerical and experimental verification of a metasurface cloak for hiding metallic objects from low frequency radiation is presented by Teperik *et. al.* [37]. Intense research is going on in the direction to achieve invisibility using cloaking property which may have military and surveillance applications. However, such applications may also raise a few ethical issues.

Metamaterials, since its inception, have found numerous interesting applications in other fields such as acoustics, superconductivity etc. There have been tremendous interest in the field of acoustic metamaterials and various applications of such materials have been developed. It has been found that sound wave can be controlled using sub wavelength metamaterial structures [38]. Voltage tunable acoustic metasheets have been used for controlling propagation directions and focusing of acoustic waves [39]. Superconducting metamaterials have also been a promising new regime [40, 41]. Another promising area where interesting research is happening is in the fields of energy harvesting, wireless power transfer etc. [42].

1.3 Dielectric Materials

Materials can be classified based on electrical conductivity into conductors and insulators. Dielectrics are a subclass of insulators but may not be considered as ideal ones since the molecules in them strongly respond to electric field compared to pure insulators. Dielectrics also differ from conductors or metals in that they do not possess free electrons.

1.3.1 Dielectric constant and polarization

Dielectric materials constitute electron clouds bounded to ions. This electron cloud gets displaced in the presence of an applied electric field. This causes a polarization inside the material and hence an electric field is created which opposes the applied field. If a time varying field is applied, the electron cloud starts to oscillate according to the frequency of the applied field. This is called electronic polarization and it occurs usually in ultraviolet and optical frequencies. The mode of polarization is highly dependent upon the frequency of the applied electromagnetic field. At lower frequencies near infra-red, ionic polarization is observed which is associated with the stretching and bending of molecular bonds. For molecules possessing permanent dipole moment, dipolar polarization occurs at microwave frequencies.

Different analytical models have been proposed to describe the motion of electrons in a dielectric medium in the presence of external applied electric/electromagnetic field. A couple of prominent models are discussed in the following subsections.

1.3.1.1 Lorentz model

Under an external time-varying electric field of frequency ω, the electrons get displaced from their position associated with each ions. But the coulomb force ($\vec{F} = -e\vec{E}$) which act as a restoring force ($\vec{F}_{rest} = m\omega_0^2\vec{r}$) make their motion to a harmonic oscillation. Damping forces ($\vec{F}_{damp} = m\gamma\dot{\vec{r}}$) due to collisions and radiations will be also present in addition to the restoring force. Where γ is the damping constant.

The equation of motion of an electron in the presence of these competing forces can be written as (by neglecting effects of local electric fields)

$$m\ddot{\vec{r}} + m\gamma\dot{\vec{r}} + m\omega_0^2\vec{r} = -e\vec{E} \tag{1.16}$$

where, the second term represents the damping forces, third term is the restoring force and the right hand side is the applied electric force. In the equation, r is the displacement vector and ω_0 is the resonant frequency. This equation can be solved to obtain the expression for displacement of electron as

$$\vec{r} = \frac{-e\vec{E}/m}{\omega_0^2 - \omega^2 - i\gamma\omega} \tag{1.17}$$

Assuming the nucleus to be stationary, the polarization due to dipole moment of N electrons per unit volume will be,

$$\vec{P} = -Ne\vec{r} = \frac{Ne^2\vec{E}/m}{\omega_0^2 - \omega^2 - i\gamma\omega} \tag{1.18}$$

we know that,

$$\vec{P} = \varepsilon_0\chi\vec{E} \tag{1.19}$$

where χ is the electric susceptibility of the medium. From the relation between susceptibility and permittivity we can write,

$$\varepsilon = 1 + \chi = 1 + \frac{Ne^2/m\varepsilon_0}{\omega_0^2 - \omega^2 - i\gamma\omega} \tag{1.20}$$

From the above expression, it is clear that the permittivity is a complex term with real and imaginary parts.

1.3.1.2 Drude model

Drude model is a subclass of Lorentz model where the medium considered is metals or conductors. In this model electron-electron and electron-ion interactions are neglected in deriving the expression for permittivity. Further more, the oscillation frequencies will be zero due to negligible restoring force. From Eq. 1.20, the permittivity is given by

$$\varepsilon = 1 - \frac{\omega_p^2}{\omega(\omega + i/\tau)} \tag{1.21}$$

where τ is the relaxation time and

$$\omega_p = \sqrt{\frac{Ne^2\tau}{m}} \tag{1.22}$$

is the plasma frequency of the medium. Plasma is defined as the collective oscillation of electrons in the background of ions and the quanta of plasma oscillations are called plasmons. For free electron gases, (like ionosphere and free electrons in metals) there will be no restoring force. Neglecting the damping effect, we have

$$\varepsilon = \varepsilon_0[1 - \frac{Ne^2}{m\varepsilon_0\omega^2}] = \varepsilon_0[1 - \frac{\omega_p^2}{\omega^2}] \tag{1.23}$$

From this equation, we can see that when $\omega > \omega_p^2$, permittivity is positive which leads to the propagation of incident radiation through the medium. However, when $\omega < \omega_p^2$ permittivity becomes negative and the propagation constant ($\vec{k}$) become imaginary and hence the incident radiation will be attenuated.

1.3.2 Complex nature of permittivity

As explained in Sec. 1.3.1.1, the permittivity is a complex term with real and imaginary parts. The imaginary part comes from the inertia of electrons to the externally applied electromagnetic field. As the applied frequency increases, the inertia also increases, and the displacement vector will not be able to keep in phase with field changes. It causes a frictional damping which results in power loss. The out of phase polarization is characterized by complex terms in permittivity. In conductors, semiconductors, and electrolytes in addition to frictional loss, ohmic loss will also be present which will also contribute to the complex part. Complex permittivity is written as

$$\varepsilon_c = \varepsilon' - i\varepsilon'' \tag{1.24}$$

where, ε' and ε'' are real and imaginary parts of permittivity respectively. The ratio of imaginary part to real part is called loss tangent which is defined as

$$\tan\delta = \varepsilon''/\varepsilon' \tag{1.25}$$

where δ is called the loss angle. The imaginary part ε'' or loss tangent is a measure of power loss or conductivity in the medium.

1.3.3 Permittivity as a dispersion function

From the expressions for permittivity in the models explained earlier, the complex permittivity can be seen as a dispersive function.

Both real and imaginary parts of the permittivity has some characteristic shapes when plotted along with the frequency. A plot depicting the two functions in the single pole model is given in Fig. 1.8. We can see that at certain frequency (ω_l) the real part of permittivity shows an anomalous nature different from that at other frequencies. Away from ω_l, the function varies normally, *i.e.* as frequency increases permittivity also increases. This is called normal dispersion. But, at frequencies close to ω_l a sudden decrease in permittivity from a maximum value is observed. This is called the anomalous dispersion. Some times

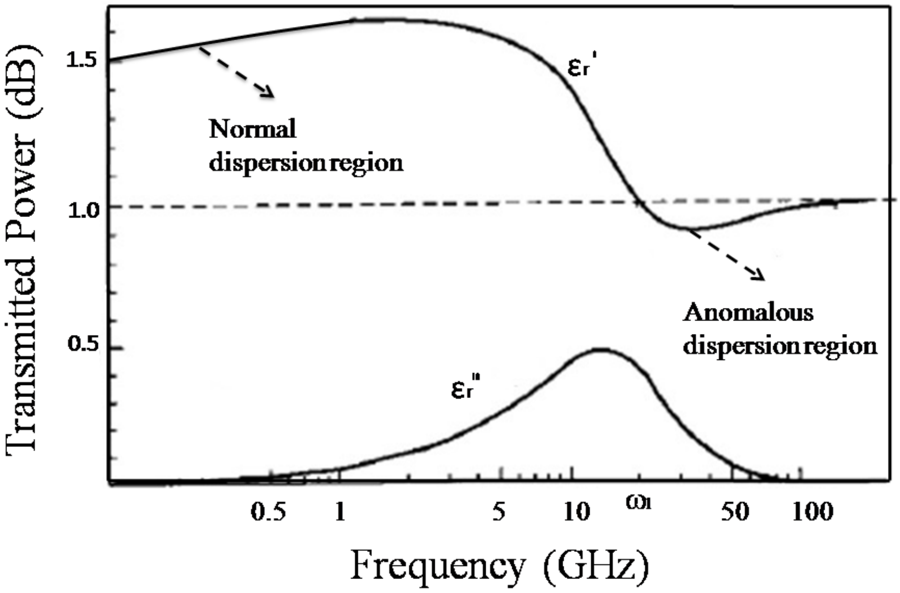

Figure 1.8: Frequency dispersion relation of complex permittivity.

the permittivity even may attain negative real values during anomalous dispersion. At this frequency domain, the imaginary part become appreciable than at other frequencies and attain large positive values. This positive imaginary part of permittivity implies that the wave is absorbed inside the medium. This is usually due to absorption of energy by resonating electrons. Hence it is called resonant absorption.

It is obvious that the dielectric constant of a material is not really a constant and is a misnomer. There are different factors that affect the value of dielectric constant of a material other than frequency of operation like temperature, humidity of atmosphere and water content. Variations in any of these parameters also affect the value of permittivity. In other words, the variations in the measured values of permittivity can in turn be used as a tool for measuring these different parameters. Thus the complex permittivity measurement becomes important in many fields. There have been a great interest in developing efficient methods for measuring the permittivity of different kinds of materials.

In the next section, we shall discuss some of the techniques for measuring permittivity.

1.4 Permittivity measurement techniques at microwave frequencies

Dielectric measurement is an important tool when it comes to characterization of materials for different applications in different fields. The characterization of materials is used for analyzing composite media (solids or liquids) and determining the composites in them. Non-linear and anisotropic nature of different materials can be understood by variations in the permittivity values. The dielectric measurement can also find applications in electronic industries where the complex permittivity values and its temperature dependence are important factors. Characterization of dielectric properties of materials is also important in food and agriculture fields. Quality and moisture control of food and agricultural products during production and packing can be used to analyze the presence of pesticides and other adulterants. In the field of medicine and pharmacy, anomalies in permittivity measurements may point to the abnormalities in tissues and may even be used for genetic analysis.

Dielectric characterization techniques differ according to the nature of the materials under test, frequency range of interest and temperature of the environment. These techniques can be classified according to the method used for measurement [43]. The methods are mainly divided into non-resonant and resonant methods. Non-resonant methods are based on the microwave propagation through the material and resonant methods are based on microwave resonance effects in the presence of the test material. Different dielectric constant measurement methods are represented as a flow chart in Fig. 1.9.

1.4.1 Non-resonant methods

For measurement of dielectric parameters, non-resonant methods are mainly used in a wide frequency range. In these kind of methods, electromagnetic wave is directed to the material under test with the help of waveguides. Transmitted or reflected waves are measured after absorption or reflection from the material. Different kinds of waveguides used for measurement are coaxial lines, planar transmission lines, hollow metallic waveguides and dielectric waveguides. Non-resonant methods are classified as reflection methods and transmission/reflection methods and are detailed below.

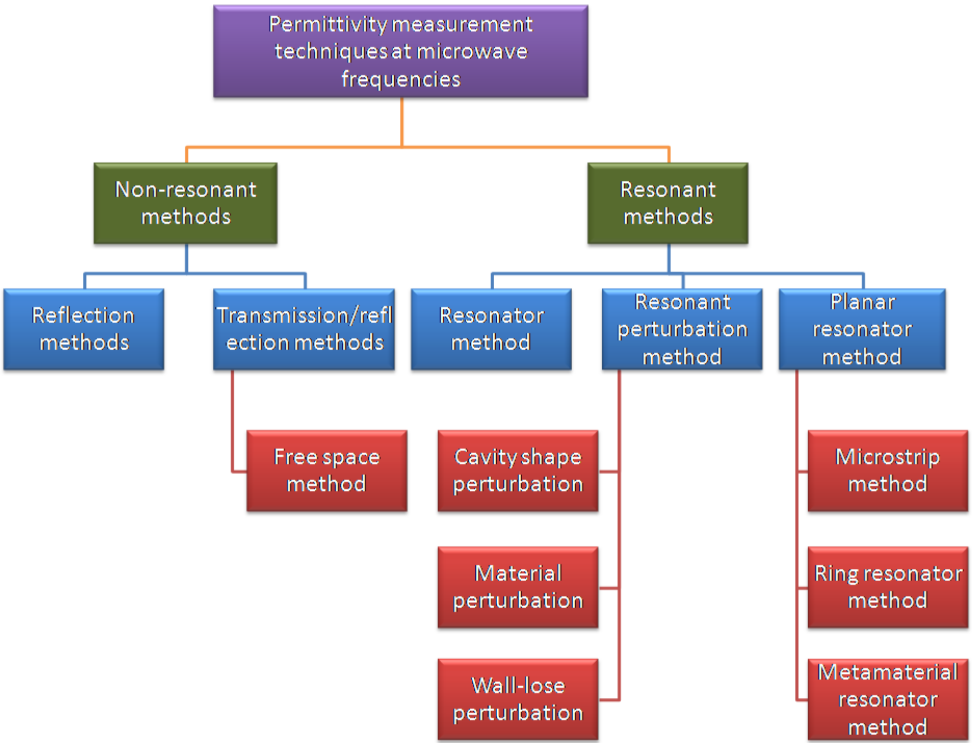

Figure 1.9: Flow chart depicting different measurement methods for permittivity.

1.4.1.1 Reflection methods

Either permittivity or permeability is calculated using reflection coefficient from measurements mainly using open ended coaxial probes. Permittivity measurement is done using open reflector measurement for non-magnetic, large size and high loss materials. The permeability of samples is measured using short reflection method where sample is electrically shorted.

1.4.1.2 Transmission/reflection methods

In transmission/reflection methods, the sample material should be inserted into the coaxial lines or waveguides. Transmission and reflection coefficients are measured in this method for obtaining the permeability and permittivity of the samples.

Severo *et al.* have presented a model for scattering parameters for non-resonant transmission/reflection and reflection technique, and equations are derived for determining the permittivity [44]. Kim *et al.* proposed a method for measuring the dielectric constant and loss tangent of ferroelectric thin films of large dielectric constant coated on substrates placed in a rectangular waveguide from numerical analysis of the scattering parameters

[45].

Free space method is another kind of non-resonant method which may use both reflection and transmission/reflection measurements. This method is non-destructive and can be used for broadband applications. They are also compatible for high temperature and high frequency applications. The method uses broadband antennas on either side of the sample which are calibrated by a suitable calibration technique initially. Several dielectric measurements have been performed in the past using free space method. Dielectric measurement of ceramic and other composite materials in the microwave frequencies is performed by Ghodgaonkar *et al.* [46]. In that work they used a reflection method to find out the real value of permittivity and comparisons are done using teflon and PVC samples. As another example for this method, Bijukumar *et al.* have developed a free space method for measuring the permittivity of compound materials in transmission/reflection methods using horn antennas [47].

1.4.2 Resonant methods

Resonant methods are usually used for permittivity measurements at single frequencies and are measured by observing the changes in resonant frequency and the Q-factor. They are mainly suitable for low-loss samples. Compared to non-resonant methods, resonant methods provide higher accuracy and sensitivity in complex permittivity measurements. Resonant methods are divided into resonator methods and resonant perturbation methods.

1.4.2.1 Resonator method

In this method the resonant frequency and Q-factor of the resonator are determined. The surface resistance of the conducting plates can also be calculated using the resonator method.

1.4.2.2 Resonant perturbation method

Unlike resonator method, resonant perturbation method uses a resonator to which the sample under test is introduced and hence changes in the resonant frequency and Q-factor of the resonator are obtained for evaluating the desired parameters. There are different types of resonant perturbation methods. Cavity shape perturbation method is one kind of resonant perturbation method which uses adjustment of the resonant frequency of the cavity. In another method, wall-lose perturbation, one of the cavity wall is replaced by the sample which changes the resonant frequency and Q-factor of the cavity. This method is used to measure the surface resistance of conductors. Cavity perturbation is another method which have found an important place in dielectric measurement techniques due to its compact and accurate nature [48, 49].

1.4.2.3 Planar resonator method

Different planar resonating structures are also used for dielectric measurements. Some of the methods are explained here.

Microstrip resonating structures are used for dielectric constant measurements. A Tee-resonator structure is used to determine the complex permittivity of the dielectric and the resistance of the conducting sheet by measuring the transmission parameters by Fulford *et al.* [50]. Demenicis *et al.* employed a coplanar wave guide linear resonator for characterization of composite ceramic screen printed thick films where the films are deposited over the resonator [51].

Ring resonator structures have also been employed for permittivity measurements. Bernard *et al.* have used a variational calculation to compute the capacitance and hence the effective permittivity of the ring resonator structure. The measured values of dielectric constant are compared with results obtained from cavity perturbation method [52].

Several dielectric measurement related works have also been done using metamaterial inspired resonator structure. Different designs are explored for improving the accuracy and sensitivity of these methods. Split Ring Resonators (SRRs) and Complementary SRRs (CSRRs) are the metamaterial resonating structures commonly used for the dielectric characterization. Their *LC* resonant property and its sensitivity to dielectric environment are utilized for finding out the complex permittivity of different kinds of materials. Spiral shaped resonators and multiple ring resonators are some of the other metamaterial inspired structures used for the dielectric study.

1.5 Brief Outline of the coming chapters

The main aim of the thesis is to introduce novel permittivity measurement techniques using resonating property of metamaterial split ring resonator structures. The proposed technique is verified using experiments and simulations. It is also extended to temperature dependent permittivity measurements of different dielectric samples.

The remaining part of the thesis is divided into five chapters. The second chapter discusses different negative permeability structures, their resonant nature, fabrication and measurement methods. It also gives an outline of the fabrication and measurement methods used for the present work.

Deriving a new formula for resonant frequency of circular SRR in terms of the capacitance and inductance of the SRR is presented in chapter 3. Derived formulas are verified using simulations and experiments. Chapter 4 proposes a complex permittivity measurement technique on the basis of the equations derived. An extrapolation method using calibration curve to measure the real part of permittivity is also introduced in this chapter. A study on the temperature dependent variations of real part of permittivity of different samples having importance in industrial and commercial applications is presented in chapter 5.

Chapter 6 presents summary of the research findings and scope for future works. Concluding remarks on the research is also presented in this chapter.

Chapter 2

Split Ring Resonators - Negative Permeability Resonating Structure

This chapter elaborates the negative permeability metamaterial Split Ring Resonators (SRR). Resonant property, negative permeability property of SRR and equivalent circuit models are discussed in this chapter. Various other negative permeability structures inspired from SRR are presented here. Tunability of SRR resonance and permeability property are explained in detail. Several applications of SRRs are also presented. The methodology adopted for fabrication of SRR and measurement of its resonant frequency are also addressed in this chapter.

Split Ring Resonators (SRRs) are basic metamaterial resonant structures constructed from non-magnetic conducting elements to exhibit negative permeability in specific frequency regions [9, 11, 10]. They are artificially engineered structures having characteristic response to electromagnetic fields. SRRs mimic the response of atoms and act as a magnetic dipole in interaction with the magnetic component of the electromagnetic wave. Their periodic arrangement leading to a bulk form exhibit homogeneous medium properties when their periodicity and dimensions are much smaller than the wavelength of the electromagnetic wave interacting with them.

2.1 Negative permeability nature of SRR

The need for negative permeability structures for realization of negative refractive index triggered intensive research in the area of metamaterials. John B. Pendry first considered an array of parallel conducting cylinders of radius r and spacing a for the above structure [9]. The expression for permeability of such a medium when alternating magnetic field applied in the axial direction of cylinders is

$$\frac{\mu}{\mu_0} = 1 - \frac{\frac{\pi r^2}{a^2}}{1 + \frac{2i\sigma}{\mu_0 \omega r}} \tag{2.1}$$

Where σ is the resistivity of the conducting material, ω if the frequency and μ_0 is the permeability of free space. This permeability is dispersive in nature with its value greater than zero indicating a limited magnetic response.

Pendry showed that range of magnetic properties can be enhanced by introducing internal capacitive elements into the structure. A structure with two concentric cylinders having splits at opposite ends prevent the current to flow around the ring and there by introducing a capacitance along with the inductance. This resulted in a resonant structure having a dispersion relation with negative permeability value at certain frequencies [9].

Such a structure is found to be highly anisotropic due to the electrical conducting path in the axial direction. To reduce the anisotropy of this structure and to remove electrical effects a modified structure with flat SRR is suggested. Fig. 2.1 shows the structural and lattice parameters of the individual and bulk SRR structures. The given structure avoids continuous conducting path and hence eliminates electrical activity along axial direction.

The equation for permeability of this structure is obtained as

$$\frac{\mu}{\mu_0} = 1 - \frac{\frac{\pi r^2}{a^2}}{1 + \frac{2il\sigma}{\mu_0 \omega r} - \frac{3lc_0^2}{ln\frac{2c}{d}\pi\omega^2 r^3}} \tag{2.2}$$

where σ is the resistivity and c_0 is the velocity of light in vacuum, *l* is the periodicity, *r* is the inner radius, *c* is the width of the ring and *d* is the spacing between the rings. The above equation can be written as

$$\mu = \frac{F\omega^2}{\omega^2 - \omega_0^2 + i\omega\Gamma} \tag{2.3}$$

where

$$F = 1 - \frac{\pi r^2}{a^2} \tag{2.4}$$

$$\Gamma = \frac{2li\sigma}{\mu_0 r} \tag{2.5}$$

$$\omega_0^2 = \frac{3lc_0^2}{\pi r^3 ln(2c/d)} \tag{2.6}$$

where ω_0 is called the resonant frequency. The permeability is found to become negative for frequencies $\omega_0 < \omega < \omega_{mp}$, where ω_{mp} is the magnetic plasma frequency and it is defined as

$$\omega_{mp} = \frac{\omega_0}{\sqrt{(1-F)}} \tag{2.7}$$

The variation of real and imaginary parts of permeability with frequencies is shown in Fig. 2.2.

The negative permeability nature of SRR was theoretically explained and experimentally verified by several researchers after Pendry's initial proposal. Frequency dependent permeability and permittivity of SRR, wire structure and composite structure are evaluated from the transmission and reflection coefficients by Smith *et al.* [12]. It is shown that the real part of permeability is negative in some frequency regions. Smith *et al.* has also experimentally proved the negative permeability of SRR [10]. Negative permeability nature of SRR is also validated and Q-factor of resonance is analyzed by Lee *et al.* [53]. Weiland *et al.* also verified the dispersion relation of the permeability of SRR and negative permeability nature is quite evident in their work [54]. Another attempt to experimentally prove the negative permeability nature of SRRs is done by Pradeep *et al.* [55] where a cavity perturbation technique is employed.

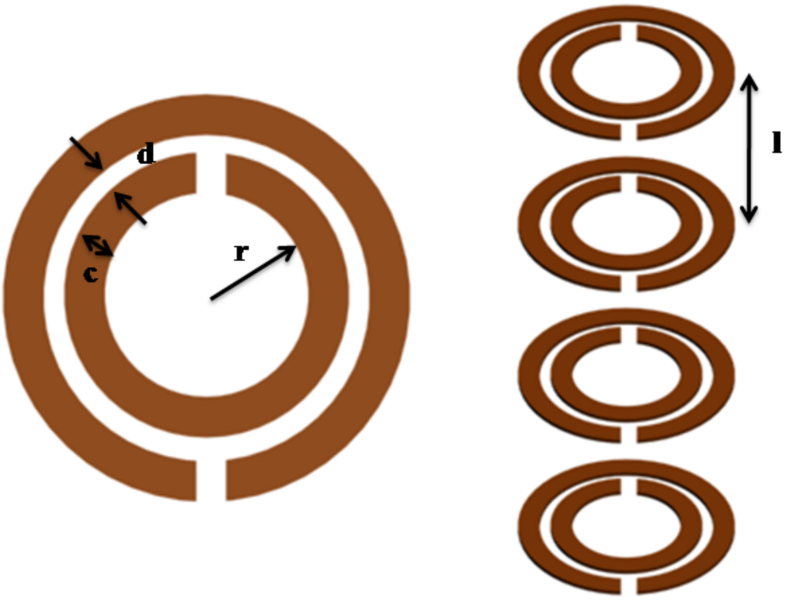

Figure 2.1: SRR structures and its stacked layers with strutural parameters.

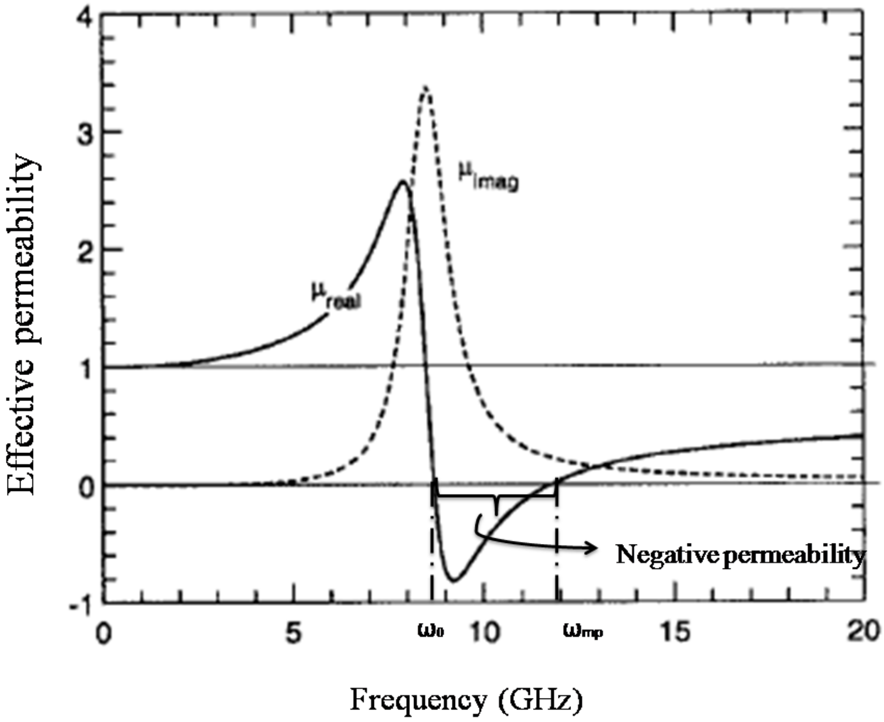

Figure 2.2: Variation of real and imaginary parts of permeability of an SRR with frequency.

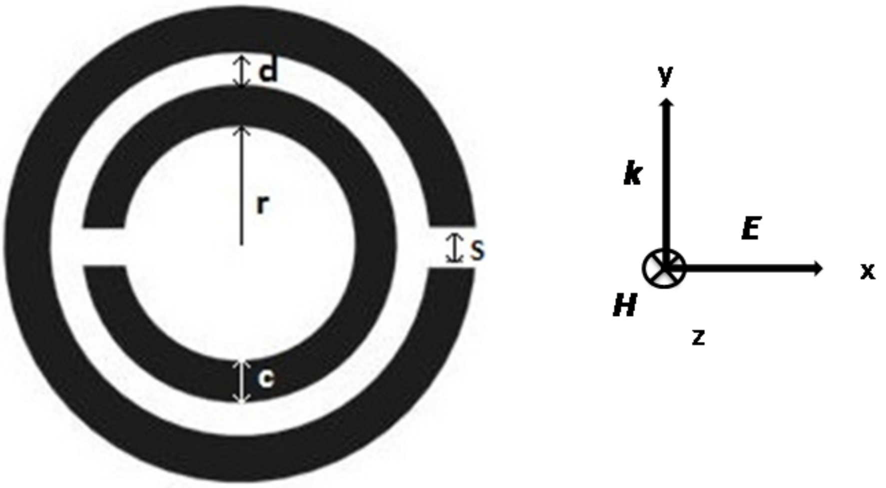

Figure 2.3: Schematic representation of the Split Ring Resonator (SRR) with its structural parameters - inner radius (*r*), ring width (*c*) split width (*s*) and spacing (*d*) along with the field directions.

SRRs with two concentric metal rings of width *c* and spacing *d* are usually fabricated on a planar dielectric substrate like printed circuit boards. The radius of the inner ring is represented as *r*. Each of the two metal rings have small split (*s*) on the diametrically opposite sides of the structure. Schematic representation of the SRR structure is shown in Fig. 2.3. The proposed SRR structures specially designed to produce negative permeability may lead to the construction of artificial negative refractive index bulk metamaterial media by suitably incorporating them with the negative permittivity counterpart (wire media).

2.2 Fabrication and measurement techniques of SRR

In this section, a brief description regarding the different fabrication techniques, geometry, resonance, tunability, equivalent circuits and some sensing applications of the SRR are presented.

2.2.1 Fabrication of SRR

Fabrication of SRR with accurate dimensions is of utmost important for getting the required resonance condition. There are several methods for the fabrication of SRR.

Figure 2.4: Block diagram representing the various steps of photo chemical etching method.

2.2.1.1 Photochemical etching method

SRRs are usually fabricated on Printed Circuit Board (PCB) laminates. Photo chemical etching method may be employed for this purpose which includes several steps as detailed below. Fig. 2.4 shows the flow chart representing different steps of photo chemical etching.

The first step of photo chemical etching is the designing of photo - masks. They are usually transparent polymer sheets printed with designs of SRR structures which are to be etched on the PCB. The required designs can be drawn using any drawing softwares like CorelDRAW and then printed on the transparent sheet.

After carefully cleaning the PCB to remove any dust, grease, oil or any other contaminants, it is coated with a photo resist material. It is a light-sensitive material which will change their chemical property when exposed to Ultra Violet (UV) radiation. After carefully dipping into the photo-resist liquid, the PCB is allowed to dry in a dark room.

The specially designed mask is then placed on the PCB and is exposed to UV rays. When photo resist is exposed to UV light, the chemical structure of the resist changes so that it becomes more soluble in the developer. This chemical change allows some of the photo-resist to be removed by a developer solution.

After developing, etching process is done where by the unwanted copper is removed. In etching process, a liquid chemical agent is used to remove the metallic layer which are not protected by photo-resist material. Usually Ferric Chloride ($FeCl_3$) solution is taken as the etching solution. When the PCB is dipped in the $FeCl_3$ solution for a sufficient time, it will react with the copper in the UV exposed area resulting in its removal. The copper in the unexposed portion will stay intact and hence we get the required SRR structure on the sheet.

2.2.1.2 Printing using milling method

Milling method is another printing technique used to fabricate electronic circuits which can also be used for SRR fabrication. It is a process of removing areas of unwanted copper from a printed circuit board with the help of a computer assisted milling machine. The method is free of chemicals as rotary cutters are used to create high quality structures printed on PCB.

2.2.2 Different types of SRR structures

The structure has an important role in determining the properties like resonant frequency, bandwidth and sensitivity of Split Ring Resonators. SRRs of different structures are designed and analyzed extensively by different researchers and proposed for several applications. Fig. 2.5(a) is the structural representation of the conventional SRR having circular shape where as Fig. 2.5(b) is its complementary structure usually named as Complimentary Split Ring Resonator (CSRR) [56, 57]. Square shaped SRR (Fig. 2.5(c)) is proposed in 2000 and analyzed later by several researchers [10, 58, 59]. Broadside Coupled SRR (BCSRR) is proposed in order to eliminate the bianisotropic effects of SRR and is widely discussed in literature (Fig. 2.5(d)) [60, 61]. A modified version of BCSRR is proposed where its two rings are separately fabricated on two pieces of same substrate which will have its added advantage of changing the spacing related capacitance (Fig. 2.5(e)) [22]. Another variant of SRR known as Double - sided Split Ring Resonator (DSRR) is made by printing two SRR structures on either sides of the substrate material [62].

Different multiple inclusion metamaterial resonating structures having effective negative permeability are analyzed through equations derived from fundamental principles (Fig. 2.5(f)) [63]. Isotropic split ring resonators having a labyrinth based structure which avoids bianisotropy is presented and later widely analyzed [64, 65]. Multi-ring SRR metamaterial design for multiband metamaterial applications is proposed by Turkmen *et al.* Beana *et al.* introduced another artificial metamaterial structure called spiral resonators which are having smaller electrical size (Fig. 2.5(g)) [66].

Metamaterial SRR structures having triangular shape (Fig. 2.5(h)) is introduced and its effective properties and other characteristics are widely analyzed by Sabah [67, 68, 69]. Omega shaped bianisotropic structures are introduced by Saadoun and Engheta and is called pseudochiral media and is proposed for reciprocal phase shifter [70]. V-shaped conducting strips etched on both faces of a substrate showing negative permeability is proposed and analyzed through numerical simulations by Ekmekci *et al.* [71]. S-shaped

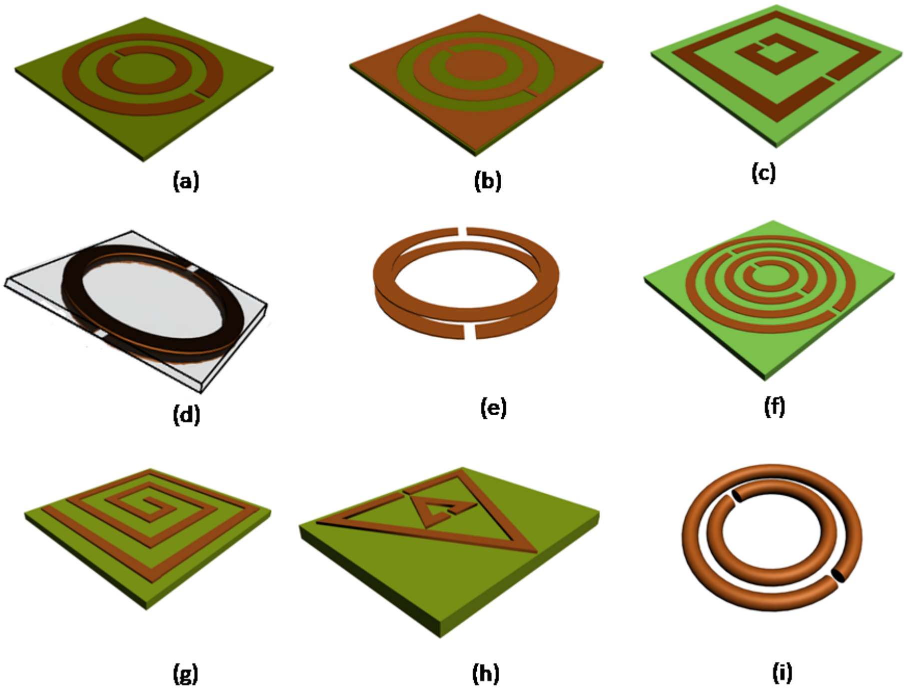

Figure 2.5: Different types of SRR structures.

resonators for negative refractive index is proposed by Hongsheng chen *et al.* [72, 73].

Flexible SRR fabricated on thin adhesive polymer films contributed to tunable resonant structures [74]. Wire SRRs (WSRR) (Fig. 2.5(i)) proposed with very high Q-values provided highly sensitive metamaterial resonating structures. They are having an added advantage of low losses as they are fabricated without using any rigid substrate material [75].

2.2.3 Resonant nature of SRR

A time varying magnetic field applied perpendicular to the surface of the structure produces currents in the ring as implied by Faraday's law (Fig. 2.6). These circulating electric current mimic magnetic dipole. Hence the metallic ring structure becomes magnetically active or show magnetic response when circulating currents are introduced. But due to the discontinuities on the rings produced by the slits, there is a charge distribution with corresponding regions of outer and inner rings possessing opposite charges. The induced charge and current distributions produce capacitance and inductance which make the structure to act as a *LC* resonant circuit. The charge concentration near the split region

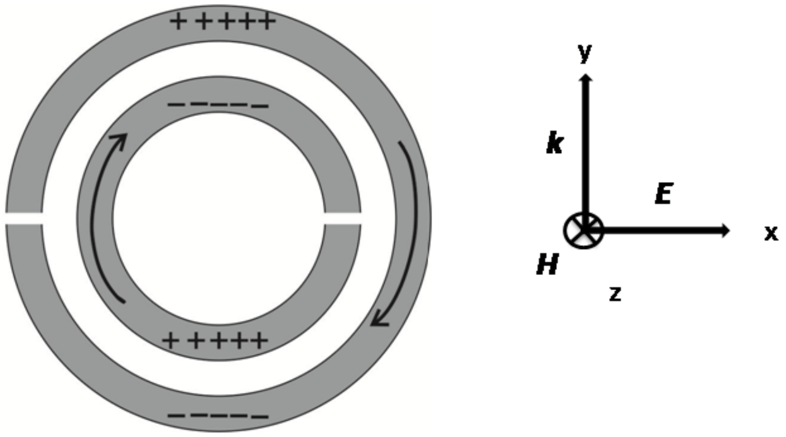

Figure 2.6: Figure of SRR with currents and charges with directions of applied electromagnetic field directions.

also add a small capacitance to the whole structure. Fig. 2.7 represents resonance curve along with the corresponding phase plot of an SRR. The resonant frequency is indicated in the figure. The phase can be seen as undergoing a sudden variation from negative values to positive values around the resonance.

When the applied magnetic field is in z direction, the currents in the two loops have the same direction. The inductance and capacitance produced due to this current produce magnetic polarizability which will lead to negative values of permeability [76]. This causes an inductive-capacitive resonant frequency which is referred to as magnetic resonant frequency. If the electric field is directed in y direction, the induced currents result in charge accumulation leading to electric polarization effect. This polarization produced by the electric field also produces a resonance usually in higher frequency region compared to the magnetic resonant frequency.

2.2.4 Resonant frequency measurements

To measure the resonant frequency of SRR, it should be exposed to an electromagnetic wave of wide frequency range. Frequency corresponding to the resonance is absorbed by the structure which may result in the corresponding change in the transmission curve. For drawing the transmission curve, a microwave source and detector connected to a Vector Network Analyzer (VNA) is used. The SRR can be placed in the applied field in different ways and are presented below.

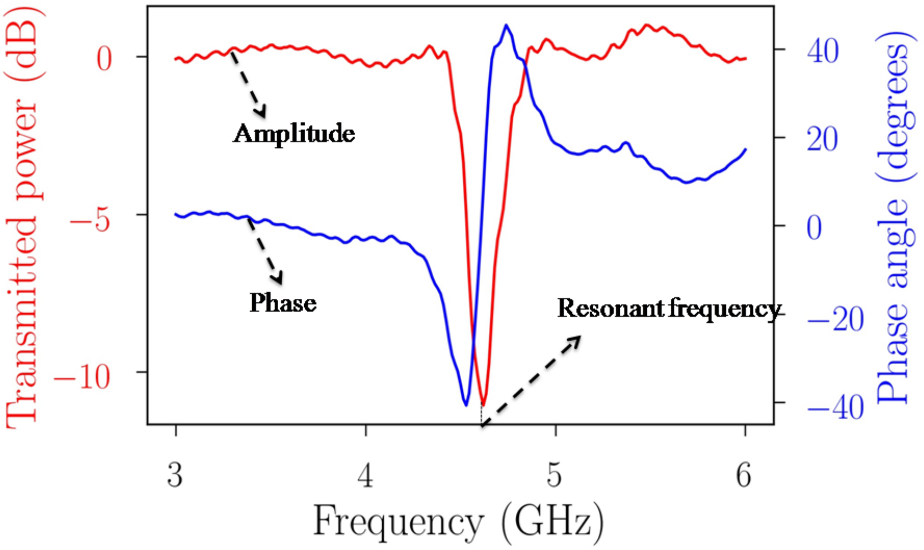

Figure 2.7: Plot showing a resonance curve of SRR along with its phase plot.

2.2.4.1 SRR between transmitting and receiving probes

The measurement of resonant frequency from the transmission curve of Split Ring Resonator structure can be done by placing it between two monopole antennas [77] connected to transmitter and receiver ports of the VNA. Initially the calibration has to be done and then the resonant frequency of SRR can be measured by placing it between the measuring probes.

2.2.4.2 Transmission line method

Microstrip transmission lines loaded with SRR can also be used to analyze the transmission and reflection properties of the resonating structure. For this, the SRR is etched side-by-side to the transmission line so that energy corresponding to the resonant frequency is absorbed by the SRR due to near field coupling [78, 79, 80].

2.2.4.3 Free space method

Transmission properties of bulk structure consisting of periodic array of SRRs can be studied by free space method. For this, two wide band horn antennas are placed on either side of the bulk sample and corresponding spectra is taken [77, 81].

2.2.5 Structural and substrate tunability

It is observed that the structural and substrate parameters determine the resonant frequency of SRR, and it is seen that even a slight variation in these parameters can change the resonant frequency. This finds numerous applications in the fields of sensors, Radio Frequency Identifiers (RFIDs) [32, 82, 83] and Micro Electro Mechanical Systems (MEMS) [84, 85].

Sensitivity in resonant frequency variation of SRR and Double - sided SRR (DSRR) due to the substrate parameter changes have been analyzed using simulations by Ekmekci *et al.* [86]. They showed that DSRR is electrically smaller than SRR. Tunability of effective property (permeability, permittivity or refractive index) of SRRs by varying substrate properties is numerically studied by Sheng *et al.* [87] and showed that effective refractive index can be switched between positive and negative values. Controlling the resonant frequency by varying aspect ratio and substrate thickness of SRRs in THz frequencies is analyzed by Chiam *et al.* [88]. Roy *et al.* studied the tailoring of resonant frequency, bandwidth and permeability of multiple inclusion negative permeability resonating structures [63]. Tuning of transmission characteristics through adjustments of lattice structure is presented by Lapine *et al.* [89]. Weiland *et al.* analyzed the resonant frequency variation of SRRs due to different structural parameters. Loading of varactor diodes and capacitors on SRR is presented as another method for frequency tuning [90, 91].

2.2.6 Equivalent circuit models

SRRs are *LC* resonating structures and can be represented as an equivalent circuit of inductor and capacitor elements. The knowledge of constitutive elements are essential for obtaining the resonant frequency of the SRR. Several researchers have analyzed the properties of SRRs and suggested equivalent circuit models and derived equations for resonant frequency.

Marques *et al.* considered the design formulas for microstrip transmission line and a pair of metallic strips in a dielectric for deriving the expression for capacitance of SRR [61]. They have used the expression for capacitance per unit length (C_{pul}) in terms of phase constant β and impedance Z given as [92]

$$C_{pul} = \frac{\beta}{\omega Z} \tag{2.8}$$

where ω is the frequency of the applied field.

The expression for total inductance is obtained from inductance of single equivalent ring by using variation expression $L = \frac{2U_m}{I^2}$ where $2U_m$ is the magneto static energy and I is the current intensity. Accordingly the inductance is obtained as

$$L = \frac{\mu\pi^2}{I^2}\int_0^\infty [I(k)]^2 k^2 dk \tag{2.9}$$

where $I(k)$ is the Fourier- Bessel transform of the current function on the ring.

Similar method was followed by Baena *et al.* to find an expression for inductance and capacitance of SRR [57]. Fig. 2.8(a) represents the equivalent circuit of SRR predicted by them. The equations presented in these works involved a lot of complex mathematical functions and is not in direct terms of structural parameters of SRR. Here the equation for capacitance is derived by considering only the capacitance of one surface of the SRR.

A novel theoretical equivalent circuit model (Fig. 2.8(b)) for SRR structure is proposed based on the geometry and the distribution of electric charge and current by Wu *et al.* [93, 94]. The expressions are derived using quasi-static approach for capacitance and inductance by considering the SRR as a transmission line segment. They have considered the resistors, capacitors and inductors of both the rings in terms of structural parameters. Numerical simulation is used to verify the derived expression.

Equivalent circuit model for square SRR is presented by considering each side of the SRR as individual inductors (Fig. 2.8(c)) [95]. Equation of inductance of two coplanar current sheets is taken with a correction applied to incorporate the presence of the slit [96]. The expression for capacitance is derived using the same concept as considered by Wu *et al.* [93, 94]. The expressions are verified using numerical simulations.

Another modeling of SRR based on an equivalent circuit (Fig. 2.8(d)) is done where capacitance and inductance are determined from geometric parameters [97]. An analytical study is proposed to determine different components of the equivalent circuit values. Validation of the proposed approach is done by considering mutual capacitance of two halves and gap capacitance.

An approximate expression is derived for the resonant frequency of a single Split Ring Resonator by Sydoruk *et al.* [98]. Equivalent circuit for SRR fabricated using coplanar wave guide technology is proposed by Rogla *et al.* [99].

A SRR calculator software has been developed by Pradeep *et al.* using a genetic algorithm [55]. Genetic algorithm is a numerical optimization method involving some approximations through which they have devised a method to predict the SRR parameters for a desired resonant frequency.

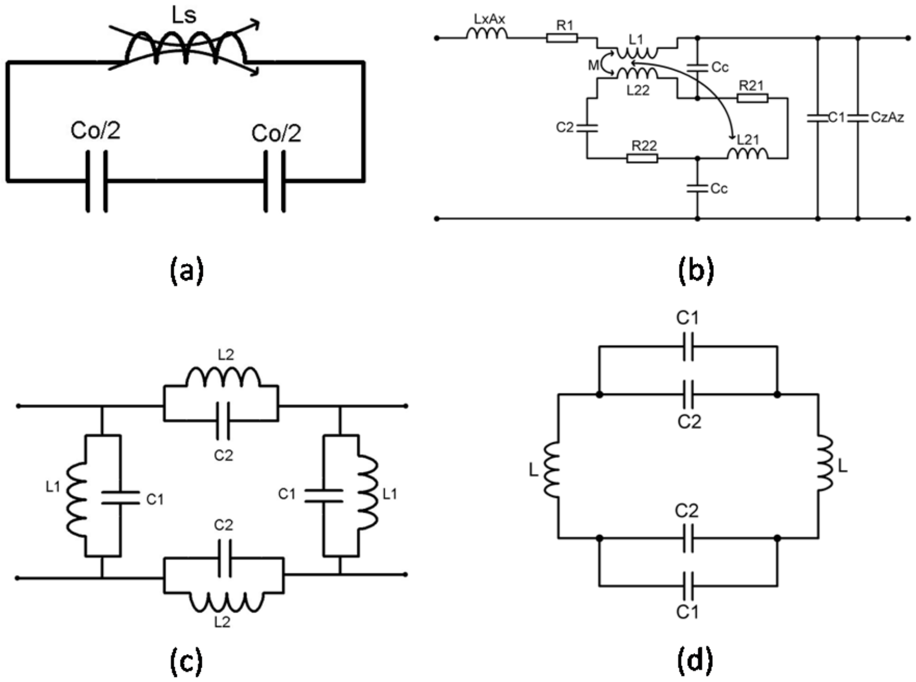

Figure 2.8: Different equivalent circuits of SRR proposed in literature.

2.2.7 Sensing applications of SRRs

Negative permeability metamaterial resonating structures, especially SRRs, are widely used for various applications due to their tunable resonance nature [74, 100]. Light weight, low cost, compactness, accuracy and sensitive properties make them suitable candidate for several sensing applications.

Displacement sensing using different SRR structures have been widely studied in literature. Transmission line loaded BCSRR and diamond shaped tapered SRR are used for alignment and displacement sensing by Horestani *et al.* [101, 102]. Rotation sensors using metamaterial inspired structures are also analyzed by Horestani *et al.* [103] and Ebrahimi *et al.* [104]. Ozbay *et al.* presented structural and health monitoring system using nested SRRs which can detect sub-micron displacements [105].

Proximity sensors are also investigated using the variations in the electric field confined at the gap of Split Ring Resonators. Proximity of a metallic object is measured using SRR and CSRR by Von Detten *et al.* [106]. A flexible probe working at very low frequencies which can detect proximity of any kind of material is presented by Zhang *et al.* [107].

Several other types of sensors like strain sensor, pressure sensor, temperature sensor, movement sensor and dielectric sensor are realized using SRRs [21, 23, 24, 108, 109].

2.2.7.1 Dielectric sensing and measurements

Dielectric sensing and measurements using SRRs have become another important field of application.

These sensors have also found many applications in material characterization studies. Permittivity and thickness measurement of solid dielectrics are done using transmission line based CSRR with the help of a calibration curve drawn using known dielectric samples [110]. Rusni *et al.* presented a dielectric sensing using transmission line loaded rectangular multiple SRR having centered gap and also aligned gap [111]. A complex permittivity measurement technique using triple Complimentary Split Ring Resonator is proposed by Hsu *et al.* [112]. Triple Complimentary Split Ring Resonator is also used for complex permittivity and thickness measurement by Yang *et al.* [113].

Complimentary Split Ring Resonators are presented as dielectric measurement sensors by Boybay *et al.* [114]. A comparison of sensitivity of SRR and CSRR is done and CSRR is found to be more sensitive. By measuring the resonant frequency and transmitted power of CSRR loaded microstripline, dielectric constant and loss tangent are calculated and presented [115]. Permittivity and thickness are shown to be measured simultaneously using CSRR having two distinct resonant frequencies by Lee *et al.* [116]. CSRR with two resonant frequencies is also used for thickness and permittivity measurement of multilayered dielectric materials [117]. CSRR is also used to determine complex permittivity of dielectric material by non-invasive method and have presented the results both numerically and experimentally [118]. A numerical study of permittivity measurement of anisotropic and lossy medium like carbon fiber reinforced polymer is done by Yilmaz *et al* using CSRR [119]. Ebrahimi *et al.* used a single CSRR coupled to a microstrip line to measure the dielectric values of different liquids and hence used it as a microfluidic sensor [80]. Double Sided Spiral SRR is used for the dielectric measurement of FR-4 boards and liquid mixtures by Benkhaoua *et al.* [120, 121]. In most of these works, the unknown values are extracted from a calibration curve drawn with the help of known values.

Dielectric constant measurement of organic liquids with the help of self sustained microwave system using SRR is presented in the works by Sekar *et al.* [122, 123]. A SRR based submersible sensor is designed and used for characterization of thin films, solids and liquids by Romera *et al.* [124]. Here expressions are derived from simulation results to find out the unknown permittivity of materials. Hexagonal shaped CSRR is used for complex permittivity measurement by employing empirical relations [125].

2.3 SRR fabrication and measurement methods used for the present study

The present study is aimed at determining the dielectric parameters by using SRRs as a dielectric sensor. The fabrication methods and novel dielectric measurement techniques proposed are briefly presented in the following sections.

2.3.1 SRR structure used

The SRRs used for the study in this thesis is of circular structure. Some typical SRRs fabricated are shown in Fig. 2.9. The Fig. 2.9(a) shows SRRs of different dimensions fabricated on FR4 circuit board whereas Fig. 2.9(b) gives SRRs fabricated on thin flexible polymer film.

2.3.2 Fabrication methods adopted

For the fabrication of SRRs on FR board, photochemical etching method and printing using milling method are used. For making SRRs on flexible polymer film direct printing technique is employed.

2.3.2.1 Photochemical etching method

The photochemical etching method described in the section 2.2.1.1 is used for fabrication of SRRs on solid substrate material. Figure 2.10 represents the process flow of the method followed. Initially photo mask is prepared and photo-resist is coated on the laminate using a dip coating machine. After exposing to ultraviolet (UV) rays, the laminate is etched using ferric chloride to get the required SRR structure.

2.3.2.2 Printing using milling method

The milling method described in section 2.2.1.2 is also used for fabricating SRRs. Though there is a limitation to the minimum dimension possible for milling gap in relation to the mill size, the edge perfection of SRR is comparatively better than the chemical etching.

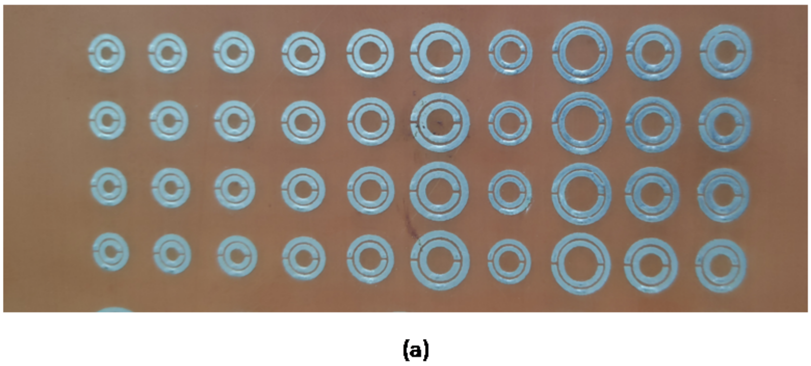
(a)

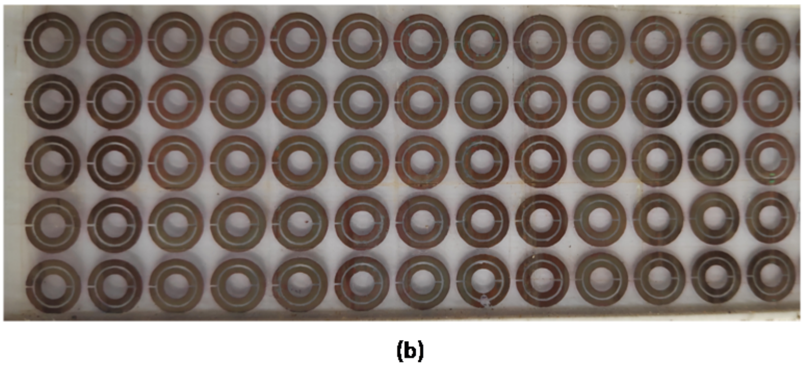
(b)

Figure 2.9: (a) SRRs of various dimensions fabricted on FR4 board (b) and on thin polymer film.

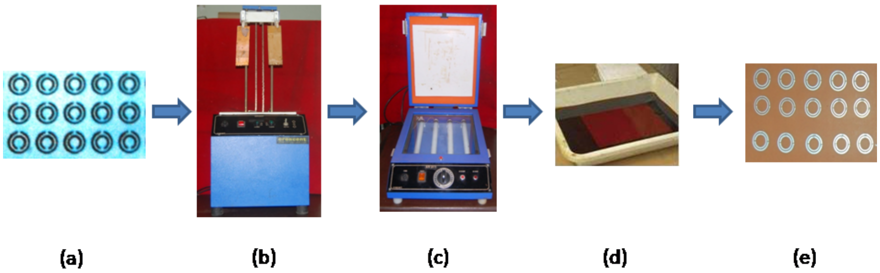
(a) (b) (c) (d) (e)

Figure 2.10: Flow diagram representing the various steps of photo chemical etching method (a) Printing of photomask (b) Dip coating unit (c) UV exposure (d) Etching in ferric chloride (e) Split Ring Resonators printed on circuit board.

Figure 2.11: Flow diagram representing the various steps of direct printing method.

2.3.2.3 Direct Printing method

Direct printing method for SRR fabrication is an easy and less time consuming method with less number of steps. Figure 2.11 gives a flowchart representing different steps of direct printing we have adopted. Initially, the structure to be printed is drawn using any drawing software employing computer. After affixing on an adhesive polymer film to one side of a thin copper sheet of 20 μm thickness having suitable area, the design is printed directly on the other side using a laser-jet printer connected to the computer. Since the printing is on thin copper film, instead of usual paper, adequate care is taken during printing. This sheet is then dipped in the ferric chloride solution for sufficient time which removes the copper from the region leaving SRR patterns. Thus the required SRR structure, will remain on the adhesive polymer sheet which will act as the substrate. The distinct advantage of this method is that, SRRs with flexible substrates can be fabricated in an easy manner [74].

2.3.3 Samples used for the study

Solid samples used for the study are glass, perspex and plastic. For analyzing the permittivity of circuit board materials, flame retardant laminates are used (FR2, FR3 nd FR4). With the intention of quality check of the food materials, powders of different pulses and cereals (wheat, corn, rice etc.) are used. Wax samples (paraffin wax, bran wax and bees wax) having uses in cosmetic and industrial applications are also employed in the study. Photographs of some selected samples are given in Fig. 2.12.

2.3.4 Resonant frequency measurement setup

The main method adopted for resonant frequency related measurement is the one with the transmitting and receiving probes connected to the VNA as detailed in section 2.2.4.1. Schematic representation and photograph of the measurement test probe are given in Fig.

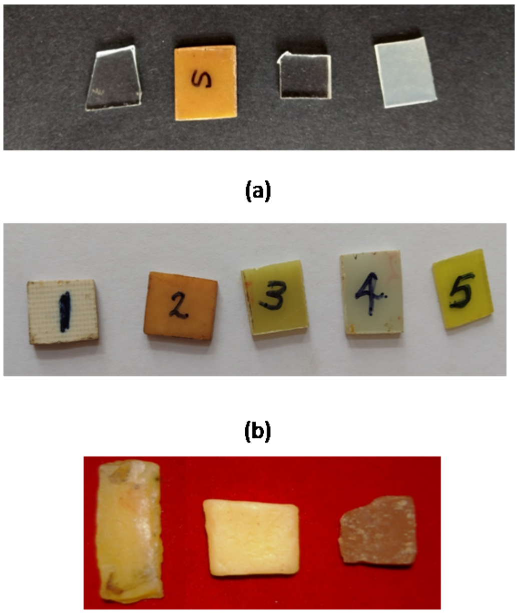

(a)

(b)

(c)

Figure 2.12: Photos of (a) Solid samples, (b) FR laminates and (c) Waxes used for the permittivity studies.

2.13.

Solid samples are prepared having same area as that of the SRR surface area and thickness grater than $c + d/2$ where c and d are width of the ring and gap between the rings of SRR respectively. Solid samples are placed directly over the SRR for resonant frequency measurements. The powdered samples and wax samples are placed in a sample holder made of transparent polymer sheet with no bottom phase. This ensures that the sample is in contact with the SRR. Photograph of wax sample placed in the sample holder on the surface of SRR is shown in the Fig. 2.14.

2.3.4.1 Temperature controlled measurement

One of the aims of the thesis is to analyze the permittivity variations with respect to the temperature. To study the temperature dependence of the complex permittivity of the test samples, suitable experimental setup to maintain and measure the temperature of the sample is to be prepared. For uniform heating of the sample, the SRR-antenna setup is placed inside a thermally insulated box made up of wood of dimensions 30 cm × 30 cm × 30 cm, and having a provision to place an infrared lamp which provide heating. Temperature measurements are done using a digital thermometer having a long metallic

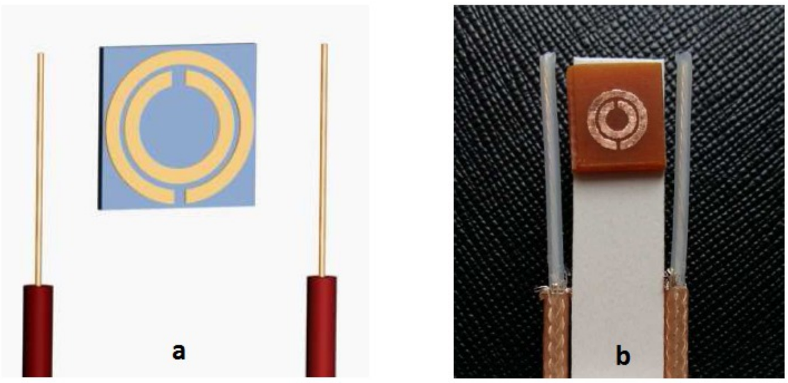

Figure 2.13: (a) Schematic representation and (b) photograph of the SRR test probe.

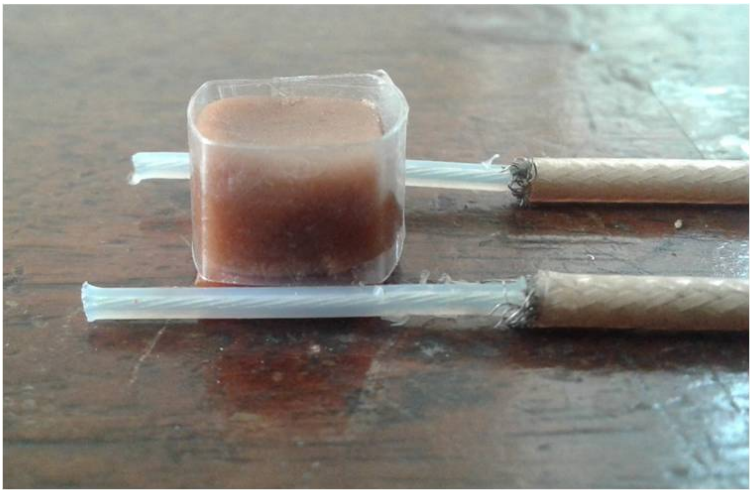

Figure 2.14: Wax sample taken in a sample holder and placed on the SRR arranged between transmitting and receiving probes.

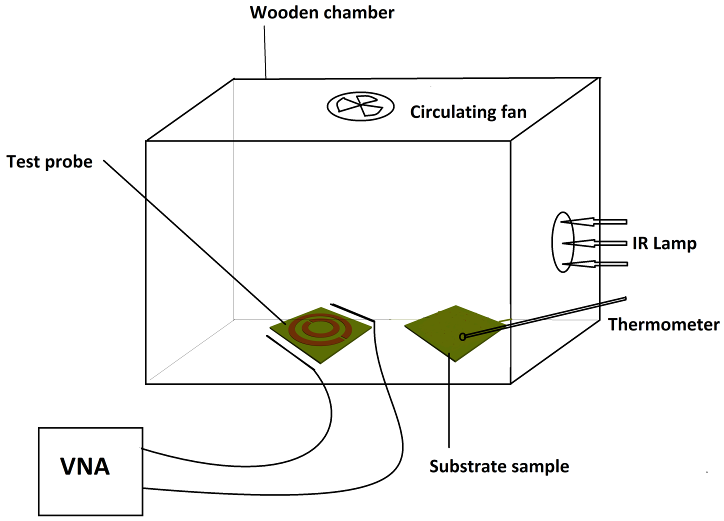

Figure 2.15: Schematic representation of measurement setup for the temperature dependent permittivity measurement.

sensor probe (with thermocouple used for measurement) which is preferred over mercury thermometer. Digital thermometer responds to sudden variations in temperature and hence is more sensitive where the readings are accurate up to 2 decimals. For accurate measurement of temperature a substrate sample is placed inside the temperature controlled box to which the thermometer tip is attached. This is done since the insertion of thermometer probe may affect the electric field distribution of the original test probe which in turn may alter the readings.

2.3.5 Simulation techniques

Simulations are used to verify the experimental results. High Frequency Structure Simulator (HFSS) is used for the same. The transmission properties are analyzed and the resonant frequencies are obtained for selected structures.

Chapter 3

Formulation of Resonant Frequency of SRR

This chapter mainly aims at deriving an equation for resonant frequency of Split Ring Resonator (SRR) in terms of the capacitance and inductance. The expression for capacitance is derived by analyzing the electric field distribution on both surfaces of SRR. SRRs of different dimensions are used to measure the resonant frequencies. The resonant frequencies of these SRRs are calculated using the derived equations. Numerical simulation is then used for resonant frequency measurements. The results using equations, experiments and simulations are compared in this chapter.

Finding an expression for the resonant frequency of the SRR is important when we have to optimize the structural parameters for desired resonant frequency for specific applications. An equivalent circuit model helps to find the expressions for capacitance and inductance in terms of the structural parameters.

In the previous chapter, different approaches to find expression for inductance and capacitance presented in literature are discussed. The equivalent circuit models proposed in these works are also discussed. In this chapter a more accurate expression for capacitance and that of the resonant frequency of SRR are derived. The effective capacitance is derived by using the basic principles of parallel plate capacitor. After considering the presence of electric field lines on both upper and lower surfaces of the SRR, which was not taken into account in previous works, the equation for capacitance is modified. The equation for inductance is taken from literature. A new equivalent circuit model is proposed based on the distribution of capacitance and inductance of the SRR. The validity of the derived equations are also verified using experiments and simulations.

3.1 Theoretical formulation of resonant frequency of SRR

An alternating magnetic field can produce a capacitive inductive resonance in SRR and the resonant frequency (f) is expressed as

$$f = \frac{1}{2\pi\sqrt{LC}} \tag{3.1}$$

where L is the effective inductance and C is the effective capacitance.

3.1.1 Field distribution near SRR

Since the SRR metalization is in the form of thin sheets, it is reasonable to imagine that charges are equally distributed on both upper and lower surfaces of the SRR and hence the fringing electric field distribution may be similar on both sides. The expected field and charge distribution of the SRR are shown in Fig. 3.1. To find the total capacitance of the SRR, an equivalent capacitive circuit is considered. The total capacitance of SRR can be considered as a combination of four capacitors, two on upper surface and two on lower surface of SRR. The two capacitors on upper surface are in series connection which are in parallel with capacitors in lower surface as shown in Fig. 3.2. If capacitances are

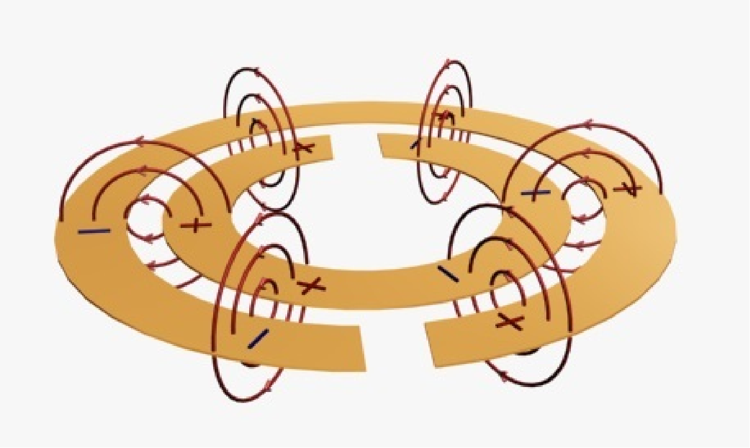

Figure 3.1: The schematic representation of the electric field and charge distribution on both surfaces of the SRR.

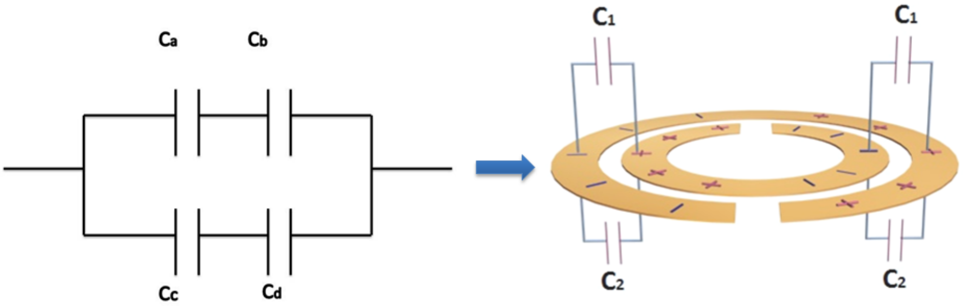

Figure 3.2: Equivalent representation of capacitance $C_1(C_a = C_b)$ and $C_2(C_c = C_d)$ on upper and lower surfaces of SRR.

C_a, C_b, C_c and C_d, the total capacitance is

$$C_{tot} = \frac{C_a + C_b}{2} + \frac{C_c + C_d}{2} \tag{3.2}$$

Capacitances C_a and C_b will be same, as the dielectric medium is same for both of the capacitors, and can be represented as C_1. Similarly the capacitances at the other side C_c and C_d will be equal and can be represented as C_2. A schematic diagram of such a distribution of capacitances is also shown in Fig. 3.2.

3.1.2 Experimental confirmation of field distribution

The experimental verification in the presence of the field and its contribution to the capacitance on both surfaces of the SRR is done by using a SRR (r = 2 mm, c = 1 mm and d = 0.1 mm) fabricated on a thin polymer film [74]. For this a copper sheet of 20 μm thickness is fixed on an adhesive polymer film of thickness 18 μm and the SRR structure is fabricated on it using direct printing method. The fabrication procedure is explained in the previous chapter. A piece of the same polymer film is fixed on the other side of the SRR for the structure to be symmetric. Accordingly, the small capacitive contribution due to the thin polymer films on both sides of the SRR will be the same. In fact, the effect of the polymer films on both sides can be neglected due to their small thickness. Resonant frequency of this structure is measured to be 4.14 GHz. A dielectric sheet of permittivity 2.45 and thickness 1.52 mm is fixed on one side of the SRR, which shifts the resonant frequency to 3.75 GHz. The corresponding shift in the resonant frequency is 0.39 GHz. Another piece of the same material with same thickness is then placed on other side of the SRR and the resonant frequency is further shifted by 0.36 GHz to 3.39 GHz. Fig. 3.3 shows these shifts in resonant frequency [27].

The experiment is repeated using another SRR fabricated on polymer film with a resonant frequency of 4.86 GHz and by using circuit board laminates of permittivity 2.5 and 2.9 and similar results are obtained. For sample of permittivity 2.5 the shifts obtained are 0.82 GHz and 0.83 GHz respectively when dielectric is placed on either sides of the SRR (Fig. 3.4). For sample of permittivity 2.9 the shifts in resonant frequency obtained are 0.76 GHz for both the cases (Fig. 3.5). Almost equal shifts in resonant frequency again verifies the presence of equal field distribution both on the upper and the lower surfaces of the SRR.

The effective capacitance of the SRR must therefore include the contribution from both sides of the SRR. After considering this contribution to evaluate the effective capacitance of the structure, the dielectric constant of various materials in relation to the resonant frequency of the SRR are calculated. When calculating the effective capacitance of SRR, the electric field on both sides - which is a major contribution - has to be considered, which was not done in earlier attempts. This important modification has resulted in reducing the error in calculating the resonant frequency of SRR considerably as will be shown in this chapter.

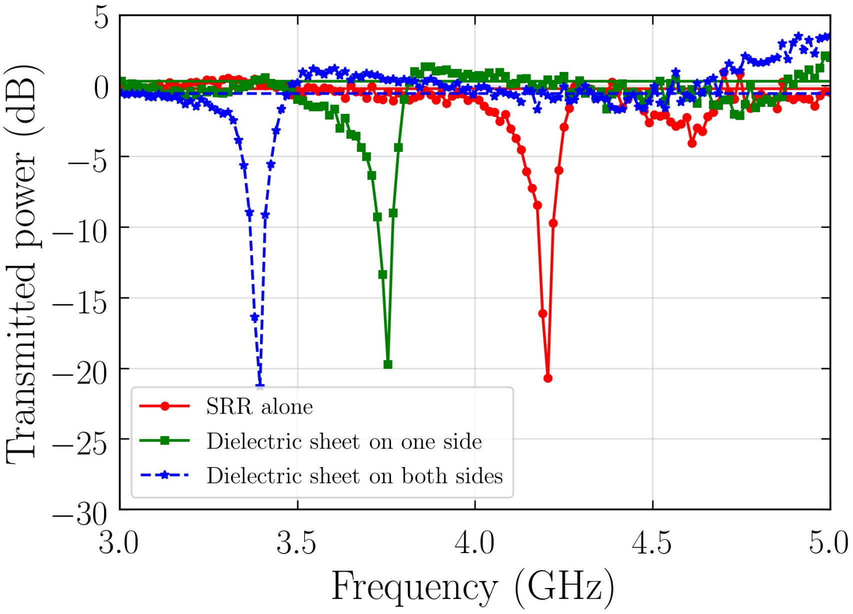

Figure 3.3: Transmission curves showing nearly equal shifts in resonant frequency when similar dielectrics of permittivity 2.45 are placed on both surfaces of the SRR.

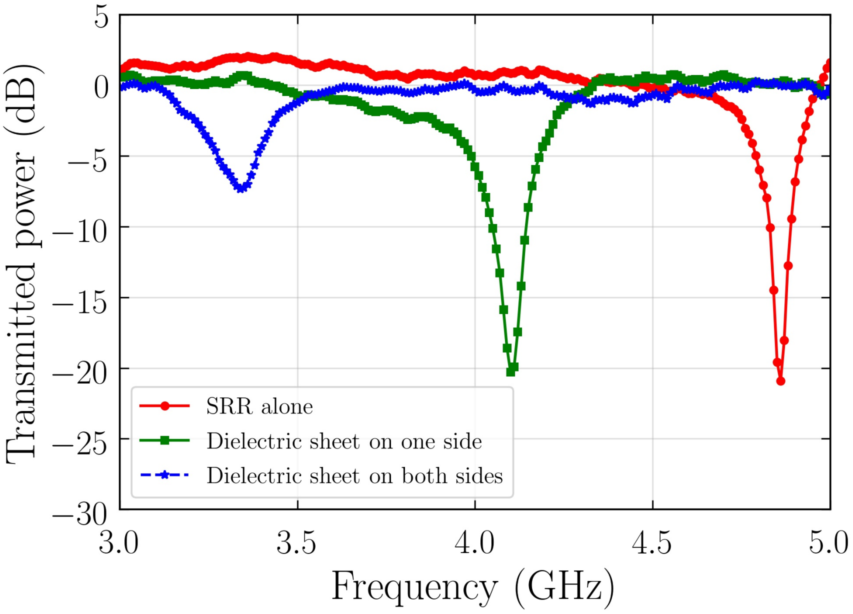

Figure 3.4: Transmission curves showing nearly equal shifts in resonant frequency when similar dielectrics of permittiviy 2.5 are placed on both surfaces of the SRR.

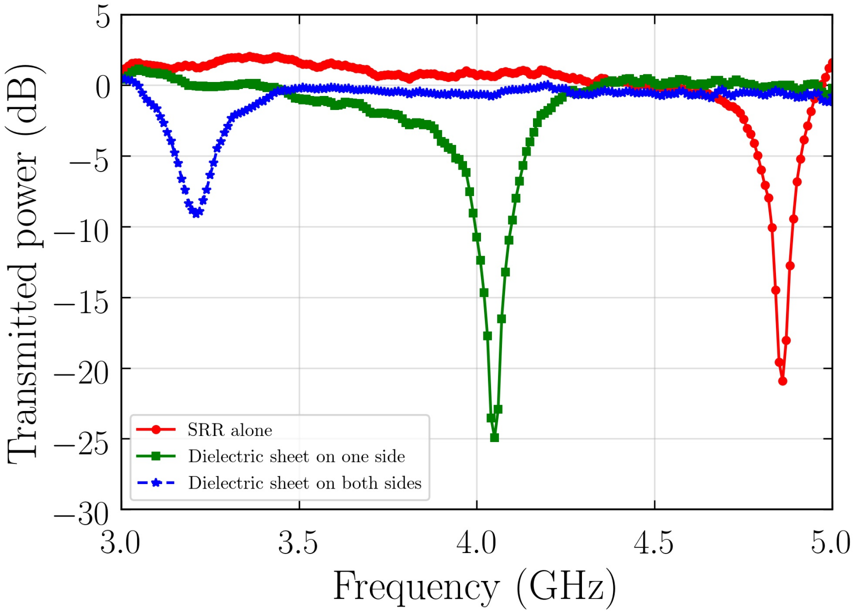

Figure 3.5: Transmission curves showing nearly equal shifts in resonant frequency when similar dielectrics of permittiviy 2.9 are placed on both surfaces of the SRR.

3.2 Derivation of effective capacitance of SRR

The presence of charge and electric field distribution on both surfaces of SRR was verified in the previous section. Although the electric field between the two rings is fringing electric field as shown in Fig. 3.1, it can be considered as analogous to a parallel plate capacitor. In literature, the capacitance of SRR was derived using variational expressions from electrostatic energy equations which included complex special functions and are tedious for calculations [57]. Transmission line equations are also used to find the expressions for capacitance [92].

To find the capacitance of a SRR, the parallel plate approximation is used. We consider two coplanar conductor strips of width c and length $2\pi a$ (where a is the average radius of the two rings = $r_{in}+c+\frac{d}{2}$) and are separated by a distance d (Fig. 3.6 and Fig. 3.7). Consider two parallel plate small strips on each planar conductors with width dr. Consider them as two conductors of capacitance with separation πr where r is the radius of the semicircle (representing the electric field lines) connecting the two sheets. The equation for parallel plate capacitor is

$$C = \frac{A\varepsilon_0}{d} \tag{3.3}$$

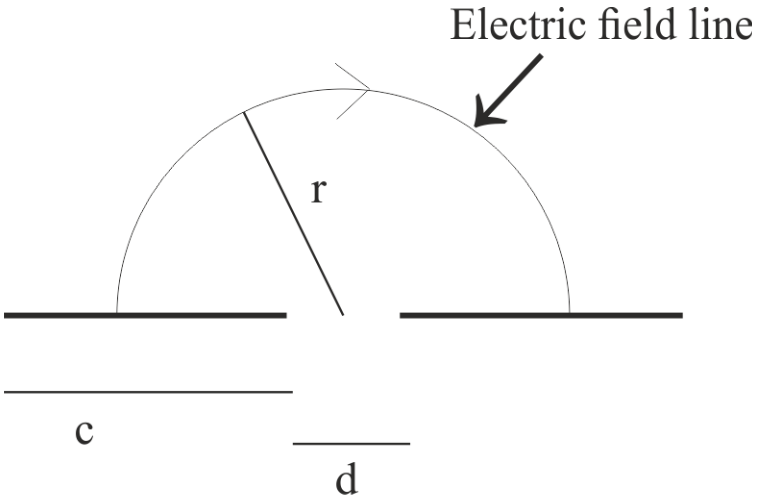

Figure 3.6: Cross sectional view of the streched SRR showing the electric field line.

where A is the area and d is the distance between them. Substituting the corresponding terms of the parallel strips, the capacitance becomes

$$C = \frac{2\pi a \varepsilon_0 dr}{\pi r} \tag{3.4}$$

The total capacitance of the conductor strip can be found out by integrating through out the width of the strips (*c*), where *r* becomes variable distance between each small capacitors. For this, the limits of the integral are *d/2* and *c+d/2*, as obvious from the figure. Then the equation becomes

$$C = \int_{d/2}^{c+d/2} \frac{2\pi a \varepsilon_0 dr}{\pi r} \tag{3.5}$$

The capacitance per unit length C_{pul} is obtained by dividing the above equation by *2πa* [27].

$$C_{pul} = \frac{\varepsilon_0}{\pi} \int_{d/2}^{c+d/2} \frac{dr}{r} \tag{3.6}$$

$$C_{pul} = \frac{\varepsilon_0}{\pi} ln \frac{2c+d}{d} \tag{3.7}$$

This is almost same as the equation for capacitance per unit length given in Pendry *et al.* [9].

Now, the total capacitance of one of the four capacitors of the equivalent circuit is $C_0 = \pi a C_{pul}$. If there is no substrate on both sides, all four capacitors are same and is equal to C_0. Hence total capacitance on upper side due to the parallel combination of two

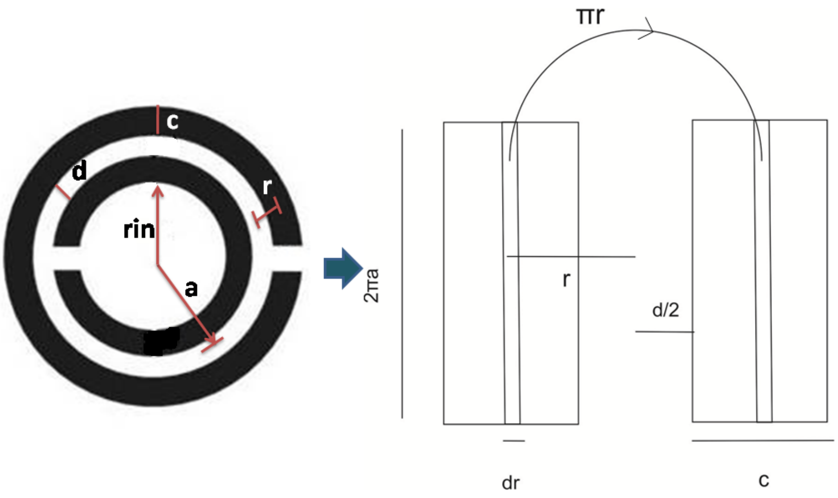

Figure 3.7: (a) Schematic representation of SRR showing average radius *a*, and spacing between rings *d* and variable for integration *r* (b) Approximated streched representation of SRR into two coplanar conducting sheets showing different parameters.

C_0 is $\frac{C_0}{2}$. Considering the contribution from both surfaces, the total capacitance of the SRR will be $\frac{C_0}{2}+\frac{C_0}{2}$ giving C_0. Therefore the total capacitance of the SRR is

$$C_{tot} = \pi a \frac{\varepsilon_0}{\pi} ln \frac{2c+d}{d} \tag{3.8}$$

If the SRR is fabricated on a dielectric substrate, the expression for capacitance of that surface includes dielectric constant contribution ε_{r1} also and is given as

$$C_{tot} = (1+\varepsilon_{r1})\pi a \frac{\varepsilon_0}{2\pi} ln \frac{2c+d}{d} \tag{3.9}$$

If the same dielectric material of same thickness is placed on the other side of the SRR, the total capacitance changes as,

$$C_{tot} = \varepsilon_{r1}\pi a \frac{\varepsilon_0}{\pi} ln \frac{2c+d}{d} \tag{3.10}$$

Instead of the same dielectric, if a material of different dielectric constant is placed on the other side, the total capacitance becomes,

$$C_{tot} = (\varepsilon_{r1}+\varepsilon_{r2})\pi a \frac{\varepsilon_0}{2\pi} ln \frac{2c+d}{d} \tag{3.11}$$

A small correction to the equation is applied in order to include the effect of curvature of the rings and the non uniformity of charge distribution and the equations 3.9 and 3.11 become

$$C_{tot} = (\varepsilon_{r1} + 1)\pi(a + \frac{d}{2})\frac{\varepsilon_0}{2\pi} ln\frac{2c + d}{\frac{d}{2}} \tag{3.12}$$

$$C_{tot} = (\varepsilon_{r1} + \varepsilon_{r2})\pi(a + \frac{d}{2})\frac{\varepsilon_0}{2\pi} ln\frac{2c + d}{\frac{d}{2}} \tag{3.13}$$

where average radius a is extended by adding a small contribution $\frac{d}{2}$. Similarly, d is replaced by $\frac{d}{2}$ in the denominator of the logarithmic term. This is for reducing the possible error which may occur due to fringing effects during the stretching process of circular SRR into straight conductors. By this assumption, almost perfect matching is obtained with experimental and simulation results which are discussed in the last part of this chapter.

3.3 Expression for inductance

The expression for inductance of SRR has been derived by different researchers by using different methods. Some of the expressions are derived using variational methods based on magnetostatic energy and include special functions like Struve and Bessel functions [57, 61]. Inductance of spiral and multiple SRR are also derived from the expressions given by Mohan [96].

In calculating the resonant frequency of SRR, the self inductance of both of the rings and the mutual inductance between the rings are considered. Here the expression for self inductance of circular current sheet and mutual inductance between two concentric circular current sheets which are derived by Mohan [96] starting with the expression of inductance between two circular filaments are taken. The derived expression for self inductance of a circular current sheet (Fig. 3.8) and for the two rings of different dimensions are

$$L_1 = \frac{\mu s_1}{2}[ln(\frac{s_1}{c_1}) + 0.9 + 0.2(\frac{c_1^2}{s_1^2})] \tag{3.14}$$

$$L_2 = \frac{\mu s_2}{2}[ln(\frac{s_2}{c_2}) + 0.9 + 0.2(\frac{c_2^2}{s_2^2})] \tag{3.15}$$

where, c_1 and c_2 are width of each rings of SRR and s_1 and s_2 are average diameter of the

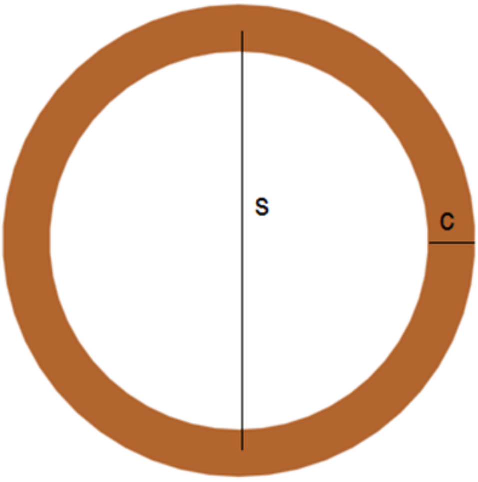

Figure 3.8: Schematic representation of a single flat metallic ring considered to derive expression for self inductance.

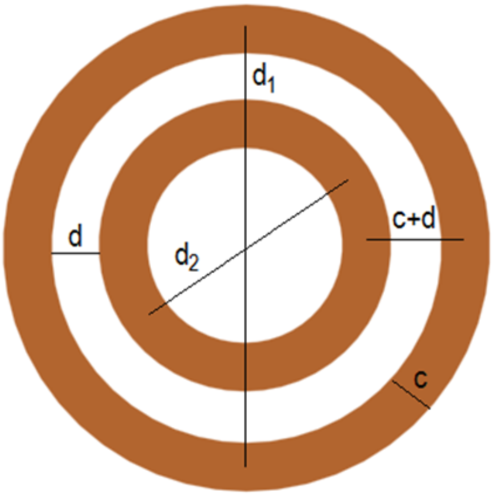

Figure 3.9: Schematic representation of two concentric flat metallic rings considered to derive expression for mutual inductance along with the dimensional parameters.

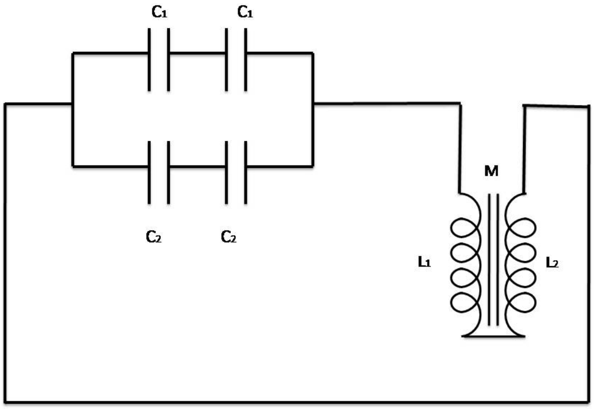

Figure 3.10: The proposed equivalent circuit of SRR.

corresponding rings.

The mutual inductance between two concentric circular current sheets is calculated using Neumann double integral method and is expressed as

$$M = \frac{\mu s}{2}[ln(\frac{1}{\rho}) - 0.6 + 0.7\rho^2 + (0.2 + \frac{1}{12\rho^2})\frac{c^2}{s^2}] \tag{3.16}$$

where $\rho = \frac{c+d}{s}$ and $s = \frac{d_1+d_2}{2}$ with d_1 and d_2 are average diameters of the inner and outer rings respectively (Fig. 3.9).

3.4 Resonant frequency

The expression for resonant frequency given in Eqn. 3.1 is modified by considering the derived expression for the total capacitance and the self and mutual inductances of the two rings. The modified expression for the resonant frequency of the SRR is given as

$$f = \frac{1}{2\pi\sqrt{(L_1 + L_2 - 2M)C_{tot}}} \tag{3.17}$$

where the self inductances are given by Eqns. 3.14 and 3.15 and mutual inductance by Eqn. 3.16. The equation for total capacitance are given by the derived Eqns. 3.12 and 3.13. Hence, the final equation for the resonant frequency with and without sample will have the form

$$f = \frac{1}{2\pi\sqrt{(L_1 + L_2 - 2M)((\varepsilon_{r1} + 1)\pi(a + \frac{d}{2})\frac{\varepsilon_0}{2\pi}ln\frac{2c+d}{\frac{d}{2}})}} \tag{3.18}$$

$$f = \frac{1}{2\pi\sqrt{(L_1 + L_2 - 2M)((\varepsilon_{r1} + \varepsilon_{r2})\pi(a + \frac{d}{2})\frac{\varepsilon_0}{2\pi}ln\frac{2c+d}{\frac{d}{2}})}} \tag{3.19}$$

This analytical expression for resonant frequency is verified experimentally and through numerical simulations.

The equivalent circuit of the SRR in terms of total capacitance C_{tot} and effective inductance can be represented by Fig. 3.10.

3.5 Verification through experiments and simulations

The expressions derived for capacitance (Eqn. 3.12) and hence the resonant frequencies (Eqns. 3.18) are verified using experiments and also using numerical simulation. For experimental verification, SRRs of different dimensions are used. Their resonant frequencies are measured by placing them between transmitting and receiving probes of the VNA and the photograph of the experimental set up is given in Fig. 3.11.

The resonant frequency of SRR for a particular dimension obtained by experiment is calculated using the derived expression (Eqn. 3.18). Simulation using Ansoft HFSS software is also used for validation of the derived equations (Fig. 3.12). The values obtained for SRRs of different dimensions using the analytical equation along with their corresponding measured and simulated values are given in Table 3.1. Typical resonance curves obtained from experiment, simulation and the calculated resonant frequency for SRR of structural parameters with r_{in}=1.6 mm, *c*=0.9 mm , *d*=0.4 mm is given in Fig. 3.13.

The Eqn. 3.19 is verified using experiments and simulation for SRR with dielectric samples in contact with them. A schematic representation of the sample placed over the test probe is given as Fig. 3.14. Two different SRRs and six different dielectric samples are selected for analysis. The samples are placed in contact with the SRR and then the resonant frequencies are obtained using experimental and simulation methods and are also calculated using the derived equation. Dimensions of selected SRRs, permittivity of substrate and samples are given in the Table 3.2. The resonant frequencies obtained using the three methods are presented in Table 3.2 for comparison. It is quite obvious from Tables 3.1 and 3.2 that there is a strong agreement between the obtained value of resonant frequency using the derived equation with the experimental and simulation results.

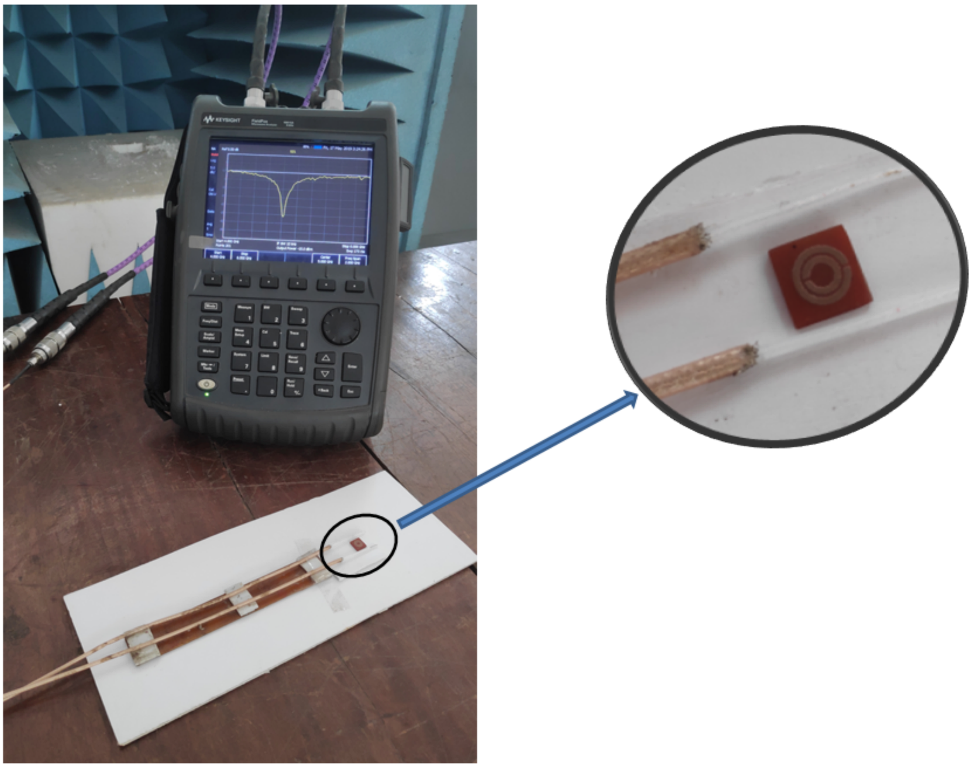

Figure 3.11: Photograph of the experimental setup along with the magnified view of the test probe.

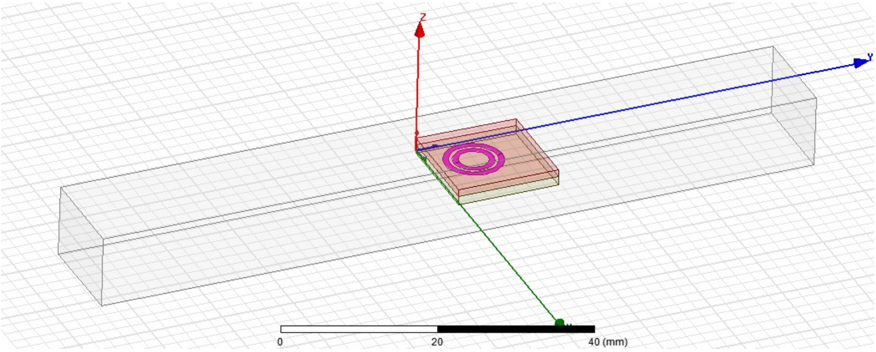

Figure 3.12: HFSS design with sample placed on the SRR test probe.

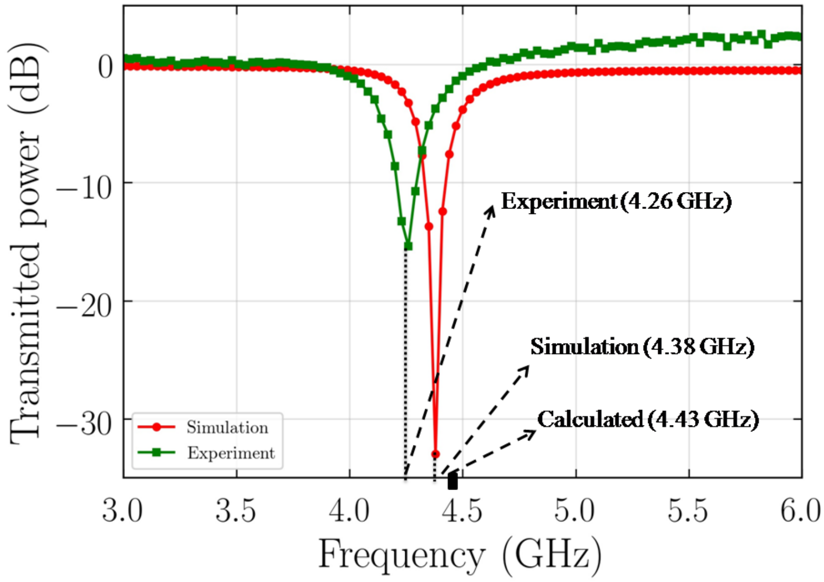

Figure 3.13: Resonance curves obtained from experiment and simulation for SRR of structural parameters r_{in}=1.6 mm, c=0.9 mm, d=0.4 mm. The resonant frequencies from experiment, simulation and calculation are also given.

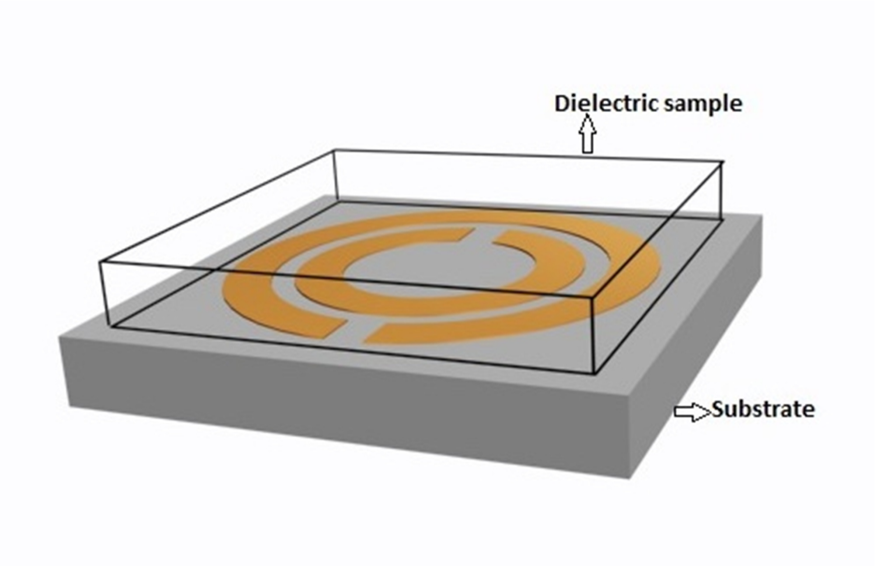

Figure 3.14: Schematic representation of SRR test probe and the dielectric sample placed over it.

Table 3.1: Resonant frequencies of SRR structures obtained from experiment, simulation and numerial calcultion.

			Resonant frequency f_0		
r_{in}	c	d	**Measured**	**Simulated**	**Calculated**
1.0	0.60	0.4	5.697	5.88	5.81
2.0	0.75	0.5	3.456	3.52	3.52
1.3	0.65	0.4	4.926	4.95	4.87
1.6	0.90	0.4	4.26	4.38	4.43
1.6	1.10	0.2	3.8	4.08	4.03
1.625	0.68	0.4	4.317	4.23	4.19
1.8	0.90	0.2	4.0	4.1	4.10
2.4	0.90	0.2	3.1	3.24	3.38

Table 3.2: Comparison of resonant frequencies of SRR structures with dielectric samples placed on its surface obtained from experiment, simulation and numeric calculation.

			Permittivity ε		**Resonant frequency f_0**		
r_{in}	c	d	**Substrate**	**Sample**	**Measured**	**Simulated**	**Calculated**
2.0	0.75	0.5	3.56	2.124	3.09	3.1	3.164
				2.471	3.009	3.02	3.071
				3.571	2.402	2.5	2.454
1.0	0.6	0.4	3.56	2.310	5.02	5.21	5.139
				2.574	4.911	5.13	5.027
				3.554	4.56	4.725	4.668

3.6 Conclusion

After establishing the existence of equal electric field distribution on both sides of SRR metalization by experimental verification, a new expression for the capacitance of SRR is derived. In view of this, the expression for resonant frequency of the SRR fabricated on a substrate is modified. The required changes needed when another dielectric in the form of a sample is placed near to SRR test probe is also investigated. The obtained equations are validated for various SRRs and samples of different parameters by experiment and simulation.

The results showed that the proposed expressions are consistent with measured and simulated results. The maximum percentage error in calculating the resonant frequency with respect to simulated results is less than 2% except for one case where it is around 5%. This method of evaluation can be extended to resonating structures of other geometries to find expressions for resonant frequencies. The derived equations can also be used to find out the dielectric constant of sample materials placed in contact with the SRR, if structural and substrate parameters are known.

Chapter 4

Complex Permittivity Measurement Methods using Split Ring Resonators

This chapter presents permittivity measurement methods from the analysis of resonant frequency variations of SRRs in the presence of sample on SRR surface. In the first method, equations are derived for real and imaginary parts of permittivity of dielectric sample in terms of resonant frequencies and quality factors. The verification of results using standard cavity perturbation are also presented. The second method involves drawing of a calibration curve using some known values of permittivity of selected samples from which the dielectric constant values of unknown samples can be evaluated. Using the proposed method the dielectric constant values of some powdered food grains are determined in view of quality assessment considerations.

Precise determination of dielectric constant of materials having different size and shape are very important in the characterization studies and in its industrial, scientific and medical applications pertaining to the microwave region. The knowledge of dielectric parameters help us to identify and study the interaction of electromagnetic waves with materials which is essential for the development of manifold instrumentation and sensor applications.Various methods are proposed in the literature for dielectric studies in microwave/RF region. Some of the commonly used techniques include free space methods, transmission/reflection methods, resonant methods, near-field sensor methods etc. [43, 126, 127]

Out of the many methods used for permittivity measurement, resonant method is often preferred due to its high precision and sensitivity. Two major kinds of resonant methods are resonator method and resonant perturbation method. In the former, sample itself acts as a resonator and in the latter, sample changes the resonant properties of the resonator. We are introducing a resonant perturbation method for the measurement of complex permittivity of low loss, low dielectric value materials using metamaterial Split Ring Resonators (SRRs). The effect of dielectric environment on the resonant frequency of SRR is well studied [62, 128, 129, 130, 131]. But the determination of permittivity of a dielectric material based on the shift in the resonant frequency of metamaterial molecule is seldom found in the literature. By using transmission line based Complementary Split Ring Resonators (CSRR), Boybay *et al.* [132] have proposed a method for measuring the real part of permittivity of very low loss dielectric samples. It is based on an extraction technique where some samples with known values of dielectric constant is a pre-requisite. Another transmission line based extraction procedure proposed by Gabriel *et al.* [133] describes the permittivity characterization of solid and liquid materials using SRRs. They have employed empirical relations for the analysis of complex permittivity.

By working on the resonant perturbation method, using a single SRR as a movable test probe, a direct and easy technique to precisely determine both the real and imaginary parts of the permittivity of different solid materials is introduced. A detailed theoretical analysis based on the characteristic parameters of the SRR, along with its experimental confirmation using different test probes resonating at different frequencies is presented. The results are verified using standard cavity perturbation technique. Another simple method for measuring real part of permittivity using a calibration curve is also introduced. Dielectric constant of some powdered food samples are also analyzed with the view of current trends of high level of adulteration in food materials.

4.1 Development of theoretical model

As seen in the previous chapter, the resonant frequency of SRR is a function of effective capacitance (C_{eff}) and effective inductance (L_{eff}) and is given as

$$f = \frac{1}{2\pi\sqrt{L_{eff}C_{eff}}} \tag{4.1}$$

where, $L_{eff} = L_1 + L_2 - 2M$ (Eqns. 3.14, 3.15 and 3.16) and $C_{eff} = C_{tot}$ (Eqn. 3.12 and 3.13). For a single SRR of specific dimensions the variation in the dielectric constant changes the resonant frequency. Since the inductance L of the SRR is independent of the permittivity, the resonant frequency can be correlated to ε_{r1} and ε_{r2} through C_{tot}.

$$f \propto \frac{1}{\sqrt{C_{tot}}} \tag{4.2}$$

From Eqn. 3.13,

$$C_{tot} \propto \frac{(\varepsilon_{r1} + \varepsilon_{r2})}{2} \tag{4.3}$$

where, ε_{r1} is the dielectric constant of substrate and ε_{r2} is that of the sample. Hence the resonant frequency,

$$f \propto \frac{1}{\sqrt{\frac{\varepsilon_{r1}+\varepsilon_{r2}}{2}}} \tag{4.4}$$

Therefore, the variation in permittivity can be directly inferred from the resonant frequency when all other parameters remain constant.

4.1.1 Permittivity calculation - real part

From relation of resonant frequency, the dielectric constant of an unknown sample material can be calculated. It is possible to obtain expressions for permittivity of an unknown sample when SRR is fabricated on substrate with a known value. Even if the substrate permittivity is not known, the permittivity of the sample can be evaluated by a slightly modified equation.

4.1.1.1 Calculation in terms of known substrate permittivity

If we consider a SRR with a substrate of known dielectric constant ε_{r1} on one side and air on the other side, the resonant frequency (f_1) can be represented by using Eqn. 4.4 as

$$f_1 \propto \frac{1}{\sqrt{\frac{\varepsilon_{r1}+1}{2}}} \tag{4.5}$$

When a dielectric sample of unknown dielectric constant ε_{r2} is placed on the surface of the resonator, the air is substituted by the sample and the resonant frequency changes to

$$f_2 \propto \frac{1}{\sqrt{\frac{\varepsilon_{r1}+\varepsilon_{r2}}{2}}} \tag{4.6}$$

The ratio of Eqn. 4.5 and Eqn. 4.6 is

$$\frac{f_1}{f_2} = \frac{\sqrt{\varepsilon_{r1}+\varepsilon_{r2}}}{\sqrt{\varepsilon_{r1}+1}} \tag{4.7}$$

By rearranging this equation the expression for unknown dielectric constant of the sample is obtained as [27]

$$\varepsilon_{r2} = [(\frac{f_1}{f_2})^2(\varepsilon_{r1}+1)] - \varepsilon_{r1} \tag{4.8}$$

A plot between ε_{r2} and f_2 for different substrates of relative permittivity ε_{r1} is shown in Fig. 4.1 using Eqn. 4.8. It is clear that the value of resonant frequency decreases when the permittivity of the sample increases irrespective of the substrate permittivity. A similar lowering of resonant frequency is also seen when substrate dielectric constant increases.

4.1.1.2 Calculation in terms of unknown substrate permittivity

It is possible that in some cases, the permittivity of substrate material of SRR may be unknown. In such cases, a different relationship has to be used to find the permittivity of the sample. For this, the substrate material itself should be used as the sample. Then the resonant frequency will be

$$f_2 \propto \frac{1}{\sqrt{\varepsilon_{r1}}} \tag{4.9}$$

The ratio of Eqn. 4.5 and Eqn. 4.9 is

$$\frac{f_1}{f_2} = \frac{\sqrt{2\varepsilon_{r1}}}{\sqrt{\varepsilon_{r1}+1}} \tag{4.10}$$

After rearrangement the expression for relative permittivity of the substrate material is obtained as [27]

$$\varepsilon_{r1} = [2(\frac{f_2}{f_1})^2 - 1]^{-1} \tag{4.11}$$

Now, using this substrate permittivity ε_{r1}, we can find out the permittivity of any unknown sample using Eqn. 4.8. Hence, the measurement of the permittivity of a material becomes a simple numerical calculation from the two measured resonant frequency values f_1 and f_2 even without knowing the permittivity of the substrate, on which the resonator is etched.

4.1.2 Permittivity calculation - imaginary part

The imaginary part of permittivity is a measure of losses in the medium. The imaginary part of the complex permittivity is hence evaluated in terms of the loss factor tanδ. The presence of a lossy dielectric material in the vicinity of SRR changes the capacitive reactance through which the loss tangent is varied. Loss tangent is also called dissipation factor which is the reciprocal of quality factor of the resonator.

$$tan\delta = \frac{1}{Q} \tag{4.12}$$

At resonance, it is the Q - factor that determines the imaginary part. Quality factor is the ratio of resonant frequency to the 3bB bandwidth. As Q-factor is inversely proportional to the bandwidth, it is directly proportional to sharpness of resonant curve. Fig. 4.2 represents the resonant curve of a SRR showing +3dB bandwidth (BW).

$$Q = \frac{f_0}{BW} \tag{4.13}$$

Several researchers have tried to measure the complex permittivity of the material under test. Ebrahimi found out an empirical relation between complex permittivity and resonant characteristics [80]. Yang *et al.* derived a relation for loss tangent in terms of loss conductivity which is extracted using resonant frequency and input impedance [113]. It is seen that the loss tangent has a high impact on peak attenuation [63]. Using an empirical relation, an expression for loss tangent is derived in terms of quality factor. A linear

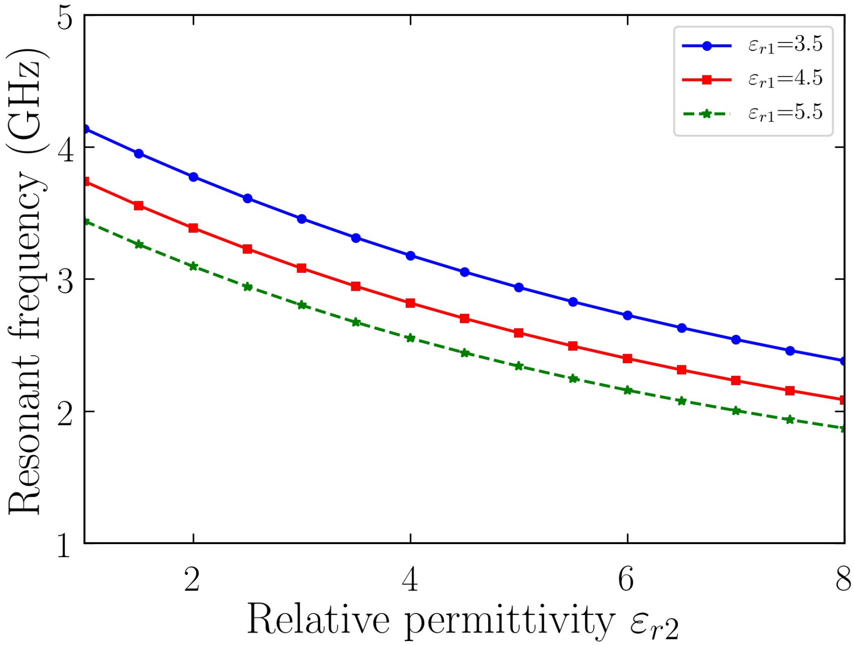

Figure 4.1: Plot showing the variation of the resonant frequency f_2 with dielectric constant of the sample ε_{r2} for different substrate values ε_{r1}.

relationship is found out between loss tangent and loss resistance by Lee *et al.*, and this relationship is used to find out loss tangent of several samples [115]. Similar techniques are followed by different researchers to find out the loss tangent of samples [118, 124].

Here an equation for finding the loss tangent of a material in terms of the Q-factors of the SRR is derived. For a resonant cavity, the expression for tanδ is given by

$$\frac{1}{Q_L} - \frac{1}{Q_0} = \tan\delta \tag{4.14}$$

where Q_0 and Q_L are the quality factors of the cavity without the sample and with the sample. In the case of the SRR resonator, the quality factor is measured from the absorption curve by considering the +3dB bandwidth from transmission minimum [21, 50, 111]. Here Q_0 is replaced with Q_{L0} which will be the quality factor of the SRR resonator when a lossless sample ($\tan\delta = 0$) of the material is assumed to be placed over the experimental probe. Q_L is the quality factor of SRR when the actual sample ($\tan\delta \neq 0$) is placed over it. The corresponding equation is given as

$$\frac{1}{Q_L} - \frac{1}{Q_{L0}} = \tan\delta \tag{4.15}$$

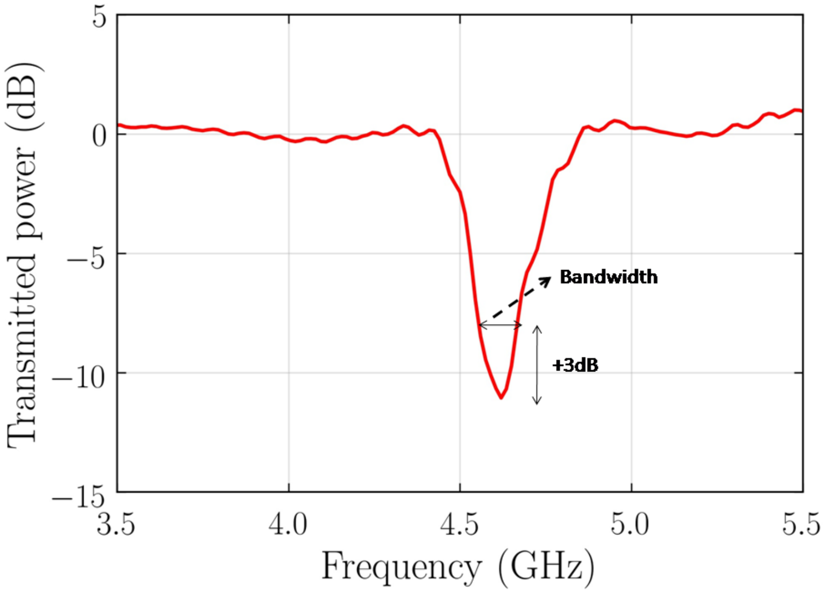

Figure 4.2: Plot showing the +3dB bandwidth from the absorption dip of a resonance curve.

Q_{L0}, which will be always greater than Q_L, can be evaluated from the energy equations as follows.

The electromagnetic energy stored in the test probe under resonance will be the sum of energy accumulation on the top and bottom sides of the SRR probe. Assuming the thickness of the substrate and the sample placed on the surface to be sufficient to accommodate the complete electric field of the SRR, the total energy of SRR is evaluated in terms of energy density $\frac{1}{2}\varepsilon_0 E^2$, for the case where no sample is placed on the SRR, will be proportional to

$$U \propto \varepsilon_{r1} + 1 \tag{4.16}$$

where ε_{r1} is the dielectric constant of the substrate. Therefore the quality factor Q_{p0} of the SRR test probe will be proportional to

$$Q_{p0} \propto \frac{\varepsilon_{r1} + 1}{l_{sub}} \tag{4.17}$$

where l_{sub} is the loss factor inside the substance. For SRR with a sample placed on its

Table 4.1: Structural parameters and resonant frequencies of SRRs used for the measurement.

Test probe	**Inner radius- *r* (mm)**	**Width of the ring- *c* (mm)**	**Spacing- *d* (mm)**	**Resonant frequency- f_1 (GHz)**
SRR-1	2.0	0.75	0.5	3.456
SRR-2	1.625	0.68	0.4	4.317
SRR-3	1.3	0.65	0.4	4.926
SRR-4	1.0	0.6	0.4	5.697

surface this relation with the same proportionality constant becomes

$$Q_{L0} \propto \frac{\varepsilon_{r1} + \varepsilon_{r2}}{l_{sub} + l_{sample}} \tag{4.18}$$

where l_{sample} is the possible loss factor of the sample and ε_{r2} is its permittivity. If the sample is assumed to be lossless Q_{L0} becomes

$$Q_{L0} = \frac{\varepsilon_{r1} + \varepsilon_{r2}}{l_{sub}} \tag{4.19}$$

By taking the ratios of Eqns. 4.19 and 4.17 [27].

$$Q_{L0} = \frac{(\varepsilon_{r1} + \varepsilon_{r2})Q_{p0}}{(\varepsilon_{r1} + 1)} \tag{4.20}$$

This Q_{L0} is substituted in Eqn. 4.15 as reference quality factor.

4.1.3 Measurement of complex permittivity of different solid samples

SRRs of four different dimensions are fabricated using photochemical etching method on glass epoxy board as described in the second chapter. For the measurement of the resonant frequency, a single SRR is placed between a transmitting and receiving probes which are connected to a Vector Network Analyzer (VNA). Fig. 3.11 shows the schematic arrangement and photograph of the experimental setup. The structural parameters of SRRs and their respective resonant frequencies are given in Table 4.1.

Samples whose dielectric constant are to be measured is placed on the top of the test probe. The minimum requirement of the sample for this particular experiment is related to its thickness, surface smoothness and area. The dielectric samples of unknown permittivity should have at least one flat surface with area greater than or equal to the area of the SRR structure so that they come in close contact with the full area of the resonator surface without any air gap. The thickness of the dielectric is so chosen that the electric field of the resonating structure is completely inside the sample. It has been experimentally verified that a thickness greater than or equal to $c + d/2$ will be sufficient for maximum inclusion of the field which is also evident from the theoretical view point. This thickness condition should be satisfied for the substrate also.

4.1.3.1 Verificaton of minimum thickness condition of samples

The electric field due to the induced charges is present on both upper and lower surfaces of SRR. The presence of electric field on both sides and its range is experimentally determined. SRR of dimensions r = 1.7 mm, c = 0.7 mm, d = 0.4 mm having very thin flexible substrate is fabricated using chemical etching method. Its resonance is measured using a network analyzer and it is found to be 7.1 GHz. To analyze the effect of the thickness of the dielectric substrate, an adhesive polymer film of thickness approximately equal to 20 μm and ε_r = 2.4 is used. The thickness is increased by placing the film on one side of the SRR one by one and the resonant frequency is noted each time. Then the experiment is repeated for the other side of the SRR also and resonant frequencies are measured for each thickness. Results are plotted in Fig. 4.3. It is observed that the resonant frequency becomes almost a constant after a certain thickness is exceeded which is found to be related to the structural parameter of the SRR as $c + d/2$. This means that a sample with thickness greater than $c + d/2$ has negligible perturbation effects on the resonant frequency. Hence, a dielectric of thickness of at least equal to $c + d/2$ will sufficiently include the whole electric field of SRR within it. Fig. 4.4 gives the schematic representation of the field regions of the SRR completely enclosed within a sample of thickness $c + \frac{d}{2}$.

From the plots we can see that the resonant frequency varies almost equally on both sides of the SRR, which shows that the presence of dielectric material alters the field distribution on both sides almost equally. This means that there is an equal contribution to the capacitance from both sides of the SRR. We have already proved in chapter 2 that the total capacitance of the SRR should include the contribution from both surfaces which is again validated here.

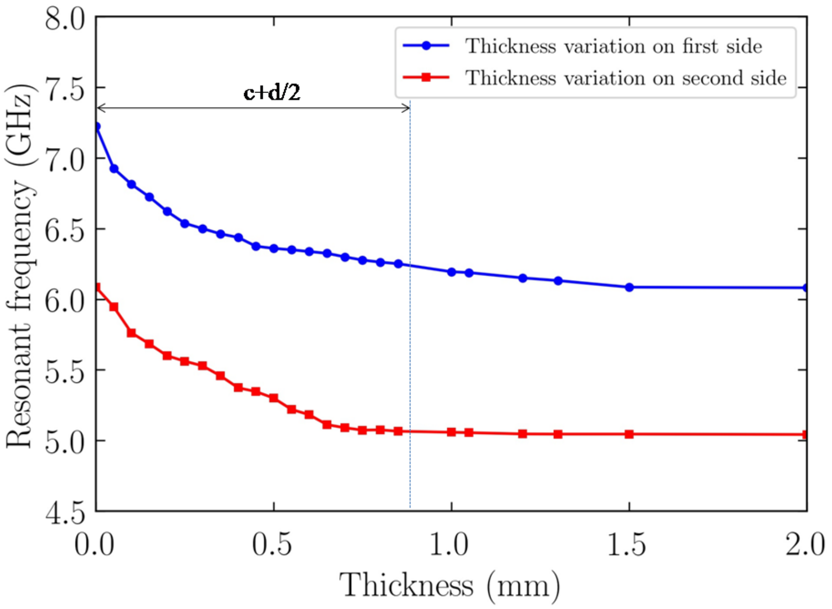

Figure 4.3: Resonant frequency variation with increasing thickness of the sample.

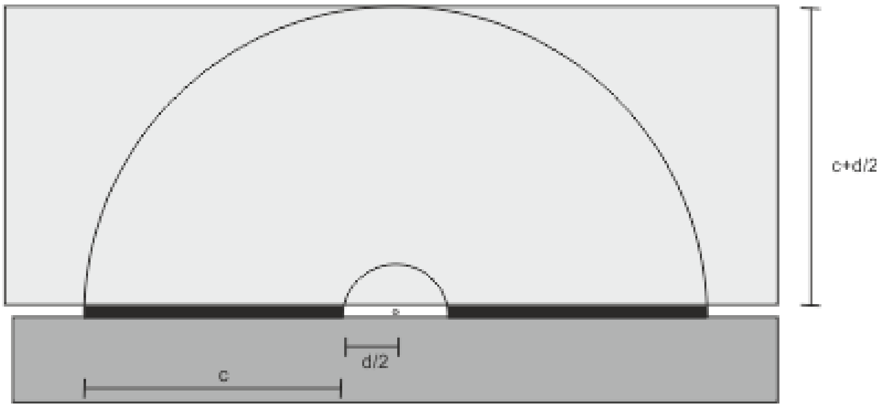

Figure 4.4: Schematic representation of field regions of a SRR along with a dielectric sample with required minimum thickness.

Five samples which are selected for study are glass, perspex, plastic and two different glass epoxy sheets out of which one is a piece of the substrate itself. The thickness of selected samples are as following: plastic - 2.85 mm, perspex - 2.12 mm, glass epoxy sample - 3.1 mm, substrate material - 2.71 mm, and for glass - 2.66 mm. Initially, the resonant frequency of the SRR-1 with known substrate permittivity ε_{r1} when no test sample placed over it is measured (f_1). Measurements are then repeated using dielectric samples and their corresponding resonant frequencies are noted (f_2). Using Eqn. 4.8 their dielectric constants (ε_{r2}) are calculated. In case, if substrate permittivity is not known, before using test samples a piece of the substrate material of the SRR itself is used as the sample and the corresponding resonant frequency is noted as f_2 and using Eqn. 4.11 ε_{r1} of the substrate is found out. Measurements are repeated using other three SRRs for all the samples.

From Eqn. 4.15 the loss factor (tanδ) of all the samples are calculated. Q_{p0} and Q_L are obtained from their corresponding transmission curves and Q_{L0} is calculated for each sample using Eqn. 4.20.

4.1.4 Results and discussions

Figures 4.5 - 4.8 show the shift in transmission curves of all the five samples from that of corresponding SRR test probes which is marked as reference. It is observed that the resonant frequencies are shifted towards lower frequencies in relation to their permittivity values. This shift is in agreement with the results predicted by various numerical and simulation methods [61, 134, 62, 130]. In all the four cases we observe that the minimum frequency shift is observed for plastic and maximum is for glass. As an example, for SRR-2, the corresponding resonant frequencies observed are 3.835 GHz and 2.992 GHz respectively. The resonant frequencies of other three samples are in between these two values as depicted in Fig. 4.6. The real part of the relative permittivity values are calculated using Eqn. 4.8. The loss tangents of all the five samples are evaluated using Eqn. 4.15. As expected the plastic sample is almost lossless ($\approx$ 0.003) while glass epoxy and the substrates of the SRR are showing relatively high loss factors ($\approx$ 0.03 to 0.04). The other two samples perspex and glass have $\tan\delta$ values around 0.01.

Tables 4.2 to 4.5 show the values of resonant frequencies along with the calculated values of real and imaginary parts of permittivity for all the five samples using the four test probes (SRR-1 to SRR-4). The Table 4.3 displays the values mentioned earlier for SRR-2.

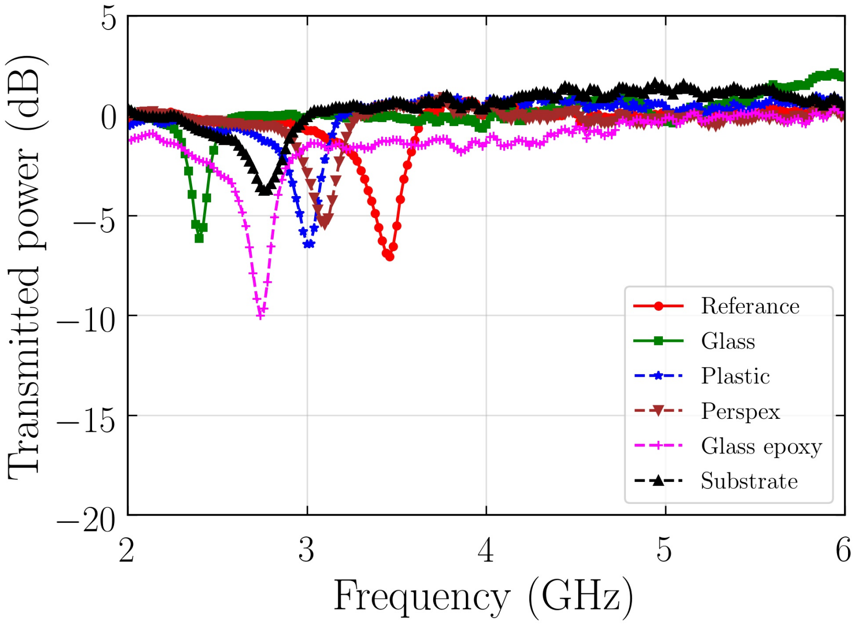

Figure 4.5: Transmission spectra showing resonant frequencies of SRR-1 for different samples.

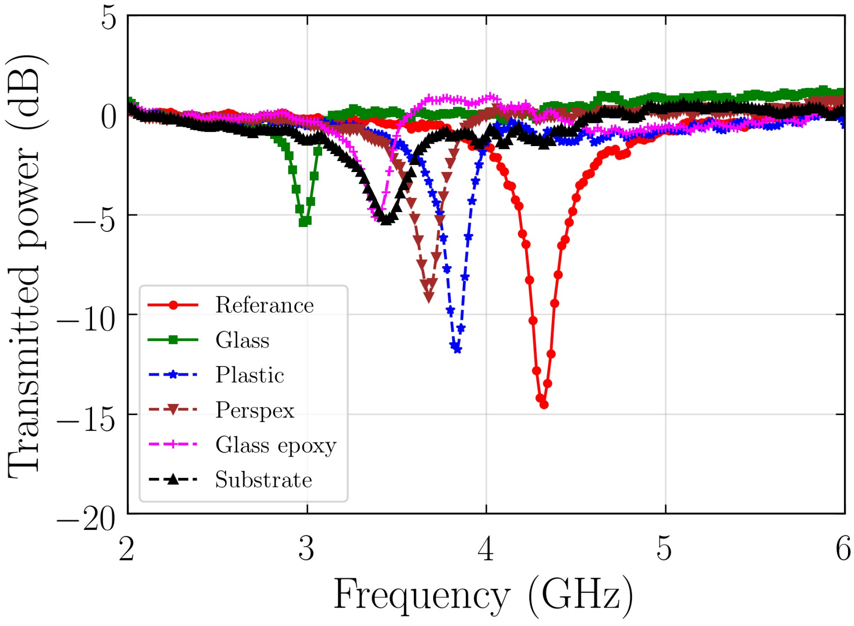

Figure 4.6: Transmission spectra showing resonant frequencies of SRR-2 for different samples.

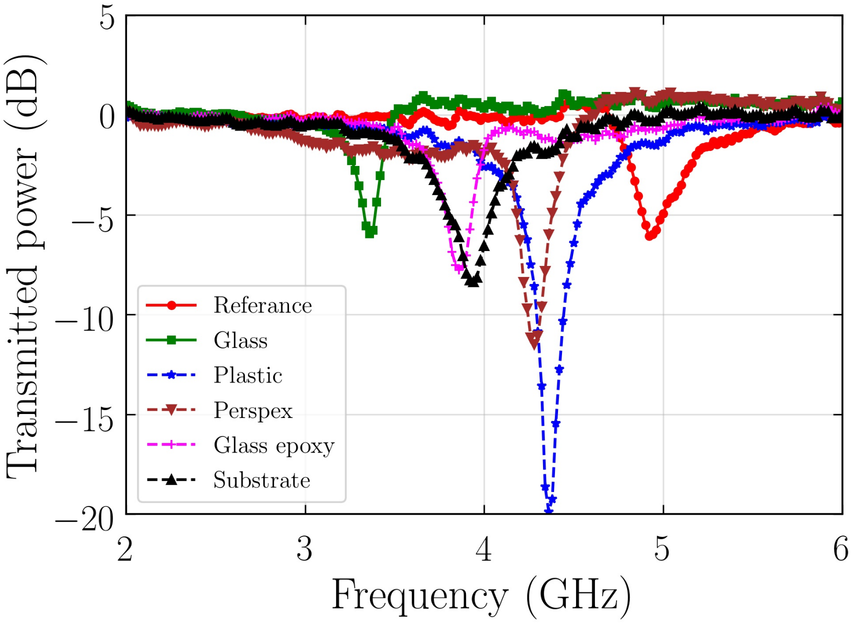

Figure 4.7: Transmission spectra showing resonant frequencies of SRR-3 for different samples.

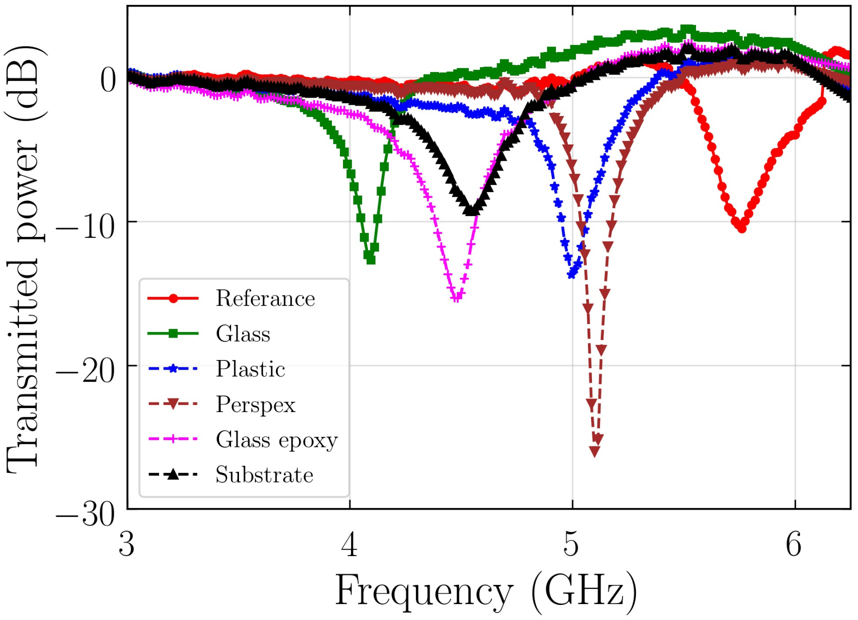

Figure 4.8: Transmission spectra showing resonant frequencies of SRR-4 for different samples.

Table 4.2: Values of complex permittivity along with resonant frequency obtained by using SRR-1 test probe.

Sample	**SRR-1**		
	f_0 **(GHz)**	ε_{r1}	$tan\delta$
Plastic	3.090	2.124	0.0039
Perspex	3.006	2.471	0.0151
Glass epoxy	2.741	3.695	0.0332
Substrate	2.763	3.571	0.0380
Glass	2.402	5.891	0.0121

Table 4.3: Values of complex permittivity along with resonant frequency obtained by using SRR-2 test probe.

Sample	**SRR-2**		
	f_0 **(GHz)**	ε_{r1}	$tan\delta$
Plastic	3.835	2.259	0.0031
Perspex	3.679	2.776	0.0131
Glass epoxy	3.386	3.944	0.0361
Substrate	3.445	3.714	0.0371
Glass	2.992	6.099	0.0094

Table 4.4: Values of complex permittivity along with resonant frequency obtained by using SRR-3 test probe.

Sample	**SRR-3**		
	f_0 **(GHz)**	ε_{r1}	$tan\delta$
Plastic	4.379	2.210	0.0035
Perspex	4.277	2.522	0.0122
Glass epoxy	3.860	3.861	0.0370
Substrate	3.930	3.62	0.0411
Glass	3.360	6.357	0.0105

Table 4.5: Values of complex permittivity along with resonant frequency obtained by using SRR-4 test probe.

Sample	**SRR-4**		
	f_0 **(GHz)**	ε_{r1}	$tan\delta$
Plastic	5.020	2.310	0.0034
Perspex	4.911	2.574	0.0151
Glass epoxy	4.483	3.804	0.0420
Substrate	4.560	3.554	0.0462
Glass	3.907	6.128	0.0108

4.1.4.1 Verification of results using cavity perturbation method

Cavity perturbation method, also known as material perturbation method, is used for the validation process. Here, the material under test is introduced into cavity and corresponding changes in the resonant frequency and Q-factor is analyzed to find out the complex permittivity of the material. Usually samples of low dielectric loss are preferred for this method. For measuring the permittivity the material is inserted into the anti-node of electric field and for permeability measurement, it is inserted into the anti-node of the magnetic field. This method can also be used to measure the surface resistance. Fig. 4.9 represents the experimental setup for cavity perturbation technique.

There have been several efforts aimed towards developing the cavity perturbation method. Among them, the work done by Waldron gave a detailed derivation of the equations and it discussed in detail about the effect of shape of the specimen and accuracy of the method [135]. There have been several applications of this method to measure dielectric constant of various materials. Dielectric behavior of vapors at microwave frequencies are measured using cavity perturbation method by Raveendranath *et al.* [136]. Banerjee *et al.* formulated an analytical solution for dielectric constant measurement using rectangular cavity [137]. Dielectric constant and loss factor of cylindrical samples are measured by Kumar *et al.* using a rectangular cavity having a small circular slot at the center to insert the sample [49]. A comparison of accuracy and importance of three different dielectric resonance techniques and cavity perturbation technique was performed by Sheen [138].

The cavity method utilizes a slotted cavity connected to a VNA through two coaxial cables to measure the transmitted power. In this method, the samples chosen should be very thin, whose width and thickness are much smaller than the resonant wavelength of the cavity. Dielectric constants are calculated from the observed shifts in the transmission

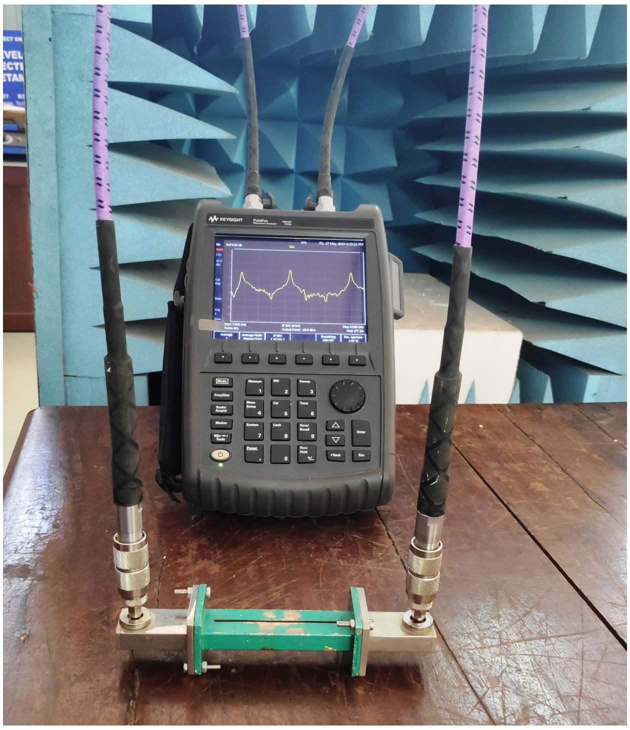

Figure 4.9: Cavity resonator connected to transmitting and receiving probes of Vector Network Analyser.

resonant peaks of the cavity when samples are inserted. The values of real and imaginary part of permittivity $\varepsilon_r^{'}$ and $\varepsilon_r^{"}$ are calculated using the following equations [49, 48]

$$\varepsilon_r^{'} = 1 + \frac{f_c - f_s}{2f_s}\frac{V_c}{V_s} \tag{4.21}$$

$$\varepsilon_r^{"} = \frac{V_c}{4V_s}\frac{Q_c - Q_s}{Q_c Q_s} \tag{4.22}$$

where f_c and f_s are resonant frequencies of the cavity without sample and with sample respectively. V_c is the volume of the cavity and V_s is the volume of the sample portion inserted into the cavity. Q_c and Q_s are quality factor of the resonance curve without sample and with sample respectively.

For the verification of the results obtained by SRR method, thin specimens of the samples are inserted in a rectangular waveguide cavity (X-band) connected to the VNA. The resonant frequency of the unloaded cavity is observed as 7.88 GHz. Using the dimensions of both the cavity and the sample, and by observing the shifts in the resonant frequencies and Q - factors the dielectric constants are calculated using equations of cavity

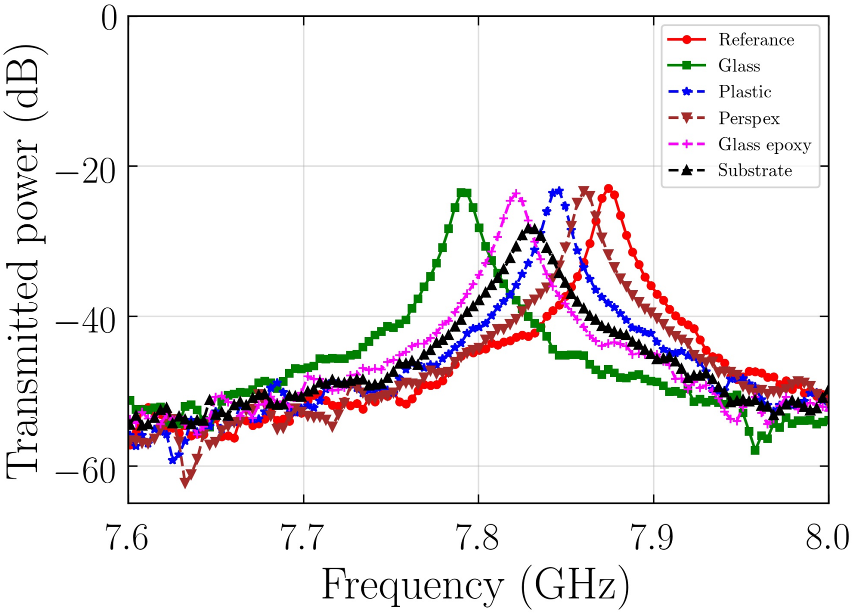

Figure 4.10: Transmission spectra showing resonant frequencies of five test samples along with that of the empty cavity.

perturbation method [48]. Figure 4.10 represents transmission spectra showing resonant frequencies of five test samples along with that of the empty cavity. Using the resonant frequencies and Q-values, real and imaginary parts of the permittivity are calculated and given in Table 4.6.

Table 4.6: Values of complex permittivity obtained by using the cavity perturbation method.

Sample	**Permittivity**	
	Real part (ε_{r1})	**Loss tangent($tan\delta$)**
Plastic	2.302	0.0036
Perspex	2.459	0.0143
Glass epoxy	3.767	0.0351
Substrate	3.583	0.0380
Glass	6.073	0.0115

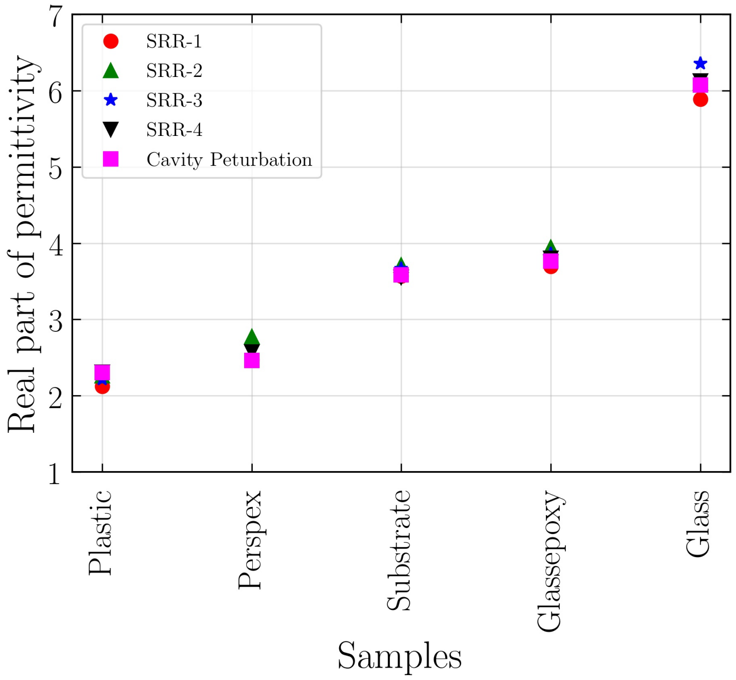

Figure 4.11: The plot showing comparison of real values of permittivity of test samples obtained using SRR probes along with cavity perturbation method.

4.1.4.2 Accuracy concerns of SRR based measurement technique

The accuracy of these measured values also depends upon the frequency interval between measurement points (sampling interval). By reducing the sampling interval we can more precisely locate the resonance dip which helps in more accurate determination of the results. Sampling interval of the order of few MHz will not change the accuracy of the results considerably. The maximum change in the $\tan\delta$ values due to the possible slight change in locating the resonant dip obtained in our measurements are, glass epoxy = ± 0.00000024, substrate = ± 0.000001, glass = ± 0.000000053, plastic = ± 0.00045 and perspex = ± 0.00037.

The values obtained by our method using SRR test probes given in Tables 4.2 - 4.5 are closely in agreement with that obtained from cavity method (Table 4.6). Figs. 4.11 and 4.12 show a comparison of real and imaginary values of permittivity of all samples measured using SRR probes along with the cavity perturbation method. Thus by simply placing the sample over SRR test probe or by placing the test probe over the sample (cases of bulk samples) we are able to precisely measure the dielectric constant and the loss factor.

Advantages of this SRR resonant method over other resonant dielectric measurement

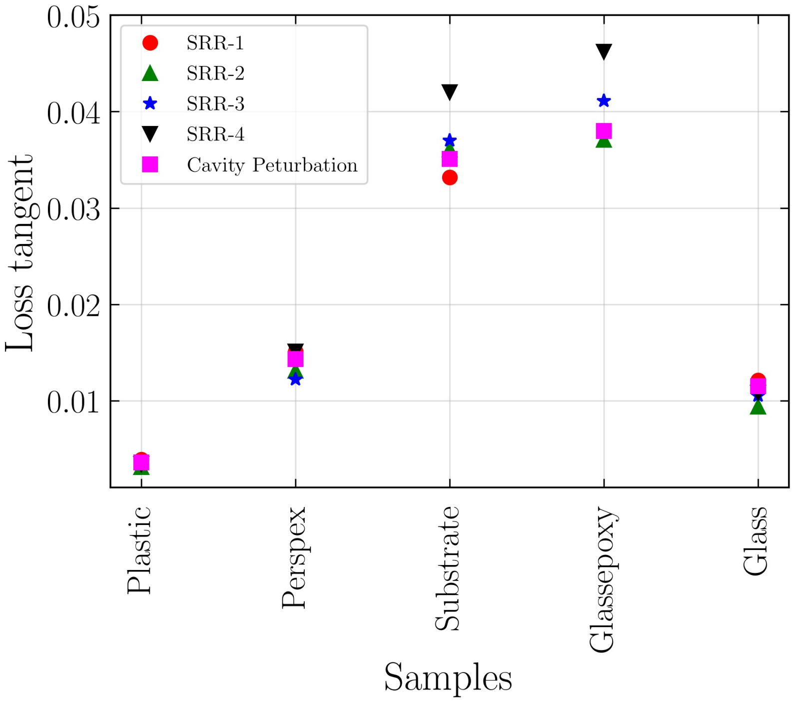

Figure 4.12: The plot showing comparison of Loss tangent values of test samples obtained using SRR probes along with cavity perturbation method.

techniques are the ease in sample preparation and the simplicity in experimental setup, which include only a SRR test probe connected to a VNA. The permittivity equations used for the calculations are also very simple. Since our SRR probe is not coupled directly with a guided wave, the theoretical formulation is straight forward and simple when compared with transmission line based SRR systems. The only condition for precise analysis is that the sample thickness should be such that the field of the resonator is completely inside the sample. This technique is extremely preferable for samples of bulk size.

It is observed that the measurement using SRR does not fully agree with the standard values when the dielectric constant increases beyond a certain limit. The relations for capacitance and permittivity given earlier are valid when the quasi-static nature is maintained for the magnetic field component. The equations for the capacitance are developed by assuming that the field over the SRR is almost constant. But when a dielectric sample of high permittivity is placed over the probe, the wavelength of the field across SRR within the sample reduces by a factor of $1/\sqrt{\varepsilon_r}$. In such situations it deviates from quasi-static approximation and the linear relationship between the capacitance and permittivity does not hold perfectly. Then the equation for the equivalent capacitance may not be expressed in the form as given in chapter 3. In such conditions, reducing the dimensions of the SRR may enhance the accuracy of measurements.

Looking into the performance efficiency of this method in comparison with some of the standard methods, [139, 140, 141, 142] the following points may be noted. In comparison with waveguide method, free space method and cavity perturbation method, the selection of size and shape of the experimental sample offers more flexibility here. All the advantages of the transmission line method such as rapid and easy measurement, ability to use at various temperature levels etc. are equally possible here along with the added feature of the provision to move the test probe towards a sample if the situation demands so. Apart from the above mentioned advantages, this is a non-destructive testing technique which may find use in the case of costly and rare samples. Since this method employs a movable test probe, it can be easily extended to the permittivity characterization of liquids by using it as a submersible probe. The air gap error usually happening in coaxial method and in planar transmission line method can be effectively minimized by proper mounting of the sample over the SRR. The presence of air gap changes the effective permittivity and hence a small reduction in the resonant frequency shift is expected. This may result in slightly lower value for the real and imaginary parts of the permittivity. Hence, for accurate results in this method, care should be taken to maintain the constant environmental conditions so as not to disturb the field distribution around the test probe during the measurements. We can also expect slight errors in experimental values due to surface imperfection of the sample and SRR fabrication errors.

4.2 Extrapolation method

In situations where we have to determine only the real part of permittivity, a SRR based simple extrapolation method can be employed. The experimental setup is same as that of previous method where instead of using analytical equation an extrapolation curve is drawn between known permittivity of some standard samples and their corresponding resonant frequencies.

The measurement of dielectric constant of any unknown sample can be obtained from this calibration curve in a straight forward and easy manner.

Table 4.7: Relative permittivities and resonant frequencies of samples for drawing calibration curve.

Sample	**Relative permittivity ε_r**	**Resonance frequency (GHz)**
Plastic	2.10	3.254
Perspex	2.45	3.118
Glass epoxy	3.571	2.863
Glass	6.07	2.647

4.2.1 Frequency - permittivity calibration graph

To draw the calibration curve, four standard samples are chosen which are plastic, perspex, glass and glass epoxy. Initially, the dielectric constants of the selected samples are measured using the standard cavity perturbation method [48].

SRR test probe used in our study is fabricated by etching it on a FR4 glass epoxy board of thickness t = 1.5 mm and dielectric constant ε_r = 3.583. The dimensions of SRR are inner radius r = 2 mm, ring width c = 0.75 mm and gap between the rings d = 0.5 mm and its resonant frequency is observed to be 3.57 GHz. The standard samples are properly mounted on the SRR without any air gap and their corresponding resonant frequencies are noted to draw the calibration curve. Table 4.7 gives the relative permittivity ε_r and resonant frequency f in GHz for the standard samples. Figure 4.13 shows the calibration curve drawn between these resonant frequencies and their dielectric constant values measured using cavity perturbation technique.

Any unknown samples whose dielectric constant is to be determined will be placed on the SRR test probe and its corresponding resonant frequency will be noticed. From the calibration curve, its real part of permittivity can be extracted out in a straight forward manner.

4.2.2 Measurement of permittivity of pulses and cereals by using extrapolation method

To demonstrate the proposed method, dielectric constant of some powdered food samples are determined.

Electromagnetic field interaction based studies are important for characterization of different materials including various types of food samples. Dielectric parameters vary according to the type and nature of the food material and hence, by analyzing the permit-

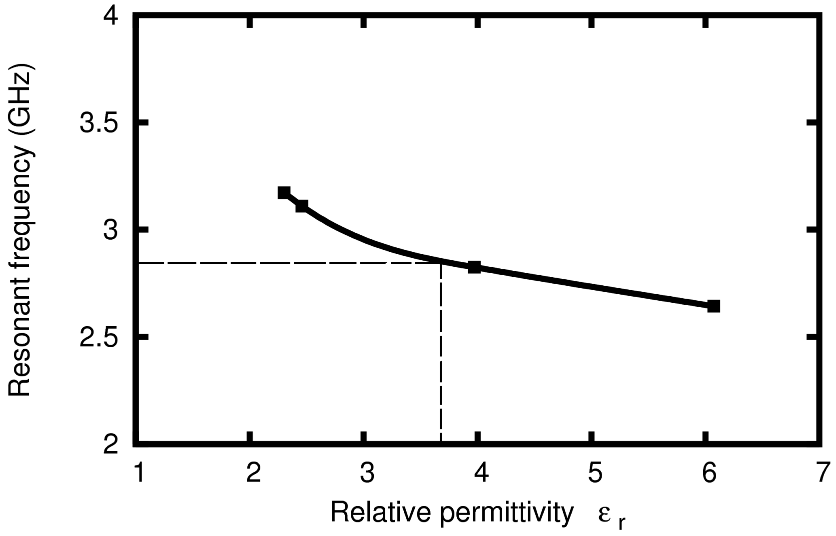

Figure 4.13: Calibration curve between resonant frequencies and relative permittivities for standard samples.

tivity we can assess the quality of food materials. The basic principles of electromagnetic properties including dielectric properties of food materials are reviewed by S. Ryynanen [143]. Knowledge of dielectric constant allows us to understand the dryness condition of edible items in packing and storing process, food quality checking, detection of unethical and illicit substitution of extraneous materials etc.

There are several methods proposed for measurement of complex permittivity of food materials in literature. An open ended coaxial probe method is proposed for frequency dependent permittivity measurement of semi-solids, liquids and powdered food samples [141]. This method is suitable mainly for high loss samples. Dependence of dielectric parameters on moisture, frequency, temperature etc. are reported for grain samples, fruits, vegetables and other food materials [144, 145, 146]. Wang *et al.* analyzed the complex permittivity changes of some food materials with variation in temperature at low frequencies for pasteurization and sterilization applications using custom-built temperature-controlled test cell connected to an impedance analyzer [147].

4.2.3 Results and discussions

We have selected four samples each for pulses and cereals, and ground them into fine powder. The pulse samples selected are green gram flour, dry cow peas flour, gram flour and soya bean flour and that of cereals are rice flour, wheat flour, all purpose flour and corn flour. The powdered sample is taken in a rectangular sample holder without any bottom sheet and it is placed coaxially with SRR ring. The sample holder should have a size greater than that of the diameter of SRR. It is made up of a thin polythene film of thickness 20 μm with sufficient height to accommodate the entire fringing field of the resonating SRR.

The transmission resonant curves of the SRR for various pulse samples are shown in Fig. 4.14. The dielectric constant of these pulse samples are then extracted from the calibration curve (Fig. 4.13) corresponding to their measured resonant frequencies. The resonant frequencies and corresponding relative permittivity obtained from calibration curve are given in Table 4.8. It is observed that the Soya bean flour has the largest resonant frequency and hence the lowest dielectric constant. The value of ε_r obtained for gram flour is slightly greater than that for Soya flour. It is clear from the graph that the other two samples green gram flour and dry cow pea flour are having almost equal resonant frequencies and hence almost same values for dielectric constant. This may be because of the fact that they are same varieties of legumes than the other two samples, powders of Soya bean and Bengal gram.

Figure 4.15 shows the transmission resonant curves for selected powdered cereal samples. A similar observation can be made from this figure that the wheat flour and the all purpose flour have equal resonant frequencies and it can be attributed to the fact that both of them are prepared from wheat. Out of all the cereal samples corn flour has the least dielectric constant and rice flour has the maximum value. The resonant frequencies and corresponding relative permittivity values of cereals are also included in Table 4.8. Selected samples give resonant frequency difference in the range of 20 MHz which helps us to precisely determine the relative permittivity with high sensitivity. Care should be taken to draw the calibration graph using the standard sample at the time of measurement of unknown samples since environmental variations like temperature and humidity may vary the resonant conditions of the SRR.

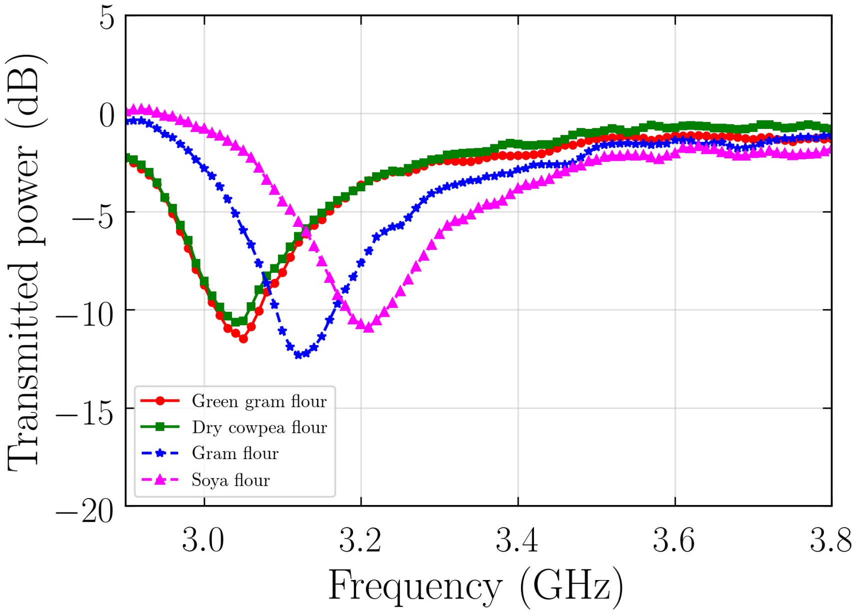

Figure 4.14: Transmission resonance curves of powdered pulses.

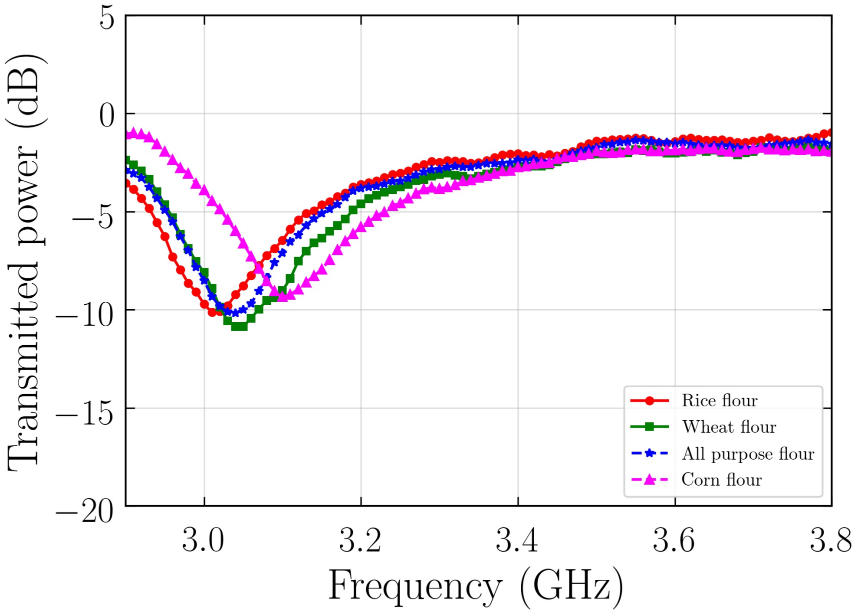

Figure 4.15: Transmission resonance curves of powdered cereals.

Table 4.8: Resonant frequency and corresponding relative permittivity of powdered pulses and cereals extracted from the calibration curve.

Sample	**Type**	**Resonant frequency f (GHz)**	**Relative permittivity ε_r**
Pulses	Green gram flour	3.20	2.212
	Dry cow pea flour	3.19	2.264
	Gram flour	3.27	2.058
	Soya flour	3.36	1.879
Cereals	Rice flour	3.16	2.333
	Wheat flour	3.19	2.264
	All purpose flour	3.19	2.264
	Corn flour	3.25	2.105

4.3 Conclusion

This chapter presents two different SRR based permittivity measurement techniques in which the first one gives detailed derivation of the analytical formulation of the complex permittivity of low loss dielectric samples. The results are experimentally verified and are confirmed by cavity perturbation method. In the second part, a simple extrapolation method is presented whereby its real part of permittivity can be extracted in a quick and straight forward way using the same experimental set up as that of the first method.

Chapter 5

Temperature Dependent Permittivity Measurement of Different Solid Samples

The temperature dependent dielectric constant measurement of some solid samples is presented in this chapter. The methods presented in chapter four for permittivity measurements are used for the calculation of temperture dependent dielectric constants of samples like waxes, flame retardent boards etc.

Among the material characterization studies, the precise determination of dielectric constant at different working environments is important from the application point of view. Out of these different parameters the variation of dielectric constant with temperature finds its use in different sensor applications in the fields of medical instrumentation, electronic and electrical industry etc.

There are several techniques described in the literature to determine the dielectric constant at different temperatures [43]. Among these different techniques, open-ended coaxial probe method, cavity resonance methods, quasi-optical resonator method, split-cylinder resonator method etc. are commonly employed [148, 149]. Many of these methods require specific working conditions to be satisfied for the precise determination of temperature dependence of relative permittivity.

The dependence of dielectric constant on temperature for some materials are reported [150, 151]. Factors contributing to the temperature dependence of dielectric constants of materials are analysed by E. Havinga using some alkali halides and $BaTiO_3$ as samples [150]. But the the temperature dependent dielectric constant measurement using metamaterial elements have not yet seen in literature.

As the properties of the metallic structure of resonator and the dielectric substrate upon which it is fabricated are all temperature dependent, SRR probe is also sensitive to temperature variations. Varadan *et al.* has done a study on shift in the resonant frequency of SRR in terms of the temperature dependence of its metallic structure, substrate permittivity and electrical conductivity [152]. It is reported that the resonant frequency variation is primarily affected by the change of permittivity of the substrate. Singh *et. al.* studied the effect of temperature on terahertz metamaterials fabricated on strontium titanate substrate [153].

In this chapter, dielectric constant of three sets of solid samples (FR board samples, wax samples, polymer samples) are analyzed for different temperature ranges. Two methods developed and presented in the previous chapter are used here for the calculation of permittivity values. Fig. 5.1 shows the flowchart which gives an overview of the methods and samples used for temperature dependent permittivity studies presented in this chapter.

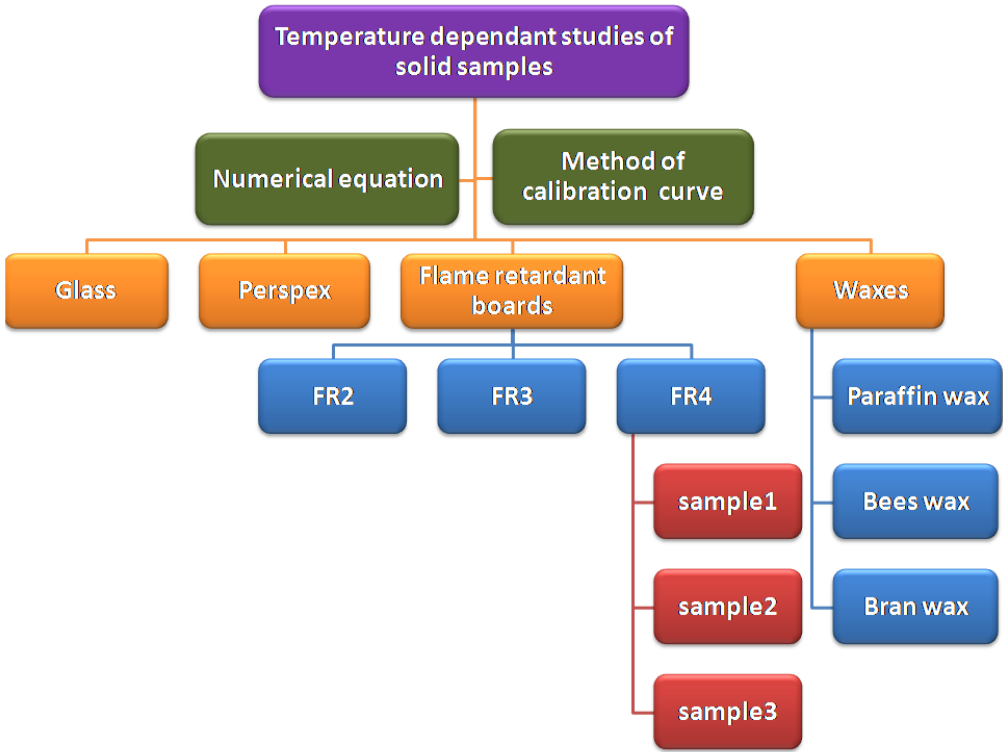

Figure 5.1: Chart representing methods and samples used for temperature dependent study.

5.1 Experimental setup and measurement methods

For the precise and easy measurement of permittivity of samples at different temperatures, a compact and flawless experimental setup and measurement methods should be used. The experimental set up is same as that was discussed in chapter four, but in order to study the temperature dependent permittivity, test probe along with the sample is kept inside a temperature controllable wooden chamber (Fig. 2.15). Temperature of the test sample placed over the SRR is gradually increased using light focused from an Infra Red (IR) lamp. A schematic digram of the test probe for the present case is shown in Fig. 5.2.

SRR of dimensions r = 2 mm, d = 0.5 mm and c = 0.75 mm is etched on a glass epoxy board (ε_r = 3.56) using photochemical etching method as explained in chapter two. Solid samples used for the analysis like FR boards, plastic and perspex can be directly placed on the surface of SRR. But, wax samples which melt with the increase in temperature should have a proper sample holder. Care is taken so that the sample holder does not disturb the SRR. A thin polymer sheet made into four sided holder is used for this pur-

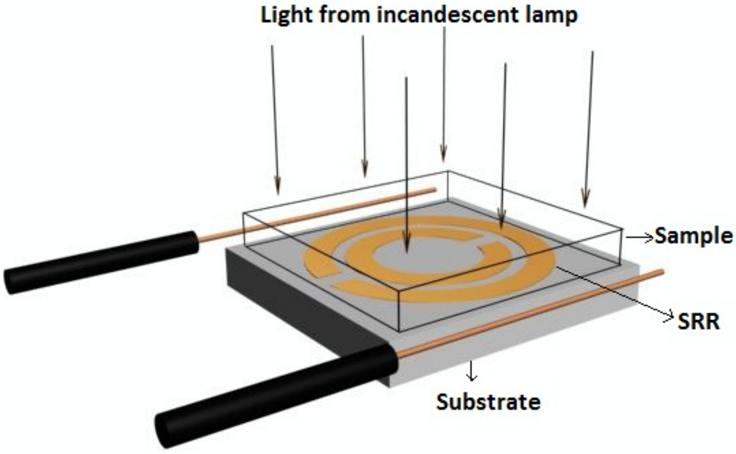

Figure 5.2: Schematic representation of the SRR test probe with light incident on it for temperature dependent perittivity study.

pose. The resonant frequency measurement method in which the SRR is placed between the transmitting and the receiving probes connected to a VNA is employed here. The experimental setup for temperature variations and measurements was explained in chapter 2.

5.1.1 Correction to measured resonant frequency

When we measure the resonant frequency of SRR with sample placed on its surface and temperature is increased from the room temperature, the SRR also heats up with the whole system which in turn changes its resonant frequency slightly. Hence to obtain an accurate value of resonant frequency due to the increasing temperature of the sample a correction must be applied to the measured resonant frequency. For this the resonant frequency of SRR without the sample is measured and is taken as f_{r0} at room temperature and f_{t0} at different temperatures. The resonant frequency corresponding to different temperatures when sample is placed on the SRR probe is measured and is labeled as f_{t1}. The shift in resonant frequency $(f_{r0} - f_{t0})$ is calculated for each temperature and it is subtracted from the resonant frequency f_{t1} as a correction.

5.1.2 Methods of calculation of dielectric constant

Two methods presented in the previous chapter for permittivity measurements are followed for the calculation of temperature dependent permittivity of different samples. The methods are briefly described here.

5.1.2.1 Calculation through analytical equations

The method based on analytical relations derived as detailed as the first method in chapter four is followed [27]. Measurement method involves placing the sample dielectric on the surface of SRR and finding the resonant frequency using VNA. From the resonant frequency of SRR without sample placed over it (f_1) and with sample placed over it (f_2, the corrected resonant frequency to accommodate the temperature dependent shift of the SRR probe) and by using the equation below (Eq. 5.1), the real part of permittivity of the sample (ε_{r2}) can be calculated.

$$\varepsilon_{r2} = [(\frac{f_1}{f_2})^2(\varepsilon_{r1} + 1)] - \varepsilon_{r1} \tag{5.1}$$

where ε_{r1} is the permittivity of the substrate material.

5.1.2.2 Calculation through calibration curve

The calibration curve drawn between resonant frequency of SRR and relative permittivity of some standard samples is used to find out the real part of permittivity of different test samples. Four standard samples selected are plastic, perspex, glass epoxy board and glass. From the cavity perturbation method [48] we obtain the dielectric constants of these samples. It is observed that resonant frequency decreases as the dielectric constant of the material increases. Relative permittivity of any unknown test sample in close contact with the surface of the SRR can be extracted from this calibration curve if corresponding resonant frequency of SRR - sample system lies on the curve. The main draw back of this method is that it is dependent on the environmental conditions and the calibration should be done during the time of each measurement.

Table 5.1: Resonant frequency of the test probe for different temperatures along with the resonant frequency shifts.

Temperature (°C)	**f_{t0} (GHz)**	**Resonant frequency shift ($\Delta f = f_{r0} - f_{t0}$)**
35	3.5613	0
40	3.5515	0.0098
45	3.54	0.0213
50	3.5199	0.0414
55	3.4911	0.0702

5.2 Polymer samples (Plastic and perspex)

Some commonly available solid samples of polymer having low dielectric constant of suitable thickness ($t > c + \frac{d}{2}$) are selected for the measurement. To study the temperature dependence of dielectric constants of polymers we choose two test samples plastic and perspex.

5.2.1 Temperature dependence of SRR

Initially the temperature dependence of SRR resonant frequency is analyzed. For this, SRR alone is placed between the transmitting and receiving probes inside the temperature control chamber. The resonant frequencies are measured at steps of 5° C from room temperature (35°C). Resonant frequency of SRR obtained without the sample is taken as f_{t0} for different temperatures and values are given in Table 5.1. The resonant frequency decreases as temperature increases. The correction factor Δf for each temperature is also shown in the Table 5.1.

5.2.2 Measurements and results

For drawing the calibration graph we have selected the dielectric samples of glass, glass epoxy board, perspex and plastic. They are then placed on the surface of SRR and their resonant frequencies in GHz obtained are 2.647, 2.863, 3.118 and 3.254 respectively. In Fig. 5.3, the transmission curves for these four samples are plotted. The dielectric constants of these samples are measured using cavity perturbation method [48] and the values obtained are 6.07, 3.571, 2.45 and 2.1 respectively and are shown in Table 5.2. In Fig. 5.4

Table 5.2: Resonant frequency and permittivity values used for drawing calibration curve.

Sample	f_0 **(GHz)**	**Permittivity** ε_r
Plastic	3.254	2.1
Perspex	3.118	2.45
Glass epoxy	2.863	3.571
Glass	2.647	6.07

we plot these resonant frequencies with their corresponding dielectric constants. It is observed that resonant frequency decreases as the dielectric constant of the material increases. Relative permittivity of any unknown test sample placed over the SRR can be extracted using the corresponding resonant frequency from this calibration graph.

The relative permittivities corresponding to the corrected resonant frequencies f for different temperatures are extracted from the calibration curve for the two samples and are given in Table 5.3. Figure 5.5 represents the transmission curve of SRR at different temperatures when perspex sample is placed over it. For calculating the temperature dependent real part of permittivity using the analytical equation (Eqn. 5.1), the following steps are taken. f_1 is the resonant frequency of test probe when no sample placed over it at room temperature and in this case it is 3.5613 GHz. f_2 is the calculated resonant frequency at different temperatures of the probe in the presence of the sample material. The values of f_2 are given as f in Table 5.3 and the calculated values of relative permittivity ε_r are also given in the same Table. It can be seen that there is only negligible variation between the calculated values and values obtained from the calibration curve. Figures showing comparison between the values by the two methods for the two samples at different temperatures are given as Fig. 5.6 and Fig. 5.7.

5.2.3 Discussions

From the values given in Table 5.3, we can see that as the temperature increases from 35°C to 55°C, the resonant frequency decreases and the dielectric constant increases accordingly. Analyzing the Table we observe that an increase of temperature by 20°C causes a small decrease in resonant frequency for both the samples. But the corresponding change observed in dielectric constant is noticeable. Perspex and plastic, show relatively small change in dielectric constant which is around 0.025 per degree Celsius.

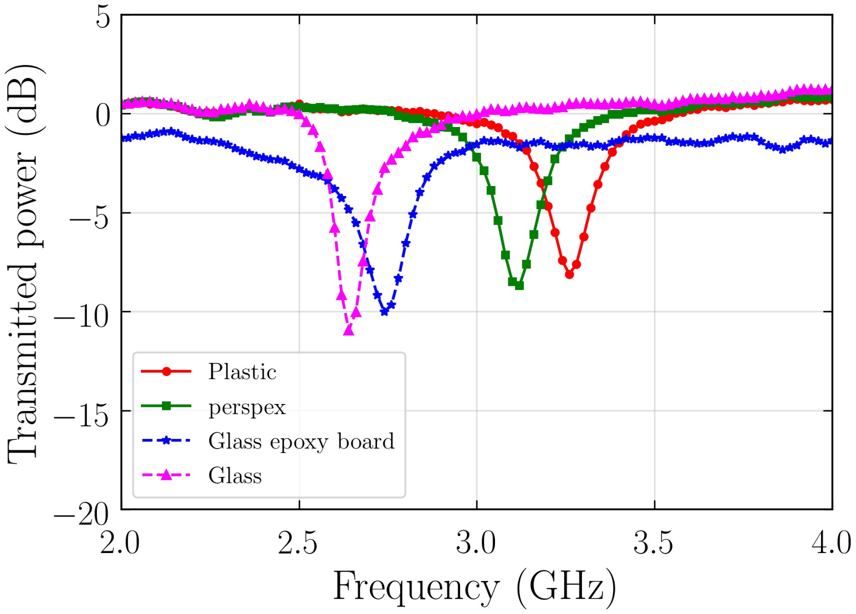

Figure 5.3: Transmission curves of SRR when different dielectric materials of known dielectric constant are placed on its surface.

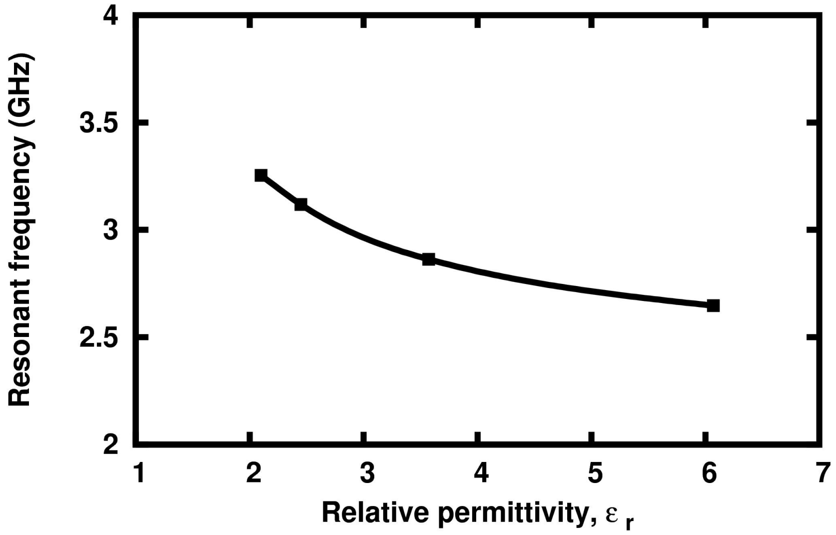

Figure 5.4: Calibration graph drawn between the resonant frequency and the relative permittivity of standard samples.

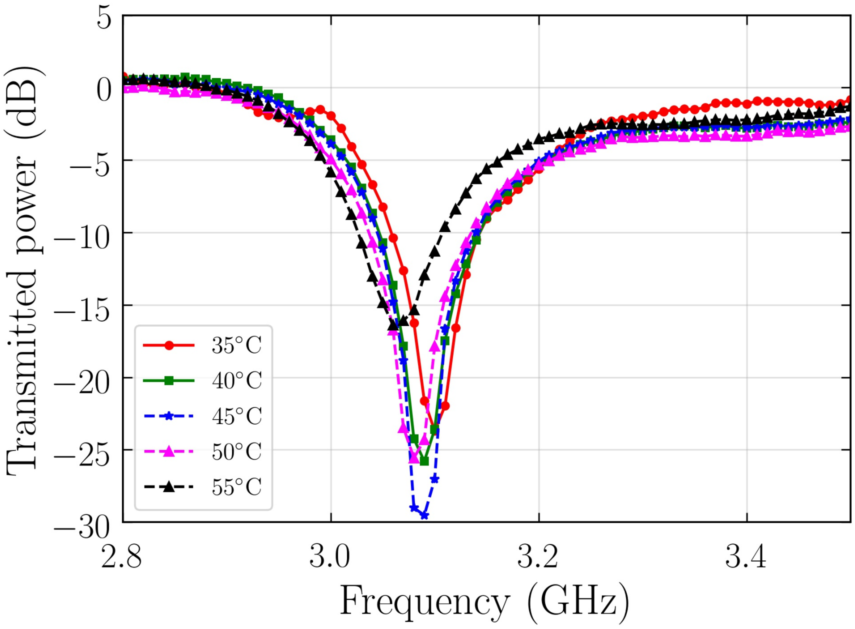

Figure 5.5: Transmission curves of SRR for different temperatures when sample is placed on its surface.

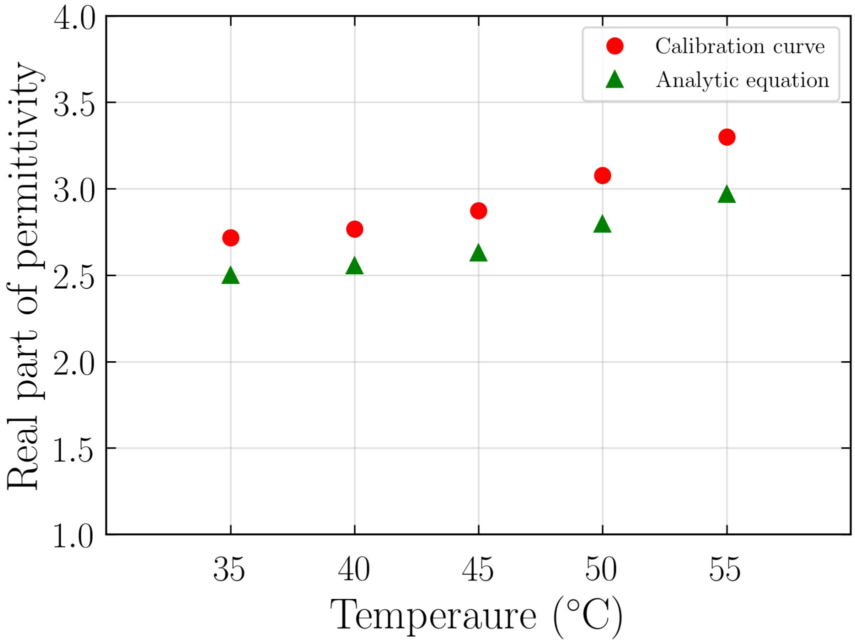

Figure 5.6: The comparison of the real part of the permittivity values obtained by calibration curve and analytical method for perspex sample.

Table 5.3: Resonant frequency and relative permittivity of various samples corresponding to different temperatures.

Sample	**Temperature (°C)**	f_{t1} **(GHz)**	$f = f_{t1} - (f_{r0} - f_{t0})$ **(GHz)**	**Real part of permittivity from the calibration graph (ε_r)**	**Real part of permittivity from equation (ε_r)**
Perspex	35	3.0920	3.0893	2.7182	2.4998
	40	3.0878	3.0753	2.7668	2.5551
	45	3.0807	3.0567	2.8732	2.6297
	50	3.0607	3.0166	3.0768	2.7954
	55	3.0495	2.9766	3.2997	2.9674
Plastic	35	3.2640	3.2613	2.0796	1.8775
	40	3.2543	3.2418	2.1188	1.9431
	45	3.2006	3.1766	2.2959	2.1713
	50	3.1882	3.1441	2.3814	2.2904
	55	3.1632	3.0903	2.5124	2.4959

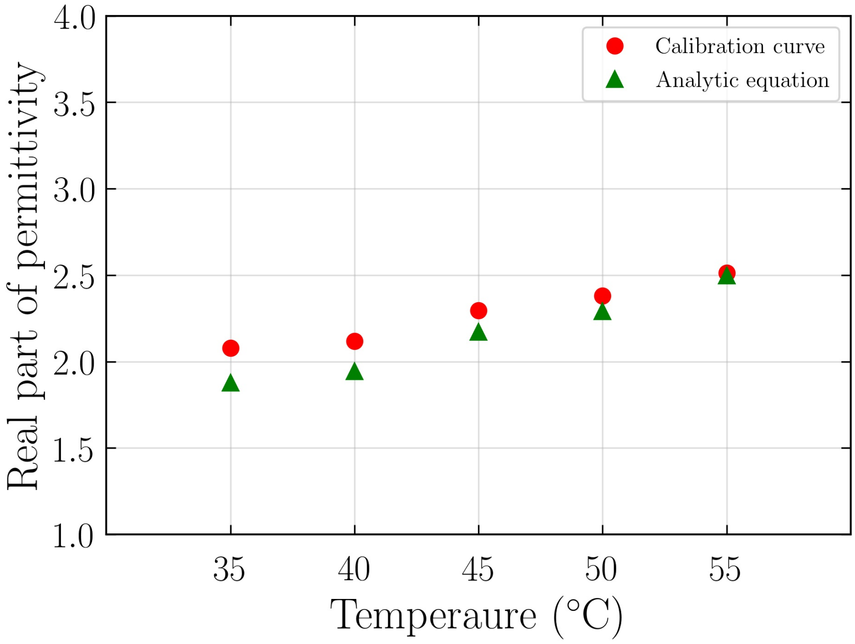

Figure 5.7: The comparison of the real part of the permittivity values obtained by calibration curve and analytical method for plastic sample.

5.3 Flame retardent circuit boards

Another set of samples used for the measurement of dielectric constant at different temperatures is Flame Retardant (FR) laminates used for Printed Circuit Boards (PCB) that have become essential part in any electronic/electromagnetic equipments. Basically they are dielectric materials with a thin layer of copper foil laminated on one or both sides. These PCB laminates (dielectrics) are made by using layers of cloth or paper along with a resin cured under temperature and pressure. Usually these laminates have 3 parts - a matrix (usually a resin), reinforcement (woven or non-woven glass fiber/paper/cotton) and a filler (usually ceramics). The materials as well as the procedures employed for making these FR laminates determines their mechanical and electrical properties. Desirable electrical properties of the PCB laminates are low dielectric constant ε (which allow rapid signal propagation), low dissipation factor tanδ (which enable it for high power applications) and thermal and frequency stability.

In different electronic circuits, even though they are protected from outer environmental temperature variations, the heat produced during operation of the various components in the circuit can affect the performance of the FR board substrate. The variation in electrical properties of the substrate can also affect the operation of the circuit as a whole. Capacitance changes in the circuit may produce some undesirable inter-electrode capacitances resulting in unwanted noises. In microwave patch antennas these dielectric changes may even change the operating wave length. Hence, the study of dependence of temperature on the electrical properties of FR laminates are an area that has to be given noticeable importance in designing microwave electronic circuits and antennas.

There are only a few attempts done in order to analyze the temperature dependence of dielectric constant of FR boards except those which are done by their manufacturers themselves. Kobayashi and Yu have tried to analyze the temperature dependence of normal and tangential components of complex permittivity of a copper clad laminated substrate using circular disc and circular cavity method [154]. The measurements are taken between -20°C and 60°C during heating and cooling. Roy *et al.* analyzed temperature dependence of substrate parameters of different materials like teflon-glass microwave laminates, RT duroid 2010 and quartz based composites [155]. Li *et al.* investigated the frequency and temperature dependence of dielectric properties of a glass fiber PCB substrate using voltage - capacitance technique [156]. The temperature dependence of dielectric constant and dissipation factor of printed circuit board on which a ring resonator is etched is studied by Heinola *et al.* in a temperature range from -30°C to 105°C [157]. A lengthy iteration method is used for the calculation of the dielectric constant and the dissipation factor. These methods to measure temperature dependence of the complex permittivity of FR boards require extensive sample preparation, bulky experimental setup and tedious calculations.

In this study, five different types of FR boards are used as samples for measurement of the temperature dependent permittivity. One each sample of FR2 and FR3 along with three samples of FR4 (FR4Brown, FR4White and FR4Yellow) are used.

5.3.1 Temperature dependence of SRR

As in the previous section, the temperature dependence of the resonant frequency of SRR test probe is analyzed initially. The resonance frequency of SRR at room temperature is denoted as f_{r0}. The resonant frequency at each temperature is noted asf_{t0} and Δf is the shift in the resonance frequency of SRR probe, due to temperature variation. The observations are given in Table 5.4.

Table 5.4: Resonant frequency of the test probe for different temperatures along with the resonant frequeny shifts.

Temperature (^0C)	**Resonant frequency (GHz) f_{t0}**	**Resonant frequency shift ($\Delta f = f_{r0} - f_{t0}$)**
33	3.60006	0
40	3.60000	0.00006
50	3.57489	0.02516
60	3.5499	0.05015
70	3.5494	0.05066
80	3.5292	0.07083

5.3.2 Measurements and results

The resonant frequencies are measured at different temperatures for the five chosen samples and the frequency variations and are given in Fig. 5.8 - 5.12. In all cases temperature is varied from room temperature (33^0C) to (80^0C). Fig. 5.8 and 5.9 are for FR2 and FR3 samples having thicknesses 1.6 mm respectively. Fig. 5.10, 5.11 and 5.12 depict resonant curves for three samples of FR4 which are FR4White (1.6 mm), FR4Brown (0.8 mm) and FR4Yellow (1.6 mm).

To draw the calibration curve, the resonant frequency of SRR with four standard samples used before are measured and given in Table 5.5 along with the permittivity values obtained from cavity perturbation method. Figure 5.13 gives the calibration curve drawn using these values. The real part of permittivity for different temperatures obtained from the calibration cure for FR2 and FR3 samples is given in Tables 5.6. The results obtained for the three FR4 samples are presented in Table 5.7.

The real parts of permittivity of each of the five samples at different temperatures are calculated using Eqn. 5.1 and are given in Tables 5.6 and 5.7 for comparison.

5.3.3 Discussions

Figures 5.14 - 5.18 show plots of comparison for values obtained from calculation using equation and from calibration curve for all the five samples. The comparison between the values obtained by two methods show that here is only negligible variations for the temperature dependent permittivity values.

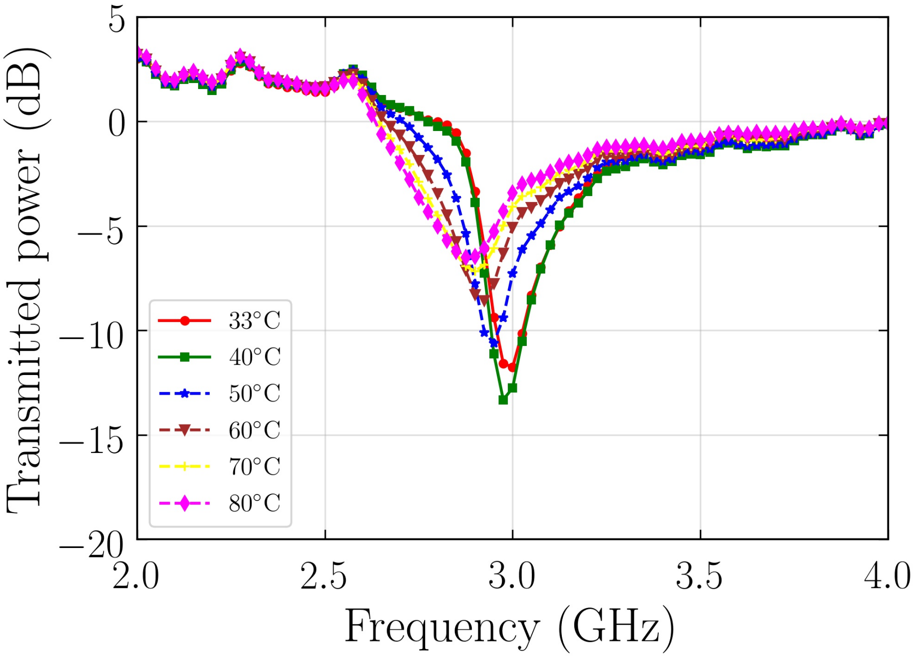

Figure 5.8: Resonant frequency curves of FR2 laminate for different temperatures.

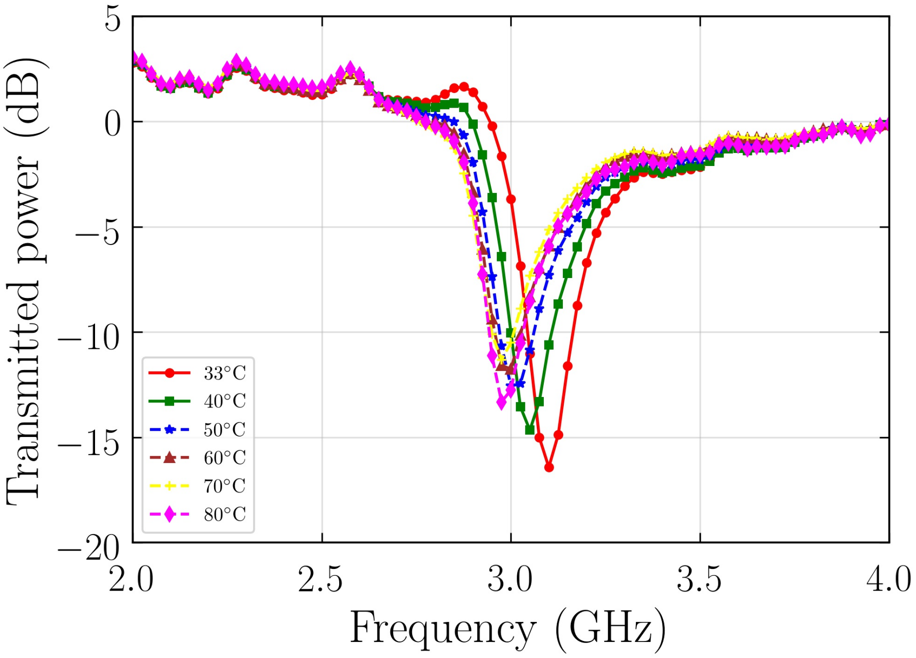

Figure 5.9: Resonant frequency curves of FR3 laminate for different temperatures.

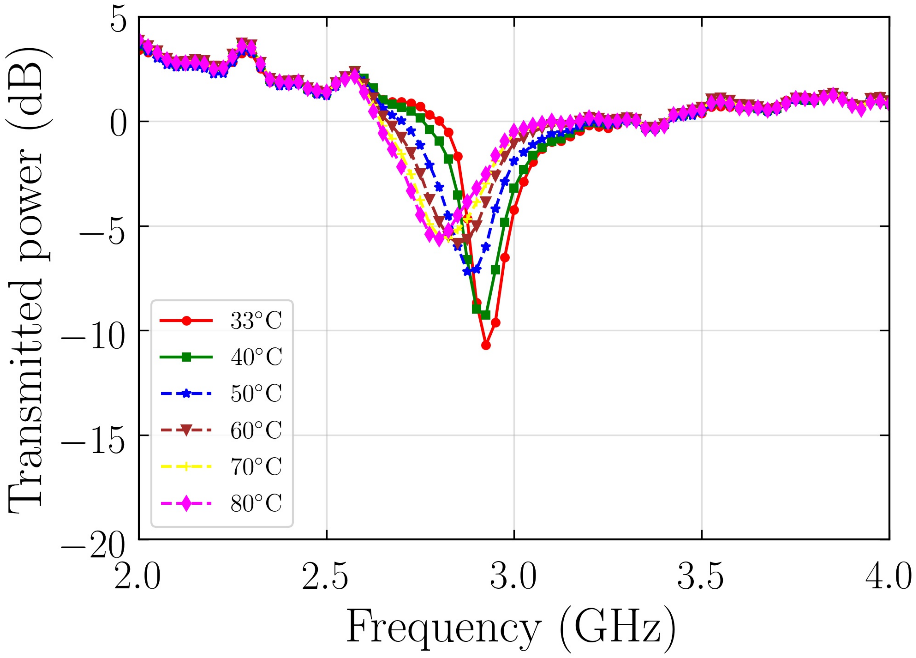

Figure 5.10: Resonant frequency curves of FR4Brown laminate for different temperatures.

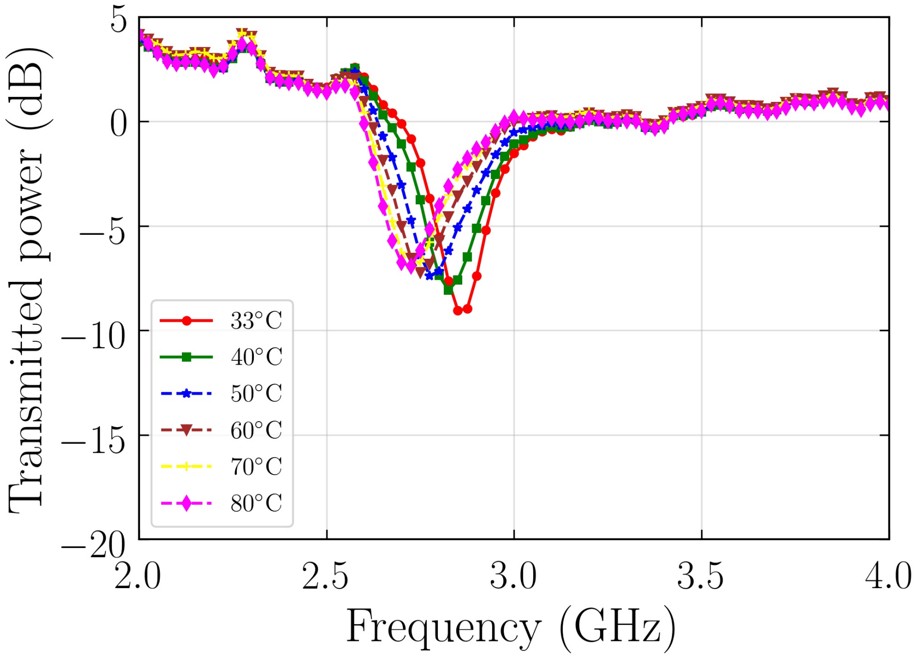

Figure 5.11: Resonant frequency curves of FR4White laminate for different temperatures.

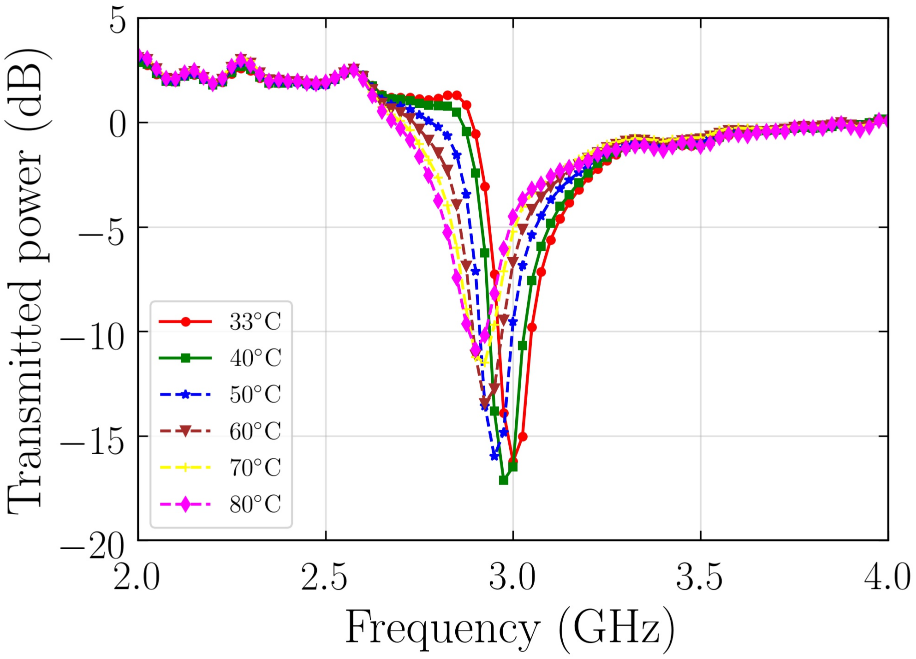

Figure 5.12: Resonant frequency curves of FR4Yellow laminate for different temperatures.

Table 5.5: Real part of permittivity and resonant frequency of samples for drawing calibration curve.

Sample	f_0 **(GHz)**	**Permittivity** ε_r
Air	3.60	1
Perspex	3.10	2.459
Glass epoxy	2.85	3.583
Glass	2.60	6.073

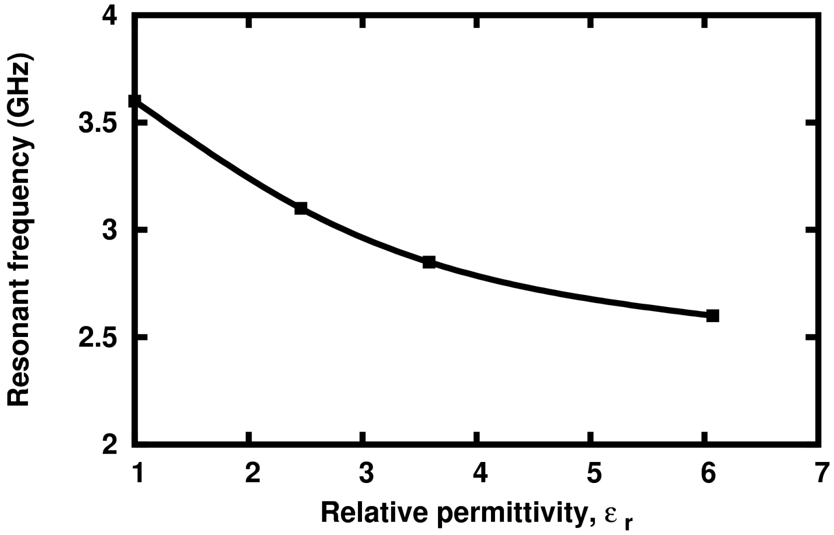

Figure 5.13: Calibration curve drawn between resonant frequency and relative permittivity for standard samples.

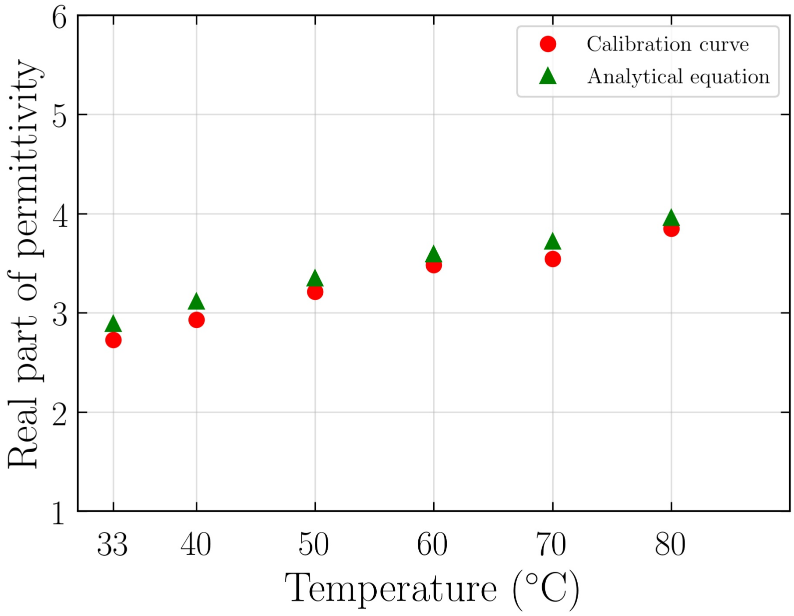

Figure 5.14: Comparison of the real part of permittivity values obtained by calibration curve and by analytical method for FR2 sample.

Table 5.6: Resonant frequency and real part of permittivity of different FR boards at different temperature.

Sample	**Temperature(^0C)**	$f_{t1}(GHz)$	$f = f_{t1} - (f_{r0} - f_{t0})$**(GHz)**	**Real part of permittivity from the calibration graph (ε_r)**	**Real part of permittivity from equation (ε_r)**
FR2	33	3.0248	3.0248	2.7278	2.8913
	40	2.9751	2.9750	2.9323	3.1179
	50	2.9494	2.9242	3.2122	3.3514
	60	2.92501	2.8748	3.4812	3.5910
	70	2.9000	2.8493	3.5458	3.7196
	80	2.8743	2.8035	3.8471	3.9594
FR3	33	3.125	3.125	2.3835	2.4917
	40	3.1000	3.0999	2.5503	2.5901
	50	3.0504	3.0252	2.7171	2.8976
	60	3.0019	2.9517	3.0400	3.2232
	70	3.0005	2.9499	3.0507	3.2315
	80	2.9751	2.9042	3.2767	3.4469

Table 5.7: Resonant frequency and real part of permittivity of different FR boards at different temperature.

Sample	**Temperature(^0C)**	$f_{t1}(GHz)$	$f = f_{t1} - (f_{r0} - f_{t0})$**(GHz)**	**Real part of permittivity from the calibration graph (ε_r)**	**Real part of permittivity from equation (ε_r)**
FR4White	33	2.8503	2.85037	3.5565	3.7145
	40	2.8252	2.82522	3.7503	3.8443
	50	2.7752	2.7501	4.3099	4.2542
	60	2.7498	2.6996	4.7404	4.5493
	70	2.7254	2.6748	5.0848	4.7004
	80	2.7251	2.6543	5.2462	4.8254
FR4Brown	33	2.9251	2.9251	3.1691	3.3472
	40	2.9246	2.9245	3.1906	3.3500
	50	2.8752	2.8500	3.5996	3.7160
	60	2.8500	2.7999	3.9225	3.9787
	70	2.8246	2.7740	4.0839	4.1201
	80	2.7996	2.7288	4.4170	4.3767
FR4Yellow	33	3.0000	3.0000	2.8139	3.0066
	40	2.9749	2.9748	2.964	3.1183
	50	2.9499	2.9247	3.1583	3.3491
	60	2.92525	2.8750	3.4597	3.5930
	70	2.92521	2.8750	3.4812	3.5930
	80	2.8999	2.8290	3.7503	3.8244

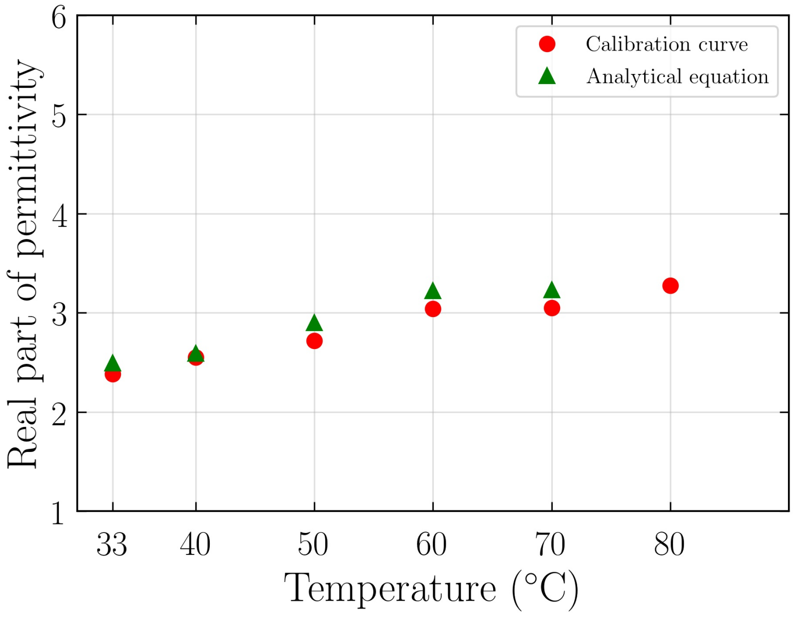

Figure 5.15: Comparison of the real part of permittivity values obtained by calibration curve and by analytical method for FR3 sample.

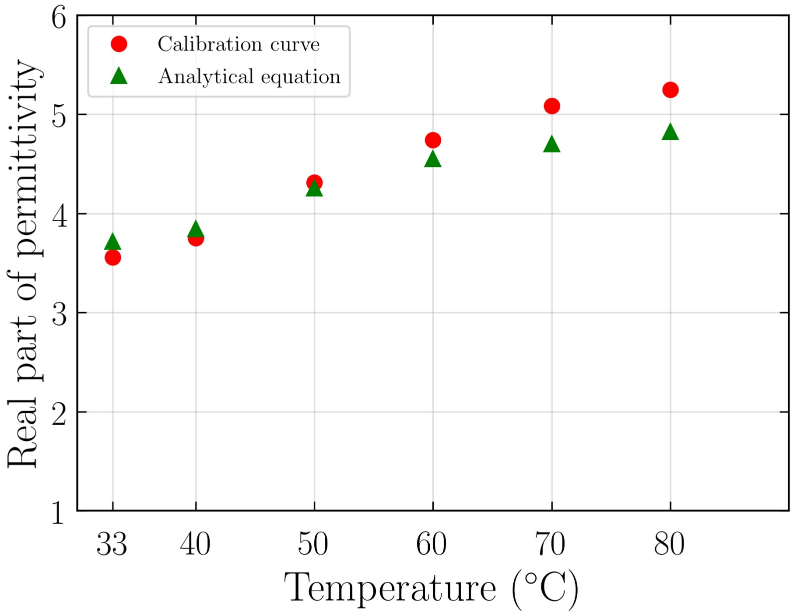

Figure 5.16: Comparison of the real part of permittivity values obtained by calibration curve and by analytical method for FR4White sample.

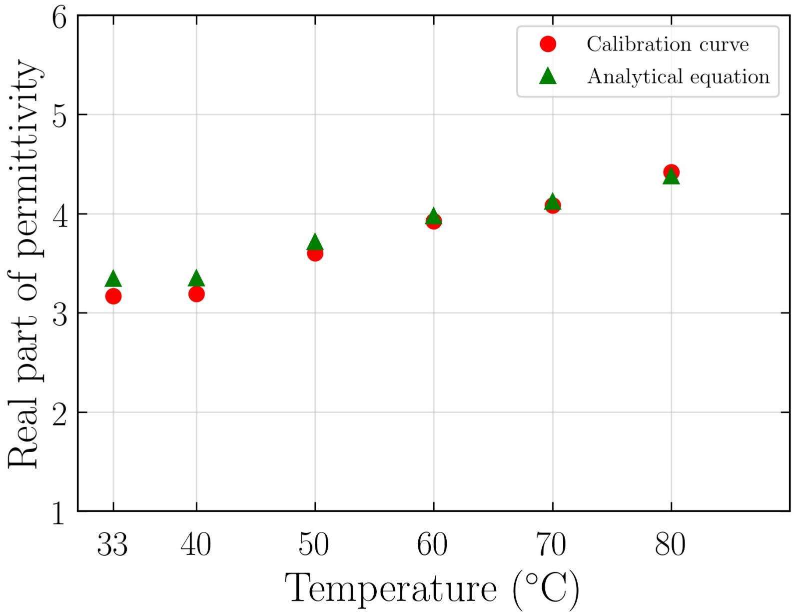

Figure 5.17: Comparison of the real part of permittivity values obtained by calibration curve and by analytical method for FR4Brown sample.

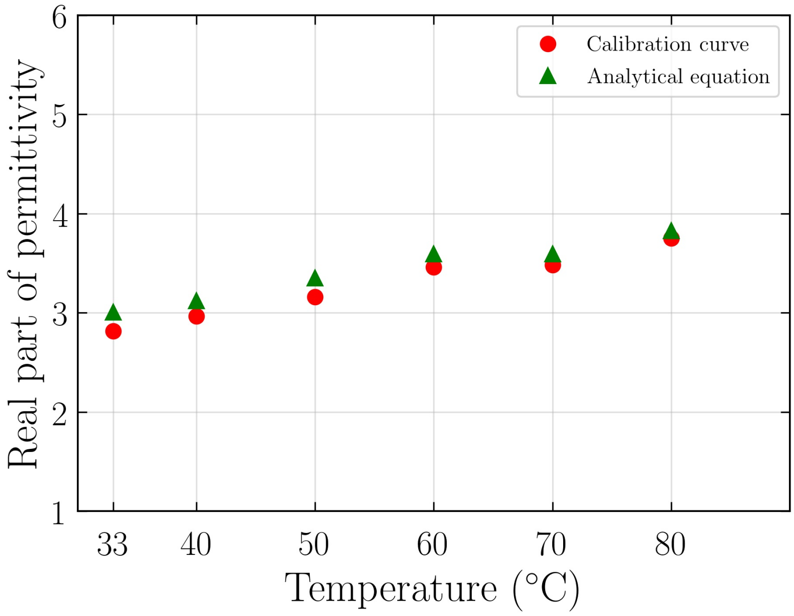

Figure 5.18: Comparison of the real part of permittivity values obtained by calibration curve and by analytical method for FR4Yellow sample.

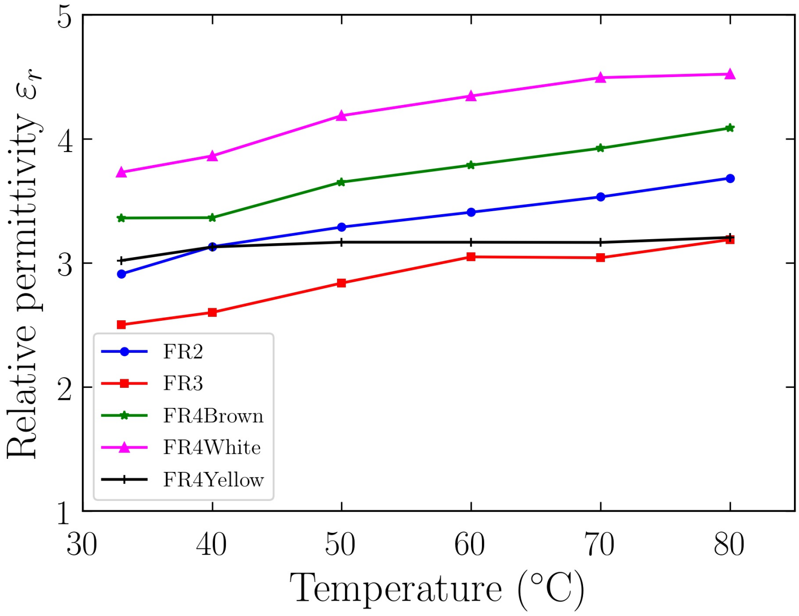

Figure 5.19: Variation of real part of permittivity with temperature for five different samples.

Figure 5.19 shows the variation of the real part of permittivity with the increase in the temperature for the five samples used for the study which show an increase with increasing temperature. From the figure the variation in the permittivity can be found to be not very negligible (0.2/10° C).

In electronic/electromagnetic systems handling relatively high power, there is a very strong chance for the increase of temperature to not so small changes, which may result in unwanted noise factors owing to the change of permittivity values.

To verify the experimental results, simulations using HFSS are used. For each temperature, the permittivity values obtained from the experiments for the sample FR4white is assigned as the material permittivity and simulations are carried out to obtain the resonance curve. The transmission curves obtained for both experiment and simulation are shown in Fig. 5.20(a) and 5.20(b). The curve clearly show the decrease in the resonant frequency with the increase in the temperature.

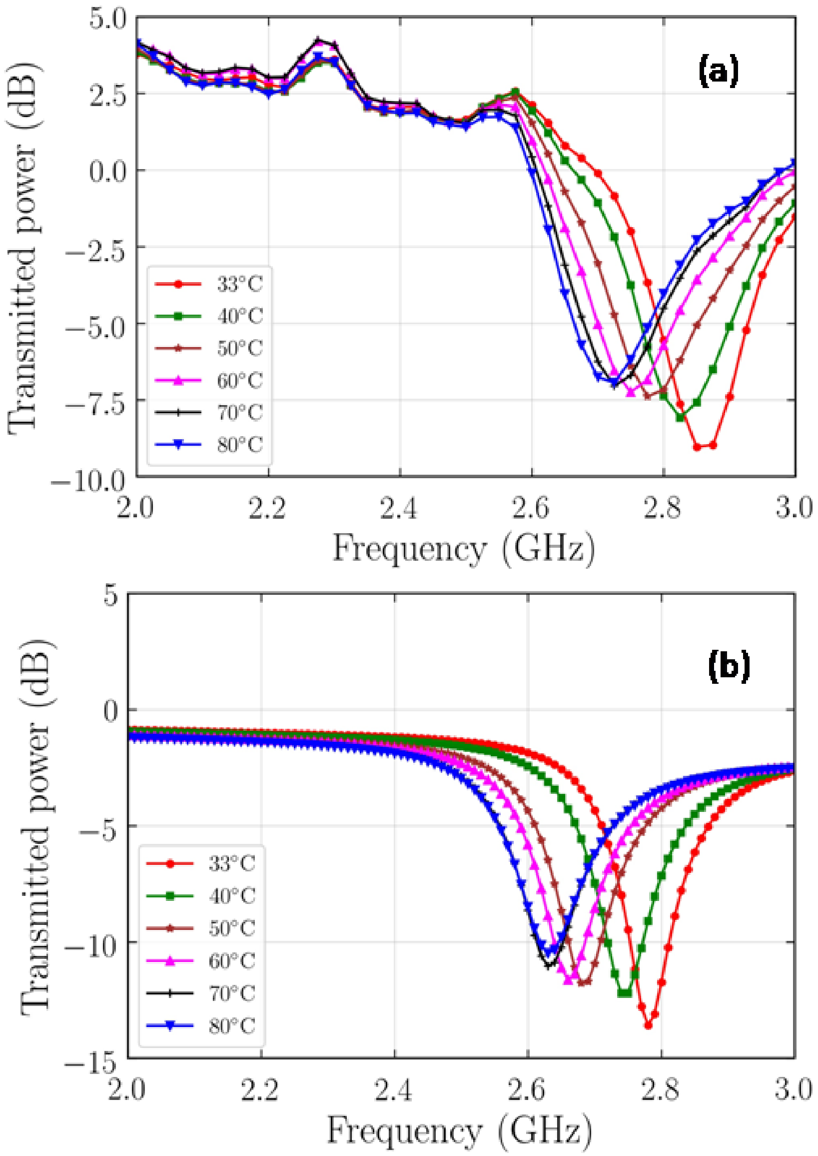

Figure 5.20: Resonant frequency curves of sample FR4white for different temperatures obtained by a) experiment and b) simulation.

Table 5.8: Resonant frequencies at different temperatures for FR4(white) sample from experiment and numerical simulation.

Temperature °C	**Resonant frequency from Experiment (GHz)**	**Resonant frequency from simulation (GHz)**
33	2.850378	2.78
40	2.824603	2.74
50	2.749488	2.69
60	2.699077	2.66
70	2.673912	2.63
80	2.654017	2.63

5.4 Wax samples

Three different waxes are chosen as a third set of sample for study of temperature dependent dielectric constant. Several industrial and household applications like lubricants, cosmetics, candles etc. utilizes the diverse properties of waxes. Like all dielectrics, structural and electrical properties of waxes are dependent upon temperature. There are several techniques existing for measurement of relative permittivity of dielectric samples at higher temperatures. Analysis of variations in dielectric constant with temperature of the material shellac is done by Srivastava *et. al.* [158]. A study on electric properties such as dielectric constant and dielectric loss is conducted in the p-band microwave frequencies for the solid samples of bees wax, paraffin wax and micro crystalline wax using Von Hippel method at room temperatures [159]. The analysis in the above referred work is done for wax samples after heat treatment also. But a detailed study on permittivity variation of wax samples under continuous variation of temperature is not found in the literature. Here the study of temperature dependence of dielectric constant of three wax samples (bees wax, bran wax and paraffin wax) is carried out by using split ring resonator (SRR).

5.4.1 Temperature dependence of SRR

Since the environmental conditions affect the sensitivity of the test probe, the resonant frequency data for the calibration need to be taken before performing the permittivity

Table 5.9: Resonant frequency of the test probe for different temperatures along with the resonant frequeny shifts.

Temperature (^0C)	**Resonant frequency (GHz) f_{t0}**	**Resonant frequency shift($\Delta f = f_{r0} - f_{t0}$)**
30	3.4578	0
35	3.4333	0.0245
40	3.4184	0.0394
45	3.4039	0.0544
50	3.3898	0.0680
55	3.3710	0.0868
60	3.3518	0.1060

measurement. As in the earlier cases, the resonant frequency of SRR test probe alone is measured at different temperatures and the values are represented as f_{t0} along with the shift in resonant frequency (Δf) and are given in Table 5.9.

5.4.2 Measurements and results

The calibration curve has been drawn between resonant frequency of SRR and relative permittivity of samples. For this we have selected four samples - glass, glass epoxy board, perspex and plastic. They are then placed on the surface of SRR (Fig. 5.2) and their resonant frequencies in GHz obtained are 2.48, 2.8797, 3.0398 and 3.1199 respectively. From the cavity perturbation method [48] we obtain the dielectric constants of these samples as 6.07, 3.58, 2.45 and 2.1 respectively. Fig. 5.21 is the calibration curve thus obtained. It is observed that resonant frequency decreases as the dielectric constant of the material increases. Relative permittivity of any unknown test sample in close contact with the surface of the SRR can be extracted from this calibration curve if corresponding resonant frequency of SRR - sample system lies on the curve. Table 5.10 gives the resonant frequency and permittivity values used for drawing the calibration curve.

Different test samples of waxes are placed on the SRR and corresponding resonant frequencies are measured and are represented as f_{t1}. The shift in resonant frequency ($f_{r0} - f_{t0}$) for each temperature is calculated as a correction factor and subtracted it from f_{t1}. The obtained resonant frequency f is the corrected resonant frequency. The values

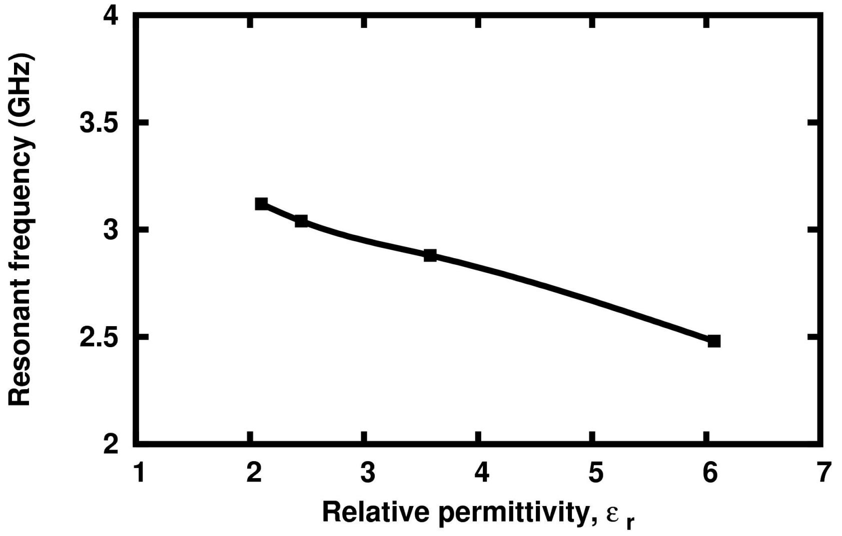

Figure 5.21: Calibration curve between the resonant frequency and the relative permittivity of four standard samples.

Table 5.10: Real part of permittivity and resonant frequency of samples for drawing calibration curve.

Sample	f_0 **(GHz)**	**Permittivity** ε_r
Plastic	3.1199	2.1
Perspex	3.0398	2.45
Glass epoxy	2.8797	3.58
Glass	2.4800	6.07

are presented in Table 5.11.

The permittivity values corresponding to each of the resonant frequencies (f) is found out from the calibration curve and are given in the same Table. The real part of permittivity of the three wax samples at different temperatures are calculated using Eqn. 5.1 and are given in Table 5.11 for comparison. Figs. 5.22 and 5.23 show the variation of relative permittivity of the three wax samples with increasing temperature obtained using calibration curve and analytical equation respectively.

5.4.3 Discussions

The resonant frequency of SRR decreases as the temperature of the sample in contact with it increases. This is due to an increase in relative permittivity with increase in tempera-

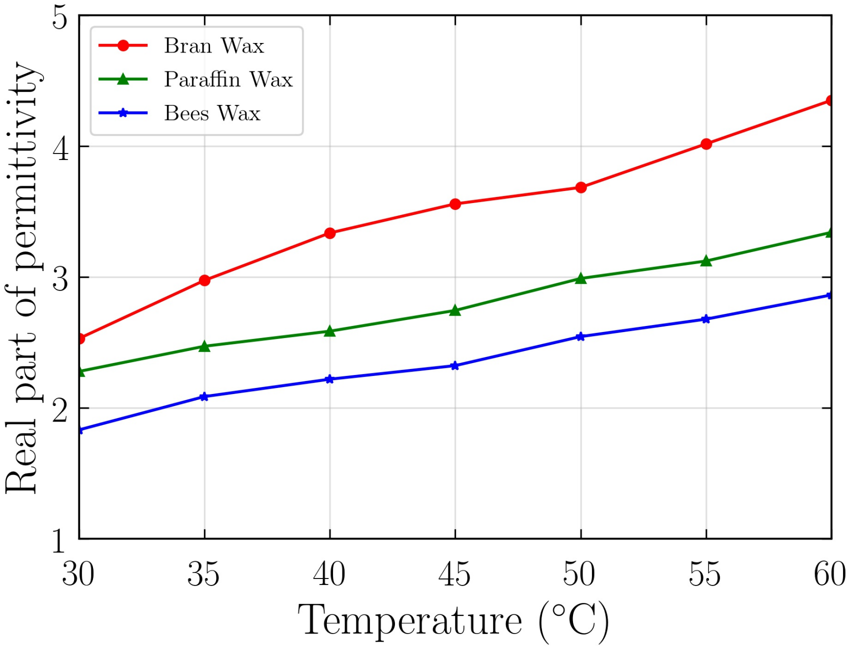

Figure 5.22: Relative permittivity variation with temperature for bran wax, paraffin wax and bees wax samples obtained from calibration curve.

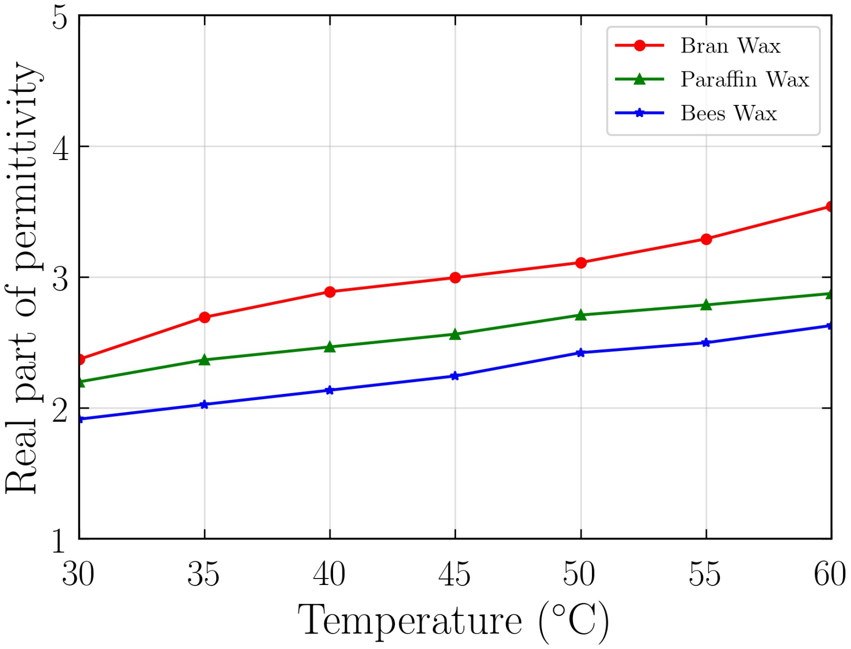

Figure 5.23: Relative permittivity variation with temperature for bran wax, paraffin wax and bees wax samples obtained from analytical equation.

Table 5.11: Resonant frequency and relative permittivity of wax samples corresponding to different temperatures.

Sample	**Temperature(^0C)**	$f_{t1}(GHz)$	$f = f_{t1} - (f_{r0} - f_{t0})$**(GHz)**	**Real part of permittivity from the calibration graph (ε_r)**	**Real part of permittivity from equation (ε_r)**
Bran Wax	30	3.044	3.032	2.5298	2.3707
	35	2.989	2.953	2.9737	2.6922
	40	2.960	2.908	3.3361	2.8872
	45	2.950	2.884	3.5582	2.9950
	50	2.939	2.859	3.6840	3.1101
	55	2.919	2.821	4.0166	3.2910
	60	2.889	2.771	4.3496	3.5405
Paraffin Wax	30	3.090	3.077	2.2785	2.1985
	35	3.070	3.033	2.4708	2.3667
	40	3.06	3.008	2.5859	2.4657
	45	3.05	2.984	2.7444	2.5630
	50	3.03	2.949	2.9886	2.7092
	55	3.03	2.931	3.1218	2.7864
	60	3.03	2.911	3.3410	2.8739
Bees Wax	30	3.168	3.156	1.8321	1.9138
	35	3.160	3.124	2.0864	2.0265
	40	3.146	3.094	2.2192	2.1353
	45	3.131	3.065	2.3229	2.2436
	50	3.100	3.019	2.5447	2.4218
	55	3.099	3.000	2.6779	2.4978
	60	3.087	2.968	2.8628	2.6292

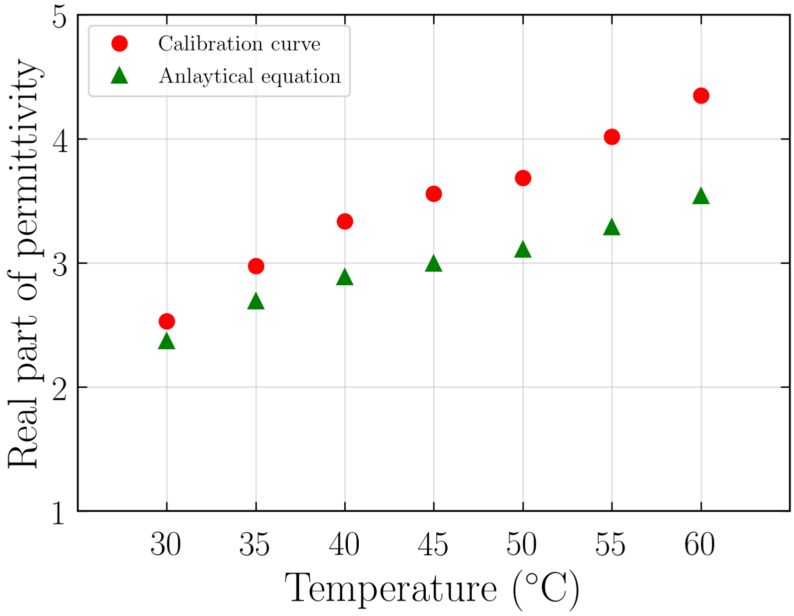

Figure 5.24: Comparison of the real part of permittivity values obtained by calibration curve and by analytical method for Bran wax.

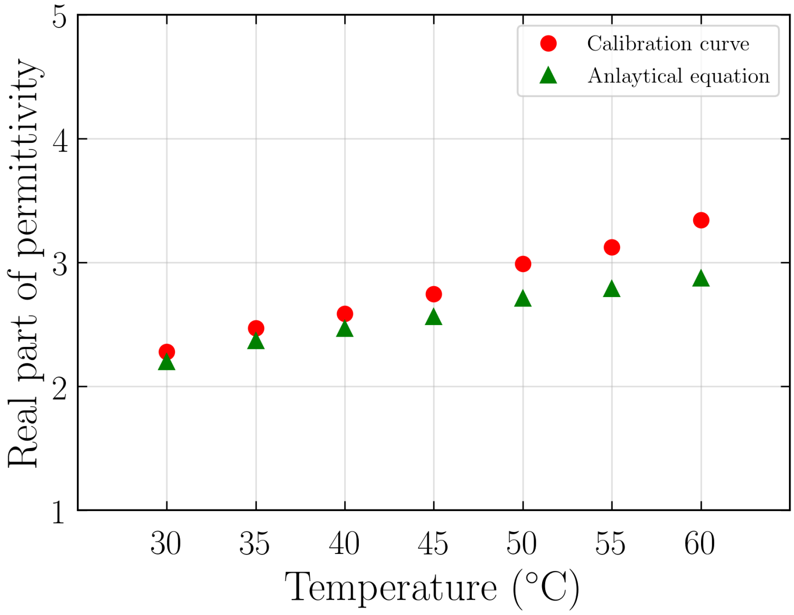

Figure 5.25: Comparison of the real part of permittivity values obtained by calibration curve and by analytical method for Paraffin wax.

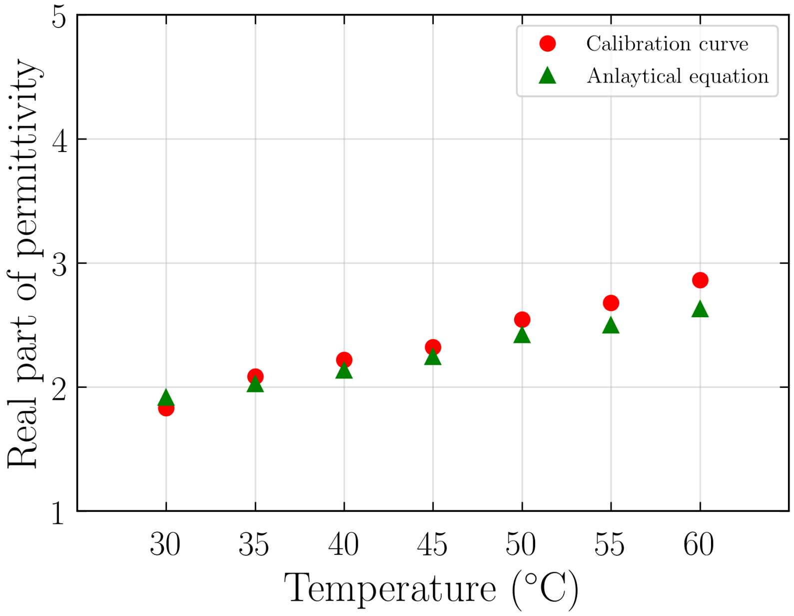

Figure 5.26: Comparison of the real part of permittivity values obtained by calibration curve and by analytical method for Bees wax.

ture. By analyzing Fig. 5.22, Fig. 5.23 and Table 5.11 we can conclude that the relative permittivity varies almost linearly with temperature for wax samples. For an increase of 30°C in temperature, the bran wax showed a larger increase in relative permittivity (1.8198). For the same increase in temperature, bees wax and paraffin wax showed an increase by 1.0307 and 1.0625 respectively.

Fig. 5.24 -5.26 show plots of comparison for values obtained by calibration curve and by analytical equation for the three samples of waxes. The figures show a close agreement in values of real part of permittivity calculated using both the methods.

5.5 Conclusion

The temperature dependence of real part of relative permittivities of the set of samples - two polymer samples (plastic and perspex), Five Flame Retardant laminates (FR2, FR3, FR4White, FR4Brown and FR4Yellow) and three wax samples (Bran wax, Bees wax and Paraffin wax) - are carried out using SRR methods. By using extrapolation method, temperature dependence of dielectric constants of any sample with a planar surface can be found out provided its resonant frequency is on calibration curve. This method proves to be a precise and easy measurement technique compared to many other characterization methods to find the temperature dependence of dielectric constant. This method may be extended to a wide range of temperatures by properly modifying the experimental setup.

The results obtained by calibration curve are also verified by the proposed numerical method and is found to be in quite good agreement.

Chapter 6

Summary and Scope for Future Works

Investigations on the applications of resonant properties of Split Ring Resonators show that it can be used as a sensor for dielectric constant measurements. The proposed methods have advantages of simplicity and efficiency over other existing methods. The major findings of the research and the scope for the future works are discussed in this chapter.

In this thesis a novel and efficient complex permittivity measurement techniques based on metamaterial inspired Split Ring Resonator is presented. The method introduced is highly effective for precise determination of permittivity of dielectric materials having low and moderate values of dielectric constant and loss factor. The numerical equations developed for the effective capacitance and resonant frequency of the SRR and the real and the imaginary parts of the permittivity are based on a quasi-static approximation in the assumption that the size of meta-molecule SRR is very much less than the wavelength of the operating electromagnetic wave. Along with the analytical method for determining the complex permittivity, a simple and straight forward method for finding the real part of permittivity based on a calibration curve using the SRR is also introduced. The temperature dependent permittivity of a variety of samples having importance in electrical, electronic and electromagnetic applications along with those field belonging to food and cosmetic industries are analyzed here. The measured results are validated using electromagnetic simulation method showing the accuracy of the proposed equations and methods.

6.1 Major findings

The thesis presents the following major findings.

- The presence of the electric field distribution is conclusively proved on either side of the resonator structure which in earlier studies were taken only on one surface, a result leading to the important modification in the effective capacitance of the Slit Ring Resonator.
- Based on the modified effective capacitance of the SRR, a new equation for the resonant frequency is derived which closely agrees with the values obtained by measurements.
- A novel and efficient SRR based permittivity technique was introduced by deriving new analytical equation for both real and imaginary parts of complex permittivity for dielectric samples.
- Another SRR based extrapolation technique is introduced for determining the real part of the permittivity by drawing a calibration curve in terms of known value of dielectric constant of some standard samples.

- The verification of the two proposed methods for determining the permittivity is done by using electromagnetic simulation software.
- The temperature dependent variation in the value of dielectric constant are analyzed for different samples having state-of-the-art commercial and industrial importance.

6.2 Scope for future works

The dielectric characterization studies of different materials can be carried out in an easy and accurate manner by employing proposed techniques and equations. A wide variety of scanning applications such as biomedical imaging, non-destructive surface imperfection testing etc. can be carried out by making suitable instrumentation based on the above methods. The quality analysis of the food samples with a special emphasis on adulteration can be evolved into a standard quality checking procedure. In situations where high power electronic/electromagnetic circuitry is used, the possibility of unexpected non-linear noise effects due to temperature changes occurring in circuit board laminates may be identified which may lead to devices having ultra high accuracy.

6.3 Concluding remarks

After deriving the required analytical equations a novel and efficient complex permittivity measurement technique is introduced along with an easy calibration curve based method for determining the real part of permittivity. The obtained results are validated using simulations. The temperature dependent variations occurring in different types of dielectric materials are carried out in detail. The study may have a wide variety of potential applications in different quality enhancement tests and accurate measurement outputs.

Bibliography

[1] J. C. Bose, "On the rotation of plane of polarisation of electric wave by a twisted structure," *Proceedings of the Royal Society of London*, vol. 63, no. 389-400, pp. 146–152, 1898.

[2] W. E. Kock, "Metal-lens antennas," *Proceedings of the IRE*, vol. 34, no. 11, pp. 828–836, 1946.

[3] W. Rotman, "Plasma simulation by artificial dielectrics and parallel-plate media," *IRE Transactions on Antennas and Propagation*, vol. 10, no. 1, pp. 82–95, 1962.

[4] E. Yablonovitch, "Photonic band-gap structures," *JOSA B*, vol. 10, no. 2, pp. 283–295, 1993.

[5] R. M. Walser, "Electromagnetic metamaterials," in *Complex Mediums II: Beyond Linear Isotropic Dielectrics*, vol. 4467, pp. 1–16, International Society for Optics and Photonics, 2001.

[6] V. G. Veselago, "The electrodynamics of substances with simultaneously negative values of and μ," *Soviet physics uspekhi*, vol. 10, no. 4, p. 509, 1968.

[7] J. B. Pendry, A. Holden, W. Stewart, and I. Youngs, "Extremely low frequency plasmons in metallic mesostructures," *Physical review letters*, vol. 76, no. 25, p. 4773, 1996.

[8] J. B. Pendry, A. Holden, D. Robbins, and W. Stewart, "Low frequency plasmons in thin-wire structures," *Journal of Physics: Condensed Matter*, vol. 10, no. 22, p. 4785, 1998.

[9] J. B. Pendry, A. J. Holden, D. Robbins, and W. Stewart, "Magnetism from conductors and enhanced nonlinear phenomena," *IEEE Trans. Microw. Theory Techn.*, vol. 47, no. 11, pp. 2075–2084, 1999.

[10] D. R. Smith, W. J. Padilla, D. Vier, S. C. Nemat-Nasser, and S. Schultz, "Composite medium with simultaneously negative permeability and permittivity," *Physical review letters*, vol. 84, no. 18, p. 4184, 2000.

[11] D. R. Smith and N. Kroll, "Negative refractive index in left-handed materials," *Physical Review Letters*, vol. 85, no. 14, p. 2933, 2000.

[12] D. Smith, S. Schultz, P. Markoš, and C. Soukoulis, "Determination of effective permittivity and permeability of metamaterials from reflection and transmission coefficients," *Physical Review B*, vol. 65, no. 19, p. 195104, 2002.

[13] R. A. Shelby, D. R. Smith, and S. Schultz, "Experimental verification of a negative index of refraction," *science*, vol. 292, no. 5514, pp. 77–79, 2001.

[14] R. Shelby, D. Smith, S. Nemat-Nasser, and S. Schultz, "Microwave transmission through a two-dimensional, isotropic, left-handed metamaterial," *Applied Physics Letters*, vol. 78, no. 4, pp. 489–491, 2001.

[15] Y. K. Srivastava, L. Cong, and R. Singh, "Dual-surface flexible thz fano metasensor," *Applied Physics Letters*, vol. 111, no. 20, p. 201101, 2017.

[16] D.-C. Wang, S. Sun, Z. Feng, W. Tan, and C.-W. Qiu, "Multipolar-interference-assisted terahertz waveplates via all-dielectric metamaterials," *Applied Physics Letters*, vol. 113, no. 20, p. 201103, 2018.

[17] A. Xomalis, I. Demirtzioglou, Y. Jung, E. Plum, C. Lacava, P. Petropoulos, D. J. Richardson, and N. I. Zheludev, "Picosecond all-optical switching and dark pulse generation in a fibre-optic network using a plasmonic metamaterial absorber," *Applied Physics Letters*, vol. 113, no. 5, p. 051103, 2018.

[18] A. Di Falco, M. Ploschner, and T. F. Krauss, "Flexible metamaterials at visible wavelengths," *New Journal of Physics*, vol. 12, no. 11, p. 113006, 2010.

[19] C. Enkrich, M. Wegener, S. Linden, S. Burger, L. Zschiedrich, F. Schmidt, J. Zhou, T. Koschny, and C. Soukoulis, "Magnetic metamaterials at telecommunication and visible frequencies," *Physical review letters*, vol. 95, no. 20, p. 203901, 2005.

[20] H.-J. Lee and J.-G. Yook, "Biosensing using split-ring resonators at microwave regime," *Applied Physics Letters*, vol. 92, no. 25, p. 254103, 2008.

[21] H.-J. Lee, H.-S. Lee, K.-H. Yoo, and J.-G. Yook, “Dna sensing using split-ring resonator alone at microwave regime,” *Journal of Applied Physics*, vol. 108, no. 1, p. 014908, 2010.

[22] K. Sikha Simon, S. P. Chakyar, J. Andrews, and P. Joseph V, “Metamaterial split ring resonator as a sensitive mechanical vibration sensor,” in *American Institute of Physics Conference Series*, vol. 1849, 2017.

[23] R. Melik, E. Unal, N. K. Perkgoz, C. Puttlitz, and H. V. Demir, “Metamaterial based telemetric strain sensing in different materials,” *Opt. Exp.*, vol. 18, no. 5, pp. 5000–5007, 2010.

[24] R. Melik, E. Unal, N. K. Perkgoz, C. Puttlitz, and H. V. Demir, “Flexible metamaterials for wireless strain sensing,” *Appl. Phys. Lett.*, vol. 95, no. 18, p. 181105, 2009.

[25] J. Carnerero-Cano, G. Galindo-Romera, J. J. Martínez-Martínez, and F. J. Herraiz-Martínez, “A contactless dielectric constant sensing system based on a split-ring resonator-loaded monopole,” *IEEE Sensors Journal*, vol. 18, no. 11, pp. 4491–4502, 2018.

[26] N. K. Tiwari, S. P. Singh, and M. J. Akhtar, “Near field planar microwave probe sensor for nondestructive condition assessment of wood products,” *Journal of Applied Physics*, vol. 123, no. 22, p. 224502, 2018.

[27] S. P. Chakyar, S. K. Simon, C. Bindu, J. Andrews, and V. Joseph, “Complex permittivity measurement using metamaterial split ring resonators,” *Journal of Applied Physics*, vol. 121, no. 5, p. 054101, 2017.

[28] S. P. Chakyar, J. Andrews, and V. Joseph, “Temperature dependence of relative permittivity: A measurement technique using split ring resonators,” *International Journal of Mechanical, Aerospace, Industrial, Mechatronic and Manufacturing Engineering*, vol. 10, no. 6, pp. 1030–1033, 2016.

[29] B.-I. Wu, W. Wang, J. Pacheco, X. Chen, T. M. Grzegorczyk, and J. A. Kong, “A study of using metamaterials as antenna substrate to enhance gain,” *Progress In Electromagnetics Research*, vol. 51, pp. 295–328, 2005.

[30] S. Enoch, G. Tayeb, P. Sabouroux, N. Guérin, and P. Vincent, “A metamaterial for directive emission,” *Physical Review Letters*, vol. 89, no. 21, p. 213902, 2002.

[31] J. Kizhakooden, J. Jose, N. Paul, S. K. Simon, S. P. Chakyar, J. Andrews, and V. Joseph, “Metamaterial inspired featherlight artificial plasma horn antenna for astronomical and communication applications,” *Microwave and Optical Technology Letters*.

[32] H. Araujo, E. Bolzan, I. Casella, C. Capovilla, and L. Kretly, “Metamaterial-based antenna for rfid applications,” in *2014 IEEE Brasil RFID*, pp. 1–3, IEEE, 2014.

[33] H. Nakano, J. Shibayama, and J. Yamauchi, *Metamaterial-Based Antennas and a Metasurface-Based Terahertz Frequency Splitter*, pp. 159–181. Cham: Springer International Publishing, 2018.

[34] P. Yu, L. V. Besteiro, Y. Huang, J. Wu, L. Fu, H. H. Tan, C. Jagadish, G. P. Wiederrecht, A. O. Govorov, and Z. Wang, “Broadband metamaterial absorbers,” *Advanced Optical Materials*, 2018.

[35] H. Tao, N. I. Landy, C. M. Bingham, X. Zhang, R. D. Averitt, and W. J. Padilla, “A metamaterial absorber for the terahertz regime: design, fabrication and characterization,” *Optics express*, vol. 16, no. 10, pp. 7181–7188, 2008.

[36] P. Yu, J. Wu, E. Ashalley, A. Govorov, and Z. Wang, “Dual-band absorber for multispectral plasmon-enhanced infrared photodetection,” *Journal of Physics D: Applied Physics*, vol. 49, no. 36, p. 365101, 2016.

[37] T. V. Teperik, S. N. Burokur, A. de Lustrac, G. Sabanowski, and G.-P. Piau, “Experimental validation of an ultra-thin metasurface cloak for hiding a metallic obstacle from an antenna radiation at low frequencies,” *Applied Physics Letters*, vol. 111, no. 5, p. 054105, 2017.

[38] L. Cai, J. Wen, D. Yu, Z. Lu, X. Chen, and X. Zhao, “Beam steering of the acoustic metasurface under a subwavelength periodic modulation,” *Applied Physics Letters*, vol. 111, no. 20, p. 201902, 2017.

[39] S. Xiao, S. T. Tang, and Z. Yang, “Voltage-tunable acoustic metasheet with highly asymmetric surfaces,” *Applied Physics Letters*, vol. 111, no. 19, p. 194101, 2017.

[40] P. Jung, A. V. Ustinov, and S. M. Anlage, “Progress in superconducting metamaterials,” *Superconductor Science and Technology*, vol. 27, no. 7, p. 073001, 2014.

[41] S. M. Anlage, "The physics and applications of superconducting metamaterials," *Journal of Optics*, vol. 13, no. 2, p. 024001, 2010.

[42] H.-T. Zhong, X.-X. Yang, X.-T. Song, Z.-Y. Guo, and F. Yu, "Wideband metamaterial array with polarization-independent and wide incident angle for harvesting ambient electromagnetic energy and wireless power transfer," *Applied Physics Letters*, vol. 111, no. 21, p. 213902, 2017.

[43] L.-F. Chen, C. Ong, C. Neo, V. Varadan, and V. K. Varadan, *Microwave electronics: measurement and materials characterization*. John Wiley & Sons, 2004.

[44] S. L. Severo, A. A. de Salles, B. Nervis, and B. K. Zanini, "Non-resonant permittivity measurement methods," *Journal of Microwaves, Optoelectronics and Electromagnetic Applications (JMOe)*, vol. 16, no. 1, pp. 297–311, 2017.

[45] B. Kim, V. Kazmirenko, Y. Prokopenko, Y. Poplavko, and S. Baik, "Non-resonant, electrode-less method for measuring the microwave complex permittivity of ferroelectric thin films," *Measurement Science and Technology*, vol. 16, no. 9, p. 1792, 2005.

[46] D. K. Ghodgaonkar, V. V. Varadan, and V. K. Varadan, "A free-space method for measurement of dielectric constants and loss tangents at microwave frequencies," *IEEE Transactions on Instrumentation and measurement*, vol. 38, no. 3, pp. 789–793, 1989.

[47] S. Biju Kumar, U. Raveendranath, P. Mohanan, K. Mathew, M. Hajian, and L. Ligthart, "A simple free-space method for measuring the complex permittivity of single and compound dielectric materials," *Microwave and Optical Technology Letters*, vol. 26, no. 2, pp. 117–119, 2000.

[48] K. T. Mathew, *Perturbation Theory*. John Wiley Sons, Inc., 2005.

[49] A. Kumar, S. Sharma, and G. Singh, "Measurement of dielectric constant and loss factor of the dielectric material at microwave frequencies," *Progress In Electromagnetics Research*, vol. 69, pp. 47–54, 2007.

[50] A. Fulford, *Conductor and dielectric property extraction using microstrip tee resonators*. PhD thesis, 2005.

[51] L. S. Demenicis, R. A. Lima, L. F. M. Conrado, W. Margulis, and M. C. R. Carvalho, "A cpw linear resonator method for the microwave characterization of high

dielectric constant films," *Microwave and Optical Technology Letters*, vol. 49, no. 3, pp. 521–524, 2007.

[52] P. Bernard and J. Gautray, "Measurement of dielectric constant using a microstrip ring resonator," *IEEE Transactions on Microwave Theory and Techniques*, vol. 39, no. 3, pp. 592–595, 1991.

[53] H. J. Lee, H. Kim, and J. G. Yook, "Numerical estimates of artificial magnetic metamaterial inclusions at microwave frequencies: An edge coupled and a broadside coupled split ring resonator," *Journal of the Korean Physical Society*, vol. 55, no. 4, pp. 1596–1601, 2009.

[54] T. Weiland, R. Schuhmann, R. Greegor, C. Parazzoli, A. Vetter, D. Smith, D. Vier, and S. Schultz, "Ab initio numerical simulation of left-handed metamaterials: Comparison of calculations and experiments," *Journal of Applied Physics*, vol. 90, no. 10, pp. 5419–5424, 2001.

[55] A. Pradeep, S. Mridula, and P. Mohanan, "Design of an edge-coupled dual-ring split-ring resonator," *IEEE Antennas and Propagation Magazine*, vol. 53, no. 4, pp. 45–54, 2011.

[56] H. Bahrami, M. Hakkak, and A. Pirhadi, "Using complementary split ring resonators (csrr) to design bandpass waveguide filters," in *2007 Asia-Pacific Microwave Conference*, pp. 1–4, Dec 2007.

[57] J. D. Baena, J. Bonache, F. Martin, R. M. Sillero, F. Falcone, T. Lopetegi, M. A. Laso, J. Garcia-Garcia, I. Gil, M. F. Portillo, *et al.*, "Equivalent-circuit models for split-ring resonators and complementary split-ring resonators coupled to planar transmission lines," *IEEE transactions on microwave theory and techniques*, vol. 53, no. 4, pp. 1451–1461, 2005.

[58] R. W. Ziolkowski, "Design, fabrication, and testing of double negative metamaterials," *IEEE Transactions on antennas and Propagation*, vol. 51, no. 7, pp. 1516–1529, 2003.

[59] C. Saha, J. Y. Siddiqui, and Y. M. Antar, "Square split ring resonator backed coplanar waveguide for filter applications," in *General Assembly and Scientific Symposium, 2011 XXXth URSI*, pp. 1–4, IEEE, 2011.

[60] R. Marqués, F. Medina, and R. Rafii-El-Idrissi, “Role of bianisotropy in negative permeability and left-handed metamaterials,” *Physical Review B*, vol. 65, no. 14, p. 144440, 2002.

[61] R. Marqués, F. Mesa, J. Martel, and F. Medina, “Comparative analysis of edge-and broadside-coupled split ring resonators for metamaterial design-theory and experiments,” *IEEE Transactions on Antennas and Propagation*, vol. 51, no. 10, pp. 2572–2581, 2003.

[62] E. Ekmekci and G. Turhan-Sayan, “Comparative investigation of resonance characteristics and electrical size of the double-sided srr, bc-srr and conventional srr type metamaterials for varying substrate parameters,” *Prog. Electromagn. Res. B*, vol. 12, pp. 35–62, 2009.

[63] T. Roy, D. Banerjee, and S. Kar, “Studies on multiple-inclusion magnetic structures useful for millimeter-wave left-handed metamaterial applications,” *IETE Journal of Research*, vol. 55, no. 2, pp. 83–89, 2009.

[64] I. Bulu, H. Caglayan, and E. Ozbay, “Experimental demonstration of subwavelength focusing of electromagnetic waves by labyrinth-based two-dimensional metamaterials,” *Optics letters*, vol. 31, no. 6, pp. 814–816, 2006.

[65] E. Özbay, I. Bulu, and H. Caglayan, “Transmission, refraction, and focusing properties of labyrinth based left-handed metamaterials,” *physica status solidi (b)*, vol. 244, no. 4, pp. 1202–1210, 2007.

[66] J. D. Baena, R. Marqués, F. Medina, and J. Martel, “Artificial magnetic metamaterial design by using spiral resonators,” *Physical review B*, vol. 69, no. 1, p. 014402, 2004.

[67] C. Sabah and S. Uckun, “Triangular split ring resonator and wire strip to form new metamaterial,”

[68] C. Sabah, “Novel, dual band, single and double negative metamaterials: nonconcentric delta loop resonators,” *Progress In Electromagnetics Research*, vol. 25, pp. 225–239, 2010.

[69] C. Sabah, “Tunable metamaterial design composed of triangular split ring resonator and wire strip for s-and c-microwave bands,” *Progress In Electromagnetics Research*, vol. 22, pp. 341–357, 2010.

[70] M. M. Saadoun and N. Engheta, "A reciprocal phase shifter using novel pseudochiral or ω medium," *Microwave and optical technology letters*, vol. 5, no. 4, pp. 184–188, 1992.

[71] E. Ekmekçi and G. Turhan-Sayan, "Investigation of effective permittivity and permeability for a novel v-shaped metamaterial using simulated s-parameters," in *5th International Conference on Electrical and Electronics Engineering*, sn, 2007.

[72] D. Wang, L. Ran, H. Chen, M. Mu, J. A. Kong, and B.-I. Wu, "Experimental validation of negative refraction of metamaterial composed of single side paired s-ring resonators," *Applied physics letters*, vol. 90, no. 25, p. 254103, 2007.

[73] H. Chen, L. Ran, J. Huangfu, X. Zhang, K. Chen, T. M. Grzegorczyk, and J. A. Kong, "Left-handed materials composed of only s-shaped resonators," *Physical Review E*, vol. 70, no. 5, p. 057605, 2004.

[74] P. M. Ragi, K. Umadevi, P. Nees, J. Jose, M. Keerthy, and V. Joseph, "Flexible split-ring resonator metamaterial structure at microwave frequencies," *Microwave and Optical Technology Letters*, vol. 54, no. 6, pp. 1415–1416, 2012.

[75] K. Umadevi, S. P. Chakyar, S. K. Simon, J. Andrews, and V. Joseph, "Split ring resonators made of conducting wires for performance enhancement," *EPL (Europhysics Letters)*, vol. 118, no. 2, p. 24002, 2017.

[76] B. Sauviac, C. Simovski, and S. Tretyakov, "Double split-ring resonators: Analytical modeling and numerical simulations," *Electromagnetics*, vol. 24, no. 5, pp. 317–338, 2004.

[77] K. Aydin, I. Bulu, K. Guven, M. Kafesaki, C. M. Soukoulis, and E. Ozbay, "Investigation of magnetic resonances for different split-ring resonator parameters and designs," *New journal of physics*, vol. 7, no. 1, p. 168, 2005.

[78] N. Wiwatcharagoses, K. Y. Park, and P. Chahal, "Metamaterial-inspired miniaturized microwave sensing probes," in *2012 IEEE 62nd Electronic Components and Technology Conference*, pp. 2106–2111, IEEE, 2012.

[79] N. Wiwatcharagoses, K. Y. Park, and P. Chahal, "A new metamaterial unit cell for compact microstrip circuit designs," in *2011 IEEE 61st Electronic Components and Technology Conference (ECTC)*, pp. 169–172, May 2011.

[80] A. Ebrahimi, W. Withayachumnankul, S. Al-Sarawi, and D. Abbott, "High-sensitivity metamaterial-inspired sensor for microfluidic dielectric characterization," *IEEE Sensors Journal*, vol. 14, no. 5, pp. 1345–1351, 2014.

[81] I. V. Shadrivov, D. A. Powell, S. K. Morrison, Y. S. Kivshar, and G. N. Milford, "Scattering of electromagnetic waves in metamaterial superlattices," *Applied Physics Letters*, vol. 90, no. 20, p. 201919, 2007.

[82] M. Smierzchalski, S. Collardey, and K. Mahdjoubi, "A novel metamaterial-based rfid antenna with efficient of operating distance," in *2012 6th European Conference on Antennas and Propagation (EUCAP)*, pp. 3038–3041, March 2012.

[83] F. Martín, C. Herrojo, P. Vélez, L. Su, J. Mata-Contreras, and F. Paredes, "Application of metamaterial concepts to sensors and chipless RFID," *Journal of Physics: Conference Series*, vol. 963, p. 012012, feb 2018.

[84] C. Lee and C. P. Ho, "Reconfigurable mems metamaterials," in *2017 International Conference on Optical MEMS and Nanophotonics (OMN)*, pp. 1–2, Aug 2017.

[85] H. Bilgin, S. Zahertar, S. Sadeghzadeh, A. D. Yalcinkaya, and H. Torun, "A mems-based terahertz detector with metamaterial-based absorber and optical interferometric readout," *Sensors and Actuators A: Physical*, vol. 244, pp. 292 – 298, 2016.

[86] E. Ekmekci and G. Turhan-Sayan, "Sensitivity of the resonance characteristics of srr and dsrr (double-sided srr) type metamaterials to the changes in substrate parameters and the usefulness of dsrr structure for reduced electrical size,"

[87] Z. Sheng and V. V. Varadan, "Tuning the effective properties of metamaterials by changing the substrate properties," *Journal of applied physics*, vol. 101, no. 1, p. 014909, 2007.

[88] S.-Y. Chiam, R. Singh, W. Zhang, and A. A. Bettiol, "Controlling metamaterial resonances via dielectric and aspect ratio effects," *Applied Physics Letters*, vol. 97, no. 19, p. 191906, 2010.

[89] M. Lapine, D. Powell, M. Gorkunov, I. Shadrivov, R. Marqués, and Y. Kivshar, "Structural tunability in metamaterials," *Applied Physics Letters*, vol. 95, no. 8, p. 084105, 2009.

[90] I. V. Shadrivov, S. K. Morrison, and Y. S. Kivshar, "Tunable split-ring resonators for nonlinear negative-index metamaterials," *Optics Express*, vol. 14, no. 20, pp. 9344–9349, 2006.

[91] K. Aydin and E. Ozbay, "Capacitor-loaded split ring resonators as tunable metamaterial components," *Journal of Applied Physics*, vol. 101, no. 2, p. 024911, 2007.

[92] I. J. Bahl and P. Bhartia, *Microwave solid state circuit design*. Wiley-Interscience Hoboken, NJ, 2003.

[93] Q. Wu, M.-f. Wu, F.-y. Meng, J. Wu, and L.-w. Li, "Modeling the effects of an individual srr by equivalent circuit method," in *2005 IEEE Antennas and Propagation Society International Symposium*, vol. 1, pp. 631–634, IEEE, 2005.

[94] Q. Wu, M.-F. Wu, F.-Y. Meng, J. Wu, and L.-W. Li, "Srrs artificial magnetic metamaterials modeling using transmission line theory," in *presentation at Progress in Electromagnetism Research Symposium*, 2005.

[95] M. Wu, F. Meng, Q. Wu, J. Wu, and L. Li, "A compact equivalent circuit model for the srr structure in metamaterials," in *2005 Asia-Pacific Microwave Conference Proceedings*, vol. 1, pp. 4–pp, IEEE, 2005.

[96] S. S. Mohan, *The design, modeling and optimization of on-chip inductor and transformer circuits*. PhD thesis, Stanford University, 1999.

[97] S. Naoui, L. Latrach, and A. Gharsallah, "Equivalent circuit model of double split ring resonators," *Microw Opt Technol Lett*, vol. 11, no. 1, pp. 1–6, 2016.

[98] O. Sydoruk, E. Tatartschuk, E. Shamonina, and L. Solymar, "Analytical formulation for the resonant frequency of split rings," *Journal of applied physics*, vol. 105, no. 1, p. 014903, 2009.

[99] L. Rogla, J. Carbonell, and V. Boria, "Study of equivalent circuits for open-ring and split-ring resonators in coplanar waveguide technology," *IET microwaves, antennas & propagation*, vol. 1, no. 1, pp. 170–176, 2007.

[100] D. R. Smith, W. J. Padilla, D. Vier, S. C. Nemat-Nasser, and S. Schultz, "Composite medium with simultaneously negative permeability and permittivity," *Physical review letters*, vol. 84, no. 18, p. 4184, 2000.

[101] A. K. Horestani, C. Fumeaux, S. F. Al-Sarawi, and D. Abbott, "Displacement sensor based on diamond-shaped tapered split ring resonator," *IEEE Sensors Journal*, vol. 13, no. 4, pp. 1153–1160, 2013.

[102] A. K. Horestani, J. Naqui, Z. Shaterian, D. Abbott, C. Fumeaux, and F. Martín, "Two-dimensional alignment and displacement sensor based on movable broadside-coupled split ring resonators," *Sensors and Actuators A: Physical*, vol. 210, pp. 18–24, 2014.

[103] A. K. Horestani, D. Abbott, and C. Fumeaux, "Rotation sensor based on horn-shaped split ring resonator," *IEEE Sensors Journal*, vol. 13, no. 8, pp. 3014–3015, 2013.

[104] A. Ebrahimi, W. Withayachumnankul, S. F. Al-Sarawi, and D. Abbott, "Metamaterial-inspired rotation sensor with wide dynamic range," *IEEE Sensors Journal*, vol. 14, no. 8, pp. 2609–2614, 2014.

[105] B. Ozbey, E. Unal, H. Ertugrul, O. Kurc, C. M. Puttlitz, V. B. Erturk, A. Altintas, and H. V. Demir, "Wireless displacement sensing enabled by metamaterial probes for remote structural health monitoring," *Sensors*, vol. 14, no. 1, pp. 1691–1704, 2014.

[106] F. Von Detten, D. Basten, and A. Ajami, "Low-cost proximity sensor system using metamaterial structures," 2013.

[107] Z. Benniu, Z. Junqian, Z. Kaihong, and Z. Zhixiang, "A non-contact proximity sensor with low frequency electromagnetic field," *Sensors and Actuators A: Physical*, vol. 135, no. 1, pp. 162–168, 2007.

[108] H. Karim, D. Delfin, M. A. I. Shuvo, L. A. Chavez, C. R. Garcia, J. H. Barton, S. M. Gaytan, M. A. Cadena, R. C. Rumpf, R. B. Wicker, *et al.*, "Concept and model of a metamaterial-based passive wireless temperature sensor for harsh environment applications," *IEEE Sensors J.*, vol. 15, no. 3, pp. 1445–1452, 2015.

[109] S. Raghavan and V. Rajeshkumar, "An overview of metamaterials in biomedical applications," *Session 2A8*, vol. 245, pp. 25–28, 2013.

[110] M. S. Boybay and O. M. Ramahi, "Non-destructive thickness measurement using quasi-static resonators," *IEEE Microw. Compon. Lett.*, vol. 23, no. 4, pp. 217–219, 2013.

[111] I. M. Rusni, A. Ismail, A. R. H. Alhawari, M. N. Hamidon, and N. A. Yusof, "An aligned-gap and centered-gap rectangular multiple split ring resonator for dielectric sensing applications," *Sensors*, vol. 14, no. 7, pp. 13134–13148, 2014.

[112] C.-M. Hsu, K.-Z. Chen, C.-S. Lee, and C.-L. Yang, "Improved approach using multiple planar complementary split-ring resonators for accurate measurement of permittivity," in *Wireless Symposium (IWS), 2016 IEEE MTT-S International*, pp. 1–4, IEEE, 2016.

[113] C.-L. Yang, C.-S. Lee, K.-W. Chen, and K.-Z. Chen, "Noncontact measurement of complex permittivity and thickness by using planar resonators," *IEEE Transactions on Microwave Theory and Techniques*, vol. 64, no. 1, pp. 247–257, 2016.

[114] M. S. Boybay and O. M. Ramahi, "Material characterization using complementary split-ring resonators," *IEEE Transactions on Instrumentation and Measurement*, vol. 61, no. 11, pp. 3039–3046, 2012.

[115] C.-S. Lee and C.-L. Yang, "Complementary split-ring resonators for measuring dielectric constants and loss tangents," *IEEE Microwave and Wireless Components Letters*, vol. 24, no. 8, pp. 563–565, 2014.

[116] C.-S. Lee and C.-L. Yang, "Single compound complementary split-ring resonator for simultaneously measuring permittivity and thickness," in *Microwave Symposium (IMS), 2014 IEEE MTT-S International*, pp. 1–3, IEEE, 2014.

[117] C.-S. Lee and C.-L. Yang, "Thickness and permittivity measurement in multi-layered dielectric structures using complementary split-ring resonators," *IEEE Sensors Journal*, vol. 14, no. 3, pp. 695–700, 2014.

[118] M. A. H. Ansari, A. K. Jha, and M. J. Akhtar, "Design and application of the csrr-based planar sensor for noninvasive measurement of complex permittivity," *IEEE Sensors Journal*, vol. 15, no. 12, pp. 7181–7189, 2015.

[119] H. O. Yilmaz and M. S. Boybay, "Sensing in anisotropic and lossy media using complementary split ring resonators," in *Antennas and Propagation (APSURSI), 2016 IEEE International Symposium on*, pp. 499–500, IEEE, 2016.

[120] L. Benkhaoua, M. Benhabiles, and M. Riabi, "A miniaturized near-field sensor based on a double-sided spiral split-ring resonator for dielectric characterization,"

in *RF and Wireless Technologies for Biomedical and Healthcare Applications (IMWS-Bio), 2014 IEEE MTT-S International Microwave Workshop Series on*, pp. 1–3, IEEE, 2014.

[121] L. Benkhaoua, M. T. Benhabiles, S. Mouissat, and M. L. Riabi, "Miniaturized quasi-lumped resonator for dielectric characterization of liquid mixtures," *IEEE Sensors Journal*, vol. 16, no. 6, pp. 1603–1610, 2016.

[122] V. Sekar, W. J. Torke, S. Palermo, and K. Entesari, "A novel approach for dielectric constant measurement using microwave oscillators," in *Microwave Symposium Digest (MTT), 2011 IEEE MTT-S International*, pp. 1–4, IEEE, 2011.

[123] V. Sekar, W. J. Torke, S. Palermo, and K. Entesari, "A self-sustained microwave system for dielectric-constant measurement of lossy organic liquids," *IEEE Transactions on Microwave Theory and Techniques*, vol. 60, no. 5, pp. 1444–1455, 2012.

[124] G. Galindo-Romera, F. J. Herraiz-Martínez, M. Gil, and J. Juan, "Submersible printed split-ring resonator-based sensor for thin-film detection and permittivity characterization," *Sensors*, vol. 14169, p. 1, 2016.

[125] A. Raj, A. Kumar Jha, M. Ansari, M. J. Akhtar, and S. Panda, "Metamaterial-inspired microwave sensor for measurement of complex permittivity of materials," *Microwave and Optical Technology Letters*, vol. 58, no. 11, pp. 2577–2581, 2016.

[126] K. Saeed, M. F. Shafique, M. B. Byrne, and I. C. Hunter, "Planar microwave sensors for complex permittivity characterization of materials and their applications," *Edited by Md. Zahurul Haq*, p. 319, 2012.

[127] J. Sheen, "Study of microwave dielectric properties measurements by various resonance techniques," *Measurement*, vol. 37, no. 2, pp. 123–130, 2005.

[128] T. Weiland, R. Schuhmann, R. Greegor, C. Parazzoli, A. Vetter, D. Smith, D. Vier, and S. Schultz, "Ab initio numerical simulation of left-handed metamaterials: Comparison of calculations and experiments," *J. Appl. Phys.*, vol. 90, no. 10, pp. 5419–5424, 2001.

[129] S.-Y. Chiam, R. Singh, W. Zhang, and A. A. Bettiol, "Controlling metamaterial resonances via dielectric and aspect ratio effects," *Appl. Phys. Lett.*, vol. 97, p. 191906, 2010.

[130] Z. Sheng and V. V. Varadan, "Tuning the effective properties of metamaterials by changing the substrate properties," *J. Appl. Phys.*, vol. 101, no. 1, p. 014909, 2007.

[131] J. Naqui, J. Coromina, F. Martín, A. K. Horestani, and C. Fumeaux, "Comparative analysis of split ring resonators (srr), electric-lc (elc) resonators, and s-shaped split ring resonators (s-srr): Potential application to rotation sensors," in *Proc. of 2014 Mediterranean Microwave Symposium (MMS2014)*, pp. 1–5, IEEE, 2014.

[132] M. Boybay and O. M. Ramahi, "Material characterization using complementary split-ring resonators," *IEEE Trans. Instrum. Meas.*, vol. 61, pp. 3039–3046, Nov 2012.

[133] G. Galindo-Romera, F. J. Herraiz-Martínez, M. Gil, J. J. Martínez-Martínez, and D. Segovia-Vargas, "Submersible printed split-ring resonator-based sensor for thin-film detection and permittivity characterization," *IEEE Sensors Journal*, vol. 16, no. 10, pp. 3587–3596, 2016.

[134] E. Ekmekci and G. Turhan-Sayan, "Sensitivity of the resonance characteristics of srr and dsrr (double-sided srr) type metamaterials to the changes in substrate parameters and the usefulness of dsrr structure for reduced electrical size," in *PIERS Proceedings*, pp. 598–602, 2008.

[135] R. Waldron, "Perturbation theory of resonant cavities," *Proceedings of the IEE-Part C: Monographs*, vol. 107, no. 12, pp. 272–274, 1960.

[136] U. Raveendranath and K. Mathew, "The study of the dielectric behaviour of vapours of water and organic liquids at microwave frequencies," *Journal of molecular liquids*, vol. 68, no. 2-3, pp. 145–156, 1996.

[137] P. Banerjee, G. Ghosh, and S. K. Biswas, "A simple method to determine the dielectric constant of small-sized medium-loss samples at x-band frequencies," *International Journal of Electromagnetics and Applications*, vol. 1, no. 1, pp. 12–15, 2011.

[138] J. Sheen, "Study of microwave dielectric properties measurements by various resonance techniques," *Measurement*, vol. 37, no. 2, pp. 123–130, 2005.

[139] J. Baker-Jarvis, M. D. Janezic, and D. C. DeGroot, "High-frequency dielectric measurements," *IEEE Instrum. Meas. Mag.*, vol. 13, no. 2, pp. 24–31, 2010.

[140] A. P. Gregory and R. N. Clarke, "A review of rf and microwave techniques for dielectric measurements on polar liquids," *IEEE Trans. Dielectr. Electr. Insul.*, vol. 13, no. 4, pp. 727–743, 2006.

[141] S. O. Nelson and P. Bartley, "Measuring frequency-and temperature-dependent permittivities of food materials," *IEEE Trans. Instrum. Meas.*, vol. 51, no. 4, pp. 589–592, 2002.

[142] P. Bernard and J. Gautray, "Measurement of dielectric constant using a microstrip ring resonator," *IEEE Trans. Microw. Theory Techn.*, vol. 39, no. 3, pp. 592–595, 1991.

[143] S. Ryynänen, "The electromagnetic properties of food materials: a review of the basic principles," *Journal of Food Engineering*, vol. 26, no. 4, pp. 409–429, 1995.

[144] S. Nelson *et al.*, "Dielectric properties of agricultural products and some applications," *Research in Agricultural Engineering*, vol. 54, no. 2, pp. 104–112, 2008.

[145] S. Nelson, "Review of factors influencing the dielectric properties of cereal grains.," *Cereal Chemistry*, 1981.

[146] E. Nyfors and P. Vainikainen, *Industrial Microwave Sensors*. Artech House microwave library, Artech House, 1989.

[147] Y. Wang, T. D. Wig, J. Tang, and L. M. Hallberg, "Dielectric properties of foods relevant to rf and microwave pasteurization and sterilization," *Journal of Food Engineering*, vol. 57, no. 3, pp. 257–268, 2003.

[148] D. L. Gershon, J. Calame, Y. Carmel, T. Antonsen Jr, and R. M. Hutcheon, "Open-ended coaxial probe for high-temperature and broad-band dielectric measurements," *Microwave Theory and Techniques, IEEE Transactions on*, vol. 47, no. 9, pp. 1640–1648, 1999.

[149] T. Shimizu and Y. Kobayashi, "Millimeter wave measurements of temperature dependence of complex permittivity of gaas plates by a circular waveguide method," in *Microwave Symposium Digest, 2001 IEEE MTT-S International*, vol. 3, pp. 2195–2198, IEEE, 2001.

[150] E. Havinga, "The temperature dependence of dielectric constants," *Journal of Physics and Chemistry of Solids*, vol. 18, no. 23, pp. 253 – 255, 1961.

[151] Z.-Y. Cheng, R. S. Katiyar, X. Yao, and A. S. Bhalla, "Temperature dependence of the dielectric constant of relaxor ferroelectrics," *Phys. Rev. B*, vol. 57, pp. 8166–8177, Apr 1998.

[152] V. V. Varadan and L. Ji, "Temperature dependence of resonances in metamaterials," *Microwave Theory and Techniques, IEEE Transactions on*, vol. 58, no. 10, pp. 2673–2681, 2010.

[153] R. Singh, A. K. Azad, Q. Jia, A. J. Taylor, and H.-T. Chen, "Thermal tunability in terahertz metamaterials fabricated on strontium titanate single-crystal substrates," *Optics letters*, vol. 36, no. 7, pp. 1230–1232, 2011.

[154] Y. Kobayashi and J. Yu, "Temperature-dependence measurement of anisotropic complex permittivity for mic dielectric substrate," in *Microwave Conference, 1992. APMC 92. 1992 Asia-Pacific*, vol. 2, pp. 859–862, IEEE, 1992.

[155] S. K. Roy, S. K. Jha, and L. Jha, "Parametric study of temperature sensitivity for microstrip patch antenna," *84.40 Ba*, 2005.

[156] H. Li, C. Ra, G. Zhang, and W. J. Yoo, "Frequency and temperature dependence of the dielectric properties of a pcb substrate for advanced packaging applications," *J. Korean Phys. Soc*, vol. 54, pp. 1096–1099, 2009.

[157] J.-M. Heinola, K.-P. Latti, P. Silventoinen, J.-P. Strom, and M. Kettunen, "A new method to measure dielectric constant and dissipation factor of printed circuit board laminate material in function of temperature and frequency," in *Advanced Packaging Materials: Processes, Properties and Interfaces, 2004. Proceedings. 9th International Symposium on*, pp. 235–240, IEEE, 2004.

[158] S. Srjvastava, D. Ptiei, and P. Mbhendeu, "Temperature dependence of dielectric loss of shellac in microwave region," *Proceedings of the National Institute of Sciences of India: Physical sciences*, vol. 23, p. 289, 1957.

[159] M. L. Prava and A. Ahmed, "Study on dielectric behaviour of waxes in p-band region," *Journal of Chemical, Biological and Physical Sciences (JCBPS)*, vol. 3, no. 4, p. 2907, 2013.

List of Publications

1. **Sreedevi P. Chakyar**, Sikha K. Simon, C. Bindu, Jolly Andrews, and V. P. Joseph, *Complex permittivity measurement using metamaterial split ring resonators,* Journal of Applied Physics, **121**, 054101, 2017.

2. **Sreedevi P. Chakyar** , Sikha Simon K., Aathira Murali, Shanto T. A., Jolly Andrews and Joseph V. P., *Determination of Permittivity of Pulses and Cereals using Metamaterial Split Ring Resonator*, AIP conference proceedings **1849**, 020024, 2017.

3. **Sreedevi P. Chakyar**, Shanto T. A., Aathira Murali, Sikha Simon K., Nees Paul, Jolly Andrews, Joseph V. P., *Measurement of Dielectric Constant of Waxes at Different Temperatures using Split Ring Resonator Structure*, IEEE Xplore, Proceedings of International Microwave and RF Conference, 1-4, 2016.

4. **Sreedevi P. Chakyar**, Jolly Andrews, and V. P. Joseph, *Temperature dependence of relative permittivity: A measurement technique using split ring resonators.,* International Journal of Mechanical, Aerospace, Industrial, Mechatronic and Manufacturing Engineering, **10(6)**, 1057 - 1060, 2016.

5. Sikha K. Simon, **Sreedevi P. Chakyar**, Anju Sebastian, Jovia Jose, Jolly Andrews and Joseph V. P., *Broadside Coupled Split Ring Resonators as a Sensitive Tunable Sensor for Efficient Detection of Mechanical Vibrations*, Accepted in Sensing and Imaging (Springer Publications)

6. Anju Sebastian, Sikha K. Simon, **Sreedevi P Chakyar**, Jovia Jose, Jolly Andrews and Joseph V. P., *Broadside coupled split ring resonator metamaterial structure for sensitive measurement of liquid concentrations*, AIP Conference proceedings, **2082**, 070002, 2019.

7. Jovia Jose, Sikha K. Simon, Joe Kizhakooden, Anju Sebastain, **Sreedevi P Chakyar**, Nees Paul, Bindu C, Jolly Andrews, and V.P.Joseph, *Frequency Dependent Radia-*

tion Properties of Negative Permittivity Metamaterial Reflector Antenna., Progress In Electromagnetic Research Letters, **83**, 1-5, 2019.

8. Joe Kizhakooden, Jovia Jose, Nees Paul, Sikha K. Simon, **Sreedevi P. Chakyar**, Jolly Andrews and V.P. Joseph, *Metamaterial inspired featherlight artificial plasma horn antenna for astronomical and communication applications*, Microwave and Optical Technology Letters (Wiley Publishers), **61**, 777-780, 2018.

9. Nees Paul, **Sreedevi P. Chakyar**, K. S. Umadevi, Simon K. Sikha, Joe Kizhakooden, Jolly Andrews, V. P. Joseph, *Humidity Sensitive Flexible Microwave Absorbing Sheet Using PolyanilinePolytetrafluoroethylene Composite*, Arabian Journal for Science and Engineering, **44**, 553560, 2018.

10. K. S. Umadevi, **Sreedevi P. Chakyar**, Sikha K. Simon, Jolly Andrews, and V. P. Joseph, *Split ring resonators made of conducting wires for performance enhancement*, Euro Physics Letters (IOP Science), **118**, 24002, 2017.

11. Hazel Thomas, **Sreedevi P. Chakyar**, Sikha Simon K., Jolly Andrews and Joseph V. P., *Transmission Line Coupled Split Ring Resonator as Dielectric Thickness Sensor*, AIP conference proceedings, **1849**, 020003, 2017.

12. Sikha Simon K., **Sreedevi P. Chakyar**, Jolly Andrews and Joseph V. P., *Metamaterial Split Ring Resonator as a Sensitive Mechanical Vibration Sensor*, AIP conference proceedings, **1849**, 02001, 2017

13. Jovia Jose, **Sreedevi P. Chakyar**, Jolly Andrews and V. P. Joseph, *FDTD analysis of the interaction of a Gaussian pulse with negative permittivity metamaterial slab*, IEEE Conference Publications, 2016 IEEE MTTS International Conference on Numerical Electromagnetic and Multiphysics Modeling and Optimization (NEMO), 1 - 3, 2016

14. Jolly Andrews, **Sreedevi P. Chakyar**, V. P. Joseph; Vincent Mathew, *Spectral domain modeling of the effect of film purity for superconducting slotline*, IEEE Conference Publications, 2016 IEEE MTT-S International Conference on Numerical Electromagnetic and Multiphysics Modeling and Optimization (NEMO), 1 - 3, 2016

Presentations in Conferences

1. *Temperature dependence of relative permittivity: A measurement technique using split ring resonators,* in **World academy of science engineering and technology, San Francisco, USA, 18(6) Part X, 1580-1583, 9-10 June, 2016.**

2. *Measurement of Dielectric Constant of Waxes at Different Temperatures using Split Ring Resonator Structure,* in **International Microwave and RF Conference (IMaRC - 2016), Delhi, 5-9 December 2016.**

3. *Determination of Permittivity of Pulses and Cereals using Metamaterial Split Ring Resonator,* in **Optics 17, NIT Calicut, Kerala, 9-11 January 2017.**

4. *Temperature Dependence of Complex Permittivity of Flame Retardant Circuit Boards,* in **OSI - International Symposium on Optics (OSI-ISO 2018), IIT, Kanpur, 19 - 22 September 2018.**

5. *Temperature Dependence of Complex Permittivity of Flame Retardant Circuit Boards,* in **National conference on Science and applications of functional materials, St. Josephs College, Irinjalakuda, Kerala, 7 December 2018.**

6. *Study of temperature induced nonlinear effects of microwave and electronic circuits using metamaterial split ring resonators,* in **National seminar on materials, methods and sensors for electromagnetic applications, Christ College (Autonomous), Irinjalakuda, Kerala, 24-25 January 2019.**

Selected publications